Electronic Supplementary Information (ESI)

Terminal alkyne insertion into a thiolate-bridged dirhodium hydride complex derived from heterolytic cleavage of H_2

Xiangyu Zhao,[a] Dawei Yang,*[a] Yahui Zhang,[a] Baomin Wang,[a] and Jingping Qu*[ab]

[a]*State Key Laboratory of Fine Chemicals, Dalian University of Technology, Dalian, 116024, P. R. China.*

[b]*Key Laboratory for Advanced Materials, East China University of Science and Technology, Shanghai, 200237, P. R. China.*

*E-mail: qujp@dlut.edu.cn
yangdw@dlut.edu.cn

Table of Contents

I. General Materials and Methods

General Consideration. All manipulations were routinely carried out under an argon atmosphere by standard Schlenk-line techniques unless otherwise specified or Mikrouna argon-filled glove box. All solvents were dried and distilled over an appropriate drying agent under argon or nitrogen. [Cp*Rh(μ-Cl)$_3$RhCp*][BF_4],[1] [Cp*Ir(*t*-Cl)(μ-Cl)]$_2$,[2] benzene-1,2-dithiol (bdt)[3] and [Cp*Ir(bdt)][4] were prepared according to the literature. $NaBPh_4$**,** HBF_4•Et_2O, $CoCp_2$, MeONa, ferrocenium hexafluorophosphate (Fc•PF_6) and terminal alkynes were commercial available and used without further purification.

Spectroscopic Measurements. The NMR spectra were recorded on a Brüker 400 Ultra Shield spectrometer. The chemical shifts (δ) are given in parts per million relative to CD_2Cl_2 (5.32 ppm for ^{1}H; 53.84 ppm for ^{13}C). Infrared spectra were recorded on an NEXVSTM FT-IR spectrometer. ESI-HRMS were recorded on a HPLC/Q-Tof micro spectrometer, except that **D-5[PF_6]** and **D-6[PF_6]** was recorded on LTQ Orbitrap XL. Elemental analyses were performed on a Vario EL analyzer. GC was performed on an Agilent 7890B spectrometer.

X-ray Crystallography Procedures. Single-crystal X-ray diffraction studies were carried out on a Brüker SMART APEX CCD diffractometer with graphite monochromated Mo Kα radiation (λ = 0.71073 Å). Empirical absorption corrections were performed using the SADABS program,[5] Structures were solved by direct methods and refined by full-matrix least-squares based on all data using SHELX 97.[6] Anisotropic thermal displacement coefficients were determined for all non-hydrogen atoms. Hydrogen atoms were placed at idealized positions and refined with fixed isotropic displacement parameters. Atoms C32, C33 of **7c[BPh_4]** were disordered and restrained during the refining of the structure. Disordered atomic positions were split and refined using one occupancy parameter per disordered group.

II. Experimental Procedures and Analytical Data

Synthesis of [Cp*Rh(μ-η^2:η^2-bdt)(μ-Cl)RhCp*][BF_4] (1[BF_4]).

Complex [Cp*Rh(μ-Cl)$_3$RhCp*][BF_4] (405 mg, 0.61 mmol) was added to MeOH (100 mL) followed by a suspension of disodium benzene-1,2-dithiolate (Na_2bdt) in MeOH (100 mL) at −78 ℃, which was prepared by the reaction of MeONa (66 mg,

1.22 mmol) and benzene-1,2-dithiol (86 mg, 0.61 mmol) in MeOH at room temperature. The mixture was stirred overnight as it warmed to room temperature. The resulting dark red suspension was evaporated, and then the residue was extracted with CH_2Cl_2 (200 mL). The solution was evaporated to dryness in reduced pressure and the residue was washed by diethyl ether. A dark red powder of **1[BF$_4$]** (317 mg, 0.43 mmol, 70%) was obtained after the volatiles were removed in vacuum. Crystals suitable for X-ray diffraction were obtained from a CH_2Cl_2 solution layered with *n*-hexane at room temperature.

^{1}H NMR (400 MHz, CD_2Cl_2, ppm): δ 7.18 (dd, 2H, J_1 = 5.4 Hz, J_2 = 3.2 Hz, bdt-*H*), 6.71 (dd, 2H, J_1 = 5.4 Hz, J_2 = 3.2 Hz, bdt-*H*), 1.52 (s, 30H, Cp*-CH_3). ^{13}C NMR (100 MHz, CD_2Cl_2, ppm): δ 152.64 (bdt-*C*), 128.43 (bdt-*C*H), 127.01 (bdt-*C*H), 97.83 (Cp*-*C*), 8.87 (Cp*-*C*H$_3$). ESI-HRMS: Calcd. for **1**$^+$ 650.9901; Found 650.9912. Anal. Calcd. For $C_{26}H_{34}Rh_2S_2ClBF_4$: C, 42.27; H, 4.64. Found: C, 42.22; H, 4.97.

Synthesis of [Cp*Rh(μ-η^2:η^2-bdt)RhCp*] (2).

To a stirred solution of **1[BF$_4$]** (406 mg, 0.55 mmol) in 200 mL of CH_2Cl_2 was added 2 equiv. of $CoCp_2$, followed by stirring at room temperature for 12 h. Volatiles were removed in vacuum, and the crude product was extracted with *n*-hexane (3×100 mL). A dark-red powder of **2** (259 mg, 0.42 mmol, 76%) were achieved after drying in reduced pressure. Crystals of **2** suitable for the X-ray diffraction experiment were grown from saturated *n*-hexane solution at −30 °C.

^{1}H NMR (400 MHz, CD_2Cl_2, ppm): δ 6.91 (s, 2H, bdt-*H*), 6.39 (s, 2H, bdt-*H*), 1.87 (s, 30H, Cp*-CH_3). ^{13}C NMR (100 MHz, CD_2Cl_2, ppm): δ 154.58 (bdt-*C*), 126.27 (bdt-*C*H), 123.75 (bdt-*C*H), 92.79 (Cp*-*C*), 11.23 (s, Cp*-*C*H$_3$). Anal. Calcd for $C_{26}H_{34}Rh_2S_2$: C, 50.65; H, 5.56; Found: C, 50.56; H, 5.80.

Synthesis of [Cp*Ir(μ-η^2:η^2-bdt)(μ-Cl)IrCp*][BPh$_4$] (3[BPh$_4$]).

Complexes [Cp*Ir(*t*-Cl)(μ-Cl)]$_2$ (231 mg, 0.29 mmol) and [Cp*Ir(bdt)] (271 mg, 0.58 mmol) were added to CH_2Cl_2 (150 mL) followed by $NaBPh_4$ (200 mg, 0.58 mmol) at −78 ℃. The mixture was stirred as it warmed to room temperature. The resulting dark orange suspension was filtered. The filtrate was evaporated to dryness in reduced pressure and the residue was washed by diethyl ether. A yellow powder of **3[BPh$_4$]** (460 mg, 0.4 mmol, 69%) was obtained after the volatiles were removed in vacuum. Crystals suitable for X-ray diffraction were obtained from a CH_2Cl_2 solution layered

with *n*-hexane at room temperature.

^{1}H NMR (400 MHz, CD_2Cl_2, ppm): δ 7.31 (s, 8H, BPh_4-*H*), 7.22 (s, 2H, bdt-*H*), 7.02 (t, J_1 = 6.6 Hz, 8H, BPh_4-*H*), 6.87 (s, 4H, BPh_4-*H*), 6.70 (s, 2H, bdt-*H*), 1.50 (s, 30H, Cp*-CH_3). ^{13}C NMR (100 MHz, CD_2Cl_2, ppm): δ 152.37 (bdt-*C*), 136.31 (BPh_4-*C*), 127.61 (bdt-*C*H) 126.72 (bdt-*C*H), 125.98 (BPh_4-*C*H), 122.07 (BPh_4-*C*H), 90.71 (Cp*-*C*), 8.75 (Cp*-*C*H_3). ESI-HRMS: Calcd. for $\mathbf{3}^+$ 831.1033; Found 831.1060. Anal. Calcd. For $C_{50}H_{54}Ir_2S_2ClB$: C, 52.23; H, 4.73. Found: C, 52.02; H, 4.60.

Synthesis of [Cp*Ir(μ-η^2:η^2-bdt)IrCp*] (4).

To a stirred solution of **3[BPh$_4$]** (471 mg, 0.41 mmol) in 200 mL of CH_2Cl_2 was added 2 equiv. of $CoCp_2$, followed by stirring at room temperature for 12 h. Volatiles were removed in vacuum, and the crude product was extracted with *n*-hexane (3×100 mL). A brown powder of **4** (192 mg, 0.24 mmol, 58%) were achieved after drying in reduced pressure. Crystals of **4** suitable for the X-ray diffraction experiment were grown from saturated *n*-hexane solution at −30 °C.

^{1}H NMR (400 MHz, CD_2Cl_2, ppm): δ 7.08 (dd, 2H, J_1 = 5.2 Hz, J_2 = 3.2 Hz, bdt-*H*), 6.38 (dd, 2H, J_1 = 5.2 Hz, J_2 = 3.2 Hz, bdt-*H*), 1.99 (s, 30H, Cp*-CH_3). ^{13}C NMR (100 MHz, CD_2Cl_2, ppm): δ 154.54 (bdt-*C*), 124.72 (bdt-*C*H), 124.38 (bdt-*C*H), 85.88 (Cp*-*C*), 11.21 (Cp*-*C*H_3). Anal. Calcd for $C_{26}H_{34}Ir_2S_2$: C, 39.27; H, 4.31; Found: C, 39.33; H, 4.10.

Synthesis of [Cp*M(μ-η^2:η^2-bdt)(μ-H)MCp*][PF$_6$] (M = Rh, 5[PF$_6$]; M = Ir, 6[PF$_6$]).

To a stirred solution of **2** (529 mg, 0.86 mmol) or **4** (477 mg, 0.60 mmol) and 1 equiv. of Fc•PF_6 in 200 mL of THF was bubbled 1 atm of H_2, followed by stirring at 60 ℃ for 12 h under H_2 (1 atm). The resulting suspension was filtrated at room temperature, the filtrate was evaporated to dryness in reduced pressure and the residue was washed by diethyl ether and dried in reduced pressure. Crystals suitable for X-ray diffraction were obtained from a CH_2Cl_2 solution layered with *n*-hexane at room temperature.

Complex **5[PF$_6$]** (229 mg, 0.30 mmol, 35%), an orange powder, ^{1}H NMR (400 MHz, CD_2Cl_2, ppm): δ 7.22 (dd, 2H, J_1 = 5.4 Hz, J_2 = 3.2 Hz, bdt-*H*), 6.71 (dd, 2H, J_1 = 5.4 Hz, J_2 = 3.2 Hz, bdt-*H*), 1.94 (s, 30H, Cp*-CH_3), −9.84 (t, 1H, J = 26 Hz, μ-*H*). ^{13}C NMR (100 MHz, CD_2Cl_2, ppm): δ149.15 (bdt-*C*), 128.55 (bdt-*C*H), 126.61 (bdt-*C*H),

100.95 (Cp*-*C*), 10.75 (s, Cp*-*C*H_3). ESI-HRMS: Calcd. for $\mathbf{5}^+$ 617.0291; Found 617.0285 Anal. Calcd. for $C_{26}H_{35}Rh_2S_2PF_6$: C, 40.96; H, 4.63; Found: C, 41.27; H, 4.33.

Complex **6[PF$_6$]** (166 mg, 0.18 mmol, 30%), a yellow powder, ^{1}H NMR (400 MHz, CD_2Cl_2, ppm): δ 7.38 (m, 2H, bdt-*H*), 6.65 (m, 2H, bdt-*H*), 2.10 (s, 30H, Cp*-C*H*$_3$), −12.86 (s, 1H, μ-*H*). ^{13}C NMR (100 MHz, CD_2Cl_2, ppm): δ 149.10 (bdt-*C*), 127.18 (bdt-*C*H), 126.79 (bdt-*C*H), 93.23 (Cp*-*C*), 10.51 (Cp*-*C*H$_3$). ESI-HRMS: Calcd. for $\mathbf{6}^+$ 797.1439; Found 797.1454. Anal. Calcd. for $C_{26}H_{35}Ir_2S_2PF_6$: C, 33.18; H, 3.75; Found: C, 33.37; H, 3.89.

The samples of **D-5[PF$_6$]** and **D-6[PF$_6$]** were synthesized using an analogous synthetic procedure by using 1 atm of D_2 in 45% and 32% yields, respectively. ^{1}H NMR spectrum is similar to that of the unlabeled complex. There is no obvious hydride signal found in the related region. ESI-HRMS: Calcd. for D-$\mathbf{5}^+$ 618.0348; Found 618.0349. ESI-HRMS: Calcd. for D-$\mathbf{6}^+$ 798.1492; Found 798.1494.

Synthesis of [Cp*M(μ-η^2:η^2-bdt)(μ-H)MCp*][BF$_4$] (M = Rh, 5[BF$_4$]; M = Ir, 6[BF$_4$])

To a stirred solution of **2** (246 mg, 0.40 mmol) or **4** (286 mg, 0.36 mmol) in 100 mL of CH_2Cl_2 was added 1 equiv. of HBF_4•Et_2O at −78 ℃, then gradually warmed to room temperature. Volatiles were removed in vacuum. The crude product was washed by *n*-hexane and dried in reduced pressure. Crystals suitable for X-ray diffraction were obtained from a CH_2Cl_2 solution layered with *n*-hexane at room temperature.

Complex **5[BF$_4$]** (155 mg, 0.22 mmol, 55%), an orange powder, ^{1}H NMR (400 MHz, CD_2Cl_2, ppm): δ 7.22 (s, 2H, bdt-*H*), 6.70 (s, 2H, bdt-*H*), 1.94 (s, 30H, Cp*-C*H*$_3$), −9.81 (s, 1H, μ-*H*). ^{13}C NMR (100 MHz, CD_2Cl_2, ppm): δ 149.14 (bdt-*C*), 128.53 (bdt-*C*H), 126.57 (bdt-*C*H), 100.93 (Cp*-*C*), 10.72 (Cp*-*C*H$_3$). ESI-HRMS: Calcd. for $\mathbf{5}^+$ 617.0291; Found 617.0285. Anal. Calcd. for $C_{26}H_{35}Rh_2S_2BF_4$: C, 44.34; H, 5.01; Found: C, 43.97; H, 4.84

Complex **6[BF$_4$]** (222 mg, 0.25 mmol, 69%), a yellow powder, ^{1}H NMR (400 MHz, CD_2Cl_2, ppm): δ 7.38 (s, 2H, bdt-*H*), 6.66 (s, 2H, bdt-*H*), 2.10 (s, 30H, Cp*-C*H*$_3$), −12.86 (s, 1H, μ-*H*). ^{13}C NMR (100 MHz, CD_2Cl_2, ppm): δ 149.07 (bdt-*C*), 127.14 (bdt-*C*H), 126.76 (bdt-*C*H), 93.20 (Cp*-*C*), 10.49 (Cp*-*C*H$_3$). ESI-HRMS: Calcd. for

6^{+} 797.1434; Found 797.1447. Anal. Calcd. for $C_{26}H_{35}Ir_2S_2BF_4$: C, 35.37; H, 4.00; Found: C, 35.56; H, 3.70.

Synthesis of [Cp*Rh(μ-η^2:η^2-bdt)(μ-η^2:η^1-C_2H_2R)RhCp*][BPh_4] (R = H, 7a[BPh_4]; R = *n*-C_3H_7, 7b[BPh_4]; R = *n*-C_5H_{11}, 7c[BPh_4]; R = *p*-MeC_6H_4, 7d[BPh_4]; R = *p*-ClC_6H_4, 7e[BPh_4]).

To a stirred solution of **5[PF_6]** (100 mg, 0.13 mmol) in 20 mL of THF was added 1 equiv. of terminal alkyne (when acetylene, bubbled 1 atm of acetlyene gas) followed by stirring at 60 ℃ for 12 h. The resulting suspension was filtrated at room temperature, and then the filtrate was dried in reduced pressure. The residue was washed with *n*-hexane and extracted by CH_2Cl_2 (20 mL). Volatiles were removed in vacuum. The residues were washed with diethyl ether. The crude products of **7a[PF_6]−7e[PF_6]** were achieved after drying in reduced pressure. And then, to the stirred solution of the above products in 20 mL of CH_2Cl_2 was added $NaBPh_4$ (45 mg, 0.13 mmol) followed by stirring at room temperature for 12 h. The resulting suspension was filtrated at room temperature, and then the filtrate was dried in reduced pressure. The residue was washed with diethyl ether. The crude products of **7a[BPh_4]−7e[BPh_4]** were achieved after drying in reduced pressure. Crystals suitable for X-ray diffraction were obtained from a CH_2Cl_2 solution layered with *n*-hexane at room temperature.

Yield of **7a[BPh_4]** (85 mg, 0.09 mmol) was 68%. ^{1}H NMR (400 MHz, CD_2Cl_2, ppm): δ 7.31 (s, 8H, BPh_4-*H*), 7.18 (m, 1H, bdt-*H*), 7.12 (m, 1H, bdt-*H*), 7.02 (t, 8H, *J* = 7.2 Hz, BPh_4-*H*), 6.87 (t, 4H, *J* = 7.2 Hz, BPh_4-*H*), 6.70 (m, 2H, bdt-*H*), 6.23 (dd, 1H, J_1 = 15.7 Hz, J_2 = 8.6 Hz, =CH-*H*), 4.97 (d, 1H, *J* = 9.4 Hz, =CH_2-*H*), 4.56 (d, 1H, *J* = 15.7 Hz, =CH_2-*H*), 1.52 (s, 30H, Cp*-C*H*$_3$). ^{13}C NMR (100 MHz, CD_2Cl_2, ppm): δ 150.68 (bdt-*C*), 136.32 (BPh_4-*C*), 128.08 (bdt-*C*H), 127.52 (bdt-*C*H), 126.88 (H_2C=*C*H), 126.51 (H_2*C*=CH_2), 125.99 (BPh_4-*C*), 122.10 (BPh_4-*C*), 99.56 (Cp*-*C*), 99.50 (Cp*-*C*), 9.00 (Cp*-*C*H_3). ESI-HRMS: Calcd. for **7a**$^{+}$ 643.0447; Found 643.0457. Anal. Calcd. for $C_{52}H_{57}Rh_2S_2B\cdot0.5CH_2Cl_2$: C, 62.73; H, 5.82; Found: C, 62.68; H, 5.78.

Yield of **7b[BPh_4]** (85 mg, 0.08 mmol) was 65%. ^{1}H NMR (400 MHz, CD_2Cl_2, ppm): δ 7.30 (s, 8H, BPh_4-*H*), 7.17-7.12 (m, 2H, bdt-*H*), 7.02 (t, *J* = 7.2 Hz, 8H, BPh_4-*H*), 6.87 (t, 4H, *J* = 7.2 Hz, BPh_4-*H*), 6.69 (m, 2H, bdt-*H*), 4.71 (s, 1H, H_2C=CH), 4.12 (s,

1H, H_2C=CH), 2.52-2.47 (m, 2H, =CCH_2−), 1.48 (s, 30H, Cp*-CH_3), 1.41 (m, 2H, CH_2CH$_3$), 1.00 (t, 3H, J = 3.4 Hz, CH$_2$CH_3). ^{13}C NMR (100 MHz, CD_2Cl_2, ppm): δ 151.85 (bdt-*C*), 136.29 (BPh$_4$-*C*), 128.02 (bdt-*C*H), 127.91 (bdt-*C*H), 126.54 (H_2C=*C*H), 125.98 (BPh$_4$-*C*), 122.07 (BPh$_4$-*C*), 99.36 (Cp*-*C*), 24.99 (−*C*H$_2$CH$_2$−), 15.51 (−*C*H$_2$CH$_3$), 14.48 (−CH$_2$*C*H$_3$), 8.99 (Cp*-*C*H$_3$). ESI-HRMS: Calcd. for **7b**$^+$ 685.0916; Found 685.0923. Anal. Calcd. for $C_{55}H_{63}Rh_2S_2B$: C, 65.74; H, 6.32; Found: C, 65.30; H, 6.36.

Yield of **7c[BPh$_4$]** (86 mg, 0.08 mmol) was 64%. ^{1}H NMR (400 MHz, CD_2Cl_2, ppm): δ 7.30 (s, 8H, BPh$_4$-*H*), 7.18-7.12 (m, 2H, bdt-*H*), 7.02 (t, 8H, J = 7.2 Hz, BPh$_4$-*H*), 6.87 (t, 4H, J = 7.2 Hz , BPh$_4$-*H*), 6.70 (m, 2H, bdt-*H*), 4.71 (s, 1H, H_2C=C−), 4.11 (s, 1H, H_2C=C−), 2.52 (m, 2H, =CCH_2−), 1.48 (s, 30H, Cp*-CH_3), 1.36 (s, 6H, (CH_2)$_3$−), 0.95 (t, 3H, J = 6.4 Hz, −CH_3). ^{13}C NMR (100 MHz, CD_2Cl_2, ppm): δ 151.25 (bdt-*C*), 135.89 (BPh$_4$-*C*), 127.69 (bdt-*C*H), 127.47 (bdt-*C*H), 126.17 (H_2C=*C*−), 126.14 (H_2C=C−), 125.57 (BPh$_4$-*C*), 121.66 (BPh$_4$-*C*), 99.01 (Cp*-*C*), 98.95 (Cp*-*C*), 47.65 (−*C*H$_2$(CH$_2$)$_3$−), 32.25 (−*C*H$_2$(CH$_2$)$_2$−), 31.22 (−*C*H$_2$CH$_2$−), 22.82 (−*C*H$_2$CH$_3$), 13.98 (−CH$_2$*C*H$_3$), 8.62 (Cp*-*C*H$_3$). ESI-HRMS: Calcd. for **7c**$^+$ 713.1229; Found 713.1223. Anal. Calcd. for $C_{57}H_{67}Rh_2S_2B$: C, 66.28; H, 6.54; Found: C, 66.15; H, 6.78.

Yield of **7d[BPh$_4$]** (85 mg, 0.08 mmol) was 62%. ^{1}H NMR (400 MHz, CD_2Cl_2, ppm): δ 7.30 (s, 8H, BPh$_4$-*H*), 7.24 (m, 1H, bdt-*H*), 7.18 (m, 1H, bdt-*H*), 7.14 (d, 2H, J = 8 Hz, Ph-*H*), 7.08 (d, 2H, J = 8 Hz, Ph-*H*), 7.02 (t, 8H, J = 7.2 Hz, BPh$_4$-*H*), 6.87 (t, 4H, J = 7.2 Hz, BPh$_4$-*H*), 6.73 (m, 2H, bdt-*H*), 4.85 (s, 1H, H_2C=C−), 3.87 (s, 1H, H_2C=C−), 2.35 (s, 3H, Toluene-CH_3), 1.29 (s, 30H, Cp*-CH_3). ^{13}C NMR (100 MHz, CD_2Cl_2, ppm): δ 151.20 (bdt-*C*), 136.30 (BPh$_4$-*C*), 128.95 (bdt-*C*H), 128.76 (Ph-*C*), 128.71 (bdt-*C*H), 127.78 (Ph-*C*), 126.77 (H_2C=*C*−), 126.54 (H_2C=C−), 125.99 (BPh$_4$-*C*), 122.08 (BPh$_4$-*C*), 99.58 (s, Cp*-*C*), 21.22 (Toluene-*C*H$_3$), 8.61 (Cp*-*C*H$_3$). ESI-HRMS: Calcd. for **7d**$^+$ 733.0916; Found 733.0918. Anal. Calcd. for $C_{59}H_{63}Rh_2S_2B$·0.5CH_2Cl_2: C, 65.24; H, 5.89; Found: C, 65.33; H, 5.70.

Yield of **7e[BPh$_4$]** (81 mg, 0.08 mmol) was 58%. ^{1}H NMR (400 MHz, CD_2Cl_2, ppm): δ 7.30-7.27 (m, 10H, BPh$_4$-*H* and Ph-*H*), 7.25 (m, 1H, bdt-*H*), 7.19 (m, 3H, bdt-*H* and Ph-*H*), 7.02 (t, 8H, J = 7.2 Hz, BPh$_4$-*H*), 6.87 (t, 4H, J = 7.2 Hz, BPh$_4$-*H*), 6.74 (m, 2H, bdt-*H*), 4.80 (s, 1H, H_2C=C−), 3.93 (s, 1H, H_2C=C−), 1.31 (s, 30H, Cp*-CH_3). ^{13}C NMR (100 MHz, CD_2Cl_2, ppm): δ 146.47 (bdt-*C*), 136.31 (BPh$_4$-*C*), 129.93 (Ph-*C*), 128.87 (bdt-*C*H), 128.46 (Ph-*C*), 127.93 (bdt-*C*H), 126.98 (H_2C=*C*−), 126.72

(H_2C=C−), 125.95 (BPh_4-*C*), 122.10 (BPh_4-*C*), 99.89 (Cp*-*C*), 99.83 (Cp*-*C*), 8.67 (Cp*-CH_3). ESI-HRMS: Calcd. for **7e**$^+$ 753.0370; Found 753.0381. Anal. Calcd. for $C_{58}H_{60}Rh_2S_2BCl \cdot CH_2Cl_2$: C, 61.18; H, 5.40; Found: C, 60.78; H, 5.32.

Analysis of terminal alkene

To a stirred solution of **7a[BPh_4]** (96 mg, 0.1 mmol) in THF (5 mL) was added 1 equiv. of HBF_4•Et_2O (20 μL, 0.1 mmol) and 2 equiv. of $CoCp_2$ (38 mg, 0.2 mmol) followed by stirring at 60 ℃ for 12 h in sealed flask with silicone cap. The resulting ethylene and ethane gas were determined and quantified by GC. The solution was dried in reduced pressure. The residues were extracted with *n*-hexane. Complex **2** (22 mg, 0.04 mmol) were obtained by removed the volatiles and solvent in vacuum. When the vinyl complexes were **7b[BPh_4]** (211 mg, 0.21 mmol), **7c[BPh_4]** (194 mg, 0.19 mmol), **7d[BPh_4]** (119 mg, 0.11 mmol) and **7e[BPh_4]** (187 mg, 0.17 mmol), THF-d_8 (8 mL) was used as reaction solvent and mellithene (20 mg, 0.12 mmol) was added as internal standard in above conditions. The resulting 1-amylene, 1-heptene, *p*-methylstyrene, *p*-chlorostyrene and complex **2** were determined and quantified by ^{1}H NMR spectroscopy.

Entry	Vinyl-bridged dirhodium complexes	Yield (%)	
		Terminal alkenes and alkanes[a]	**2**[a]
1	**7a[BPh_4]**	40[b]	36[c]
2	**7b[BPh_4]**	8	45
3	**7c[BPh_4]**	6	45
4	**7d[BPh_4]**	22	22
5	**7e[BPh_4]**	30	44

[a]Yields were calculated based on ^{1}H NMR with mellithene as internal standard. [b]Quantitative analyses of gas products are based on GC. [c]Yield of the isolated product.

III. References

[1] M. I. Rybinskaya, A. R. Kudinov, V. S. Kaganovich, *J. Organomet. Chem.*, 1983, **246**, 279.

[2] C. White, A. Yates, P. M. Maitlis,. *Inorg. Synth.*, 1992, **29**, 228.

[3] E. Block, V. Eswarakrishnan, M. Gernon, G. Ofori-Okai, C. Saha, K. Tang, J. Zubieta, *J. Am. Chem. Soc.*, 1989, **111**, 658.

[4] R. Xi, M. Abe, T. Suzuki, T. Nishioka, K. Isobe, *J. Organomet. Chem.*, 1997, **549**, 117.

[5] G. M. Sheldrick, *SADABS, Program for area detector adsorption correction*, Institute for Inorganic Chemistry, University of Göttingen, Germany, 1996.

[6] (a) G. M. Sheldrick, *SHELXL-97, Program for refinement of crystal structures*, University of Göttingen, Germany, 1997; (b) G. M. Sheldrick, *SHELXS-97, Program for Solution of Crystal Structures*, University of Göttingen, Germany, 1997.

IV. X-ray Crystallographic Data

Table S1. Crystallographic data for **1[BF_4]**·CH_2Cl_2, **2**, **3[BPh_4]**

	1[BF_4]·CH_2Cl_2	**2**	**3[BPh_4]**
Formula	$C_{27}H_{36}Rh_2S_2Cl_3BF_4$	$C_{26}H_{34}Rh_2S_2$	$C_{50}H_{54}Ir_2S_2BCl$
Formula weight	823.66	616.47	1149.71
Crystal dimensions (mm^3)	0.28 × 0.21 × 0.20	0.39 × 0.32 × 0.27	0.31 × 0.29 × 0.28
Crystal system	Triclinic	Triclinic	Triclinic
Space group	P–1	P–1	P–1
a (Å)	8.5593(7)	9.6295(4)	10.8763(6)
b (Å)	13.7160(11)	9.8207(4)	13.0712(7)
c (Å)	13.8176(11)	15.3103(7)	17.1848(10)
α (deg)	77.0026(14)	100.9957(12)	106.9709
β (deg)	88.6155(14)	103.9408(12)	93.6316(9)
γ (deg)	88.3987(14)	106.2076(13)	108.7174(9)
Volume ($Å^3$)	1579.7(2)	1296.65(10)	2179.6(2)
Z	2	2	2
T (K)	173(2)	223(2)	100(2)
D_{calcd} ($g·cm^{-3}$)	1.732	1.579	1.752
μ (mm^{-1})	1.472	1.444	6.291
F (000)	824	624	1124
No. of rflns. collected	14171	30812	28798
No. of indep. rflns. / R_{int}	5414/0.0542	4546/0.0218	7669/0.0291
No. of obsd. rflns.[$I_0 > 2\sigma(I_0)$]	5037	4154	7283
Data / restraints / parameters	5414/12/352	4546/181/256	7669/0/505
R_1 / wR_2 [$I_0 > 2\sigma(I_0)$][a]	0.0555/0.1533	0.0523/0.1412	0.0217/0.0555
R_1 / wR_2 (all data)[a]	0.0584/0.1571	0.0584/0.1476	0.0233/0.0565
GOF (on F^2)[a]	1.049	0.962	1.062
Largest diff. peak and hole ($e·Å^{-3}$)	1.757/–2.207	1.672/–2.260	0.771/–1.550
CCDC No.	1457067	1457069	1583399

Table S2. Crystallographic data for **4**, **5[PF_6]**, **6[BF_4]**

	4	**5[PF_6]**	**6[BF_4]**
Formula	$C_{52}H_{68}Ir_4S_4$	$C_{26}H_{35}Rh_2S_2PF_6$	$C_{26}H_{35}Ir_2S_2BF_4$
Formula weight	1590.10	762.45	882.87
Crystal dimensions (mm^3)	0.29 × 0.20 × 0.18	0.38 × 0.26× 0.23	0.27 × 0.19 × 0.18
Crystal system	Triclinic	Triclinic	Triclinic
Space group	P–1	P–1	P–1
a (Å)	10.7515(5)	9.9962(5)	9.921(4)
b (Å)	15.4939(7)	11.8993(6)	11.570(5)
c (Å)	16.0369(7)	13.3880(6)	13.212(6)
α (deg)	79.6888(14)	104.4486(16)	74.619(13)
β (deg)	77.9010(14)	90.0325(17)	86.919(13)
γ (deg)	87.8163(14)	95.9034(18)	83.718(13)
Volume ($Å^3$)	2569.9(2)	1533.36(13)	1453.0(11)
Z	2	2	2
T (K)	173(2)	299(2)	278(2)
D_{calcd} ($g \cdot cm^{-3}$)	2.055	1.651	2.018
μ (mm^{-1})	10.519	1.315	9.332
F (000)	1504	764	836
No. of rflns. collected	41132	34096	23707
No. of indep. rflns. / R_{int}	9029/0.0473	5376/0.0351	5021/0.0522
No. of obsd. rflns. [$I_0 > 2\sigma(I_0)$]	8099	4588	4434
Data / restraints / parameters	9029/366/541	5376/0/338	5021/12/320
R_1 / wR_2 [$I_0 > 2\sigma(I_0)$][a]	0.0418/0.1124	0.0305/0.0789	0.0506/0.1364
R_1 / wR_2 (all data)[a]	0.0475/0.1184	0.0402/0.0858	0.0585/0.1454
GOF (on F^2)[a]	1.136	0.860	1.077
Largest diff. peak and hole ($e \cdot Å^{-3}$)	2.688/–4.213	0.517/–0.568	2.221/–3.561
CCDC No.	1457081	1457073	1457080

Table S3. Crystallographic data for **7a[BPh_4]**, **7b[BPh_4]**, **7c[BPh_4]**·CH_2Cl_2

	7a[BPh_4]	**7b[BPh_4]**	**7c[BPh_4]**·CH_2Cl_2
Formula	$C_{52}H_{57}Rh_2S_2B$	$C_{55}H_{63}Rh_2S_2B$	$C_{58}H_{69}Rh_2S_2BCl_2$
Formula weight	962.73	1004.80	1117.78
Crystal dimensions (mm^3)	0.43 × 0.36 × 0.31	0.40 × 0.37 × 0.31	0.41 × 0.34 × 0.29
Crystal system	Triclinic	Monoclinic	Triclinic
Space group	P–1	Cc	P–1
a (Å)	10.9219(5)	19.4748(9)	13.5617(6)
b (Å)	13.2492(6)	10.6687(4)	14.4090(7)
c (Å)	17.0937(8)	23.5138(11)	15.3302(7)
α (deg)	106.7571(14)	90.00	73.0429(16)
β (deg)	95.4010(15)	106.023(2)	73.0526(17)
γ (deg)	108.6766(13)	90.00	74.0362(16)
Volume ($Å^3$)	2195.89(17)	4695.7(3)	2681.2(2)
Z	2	4	2
T (K)	100(2)	96(2)	100 (2)
D_{calcd} ($g \cdot cm^{-3}$)	1.456	1.421	1.385
μ (mm^{-1})	0.882	0.828	0.829
F (000)	992	2080	1156
No. of rflns. collected	49402	48368	53411
No. of indep. rflns. / R_{int}	7713/0.0628	8198/0.0249	9291/0.0488
No. of obsd. rflns. [$I_0 > 2\sigma(I_0)$]	6995	8153	7919
Data / restraints / parameters	7713/0/514	8198/18/529	9291/1422/606
R_1 / wR_2 [$I_0 > 2\sigma(I_0)$][a]	0.0279/0.0771	0.0308/0.0777	0.0475/0.1065
R_1 / wR_2 (all data)[a]	0.0319/0.0803	0.0310/0.0779	0.0589/0.1107
GOF (on F^2)[a]	1.033	1.013	1.047
Largest diff. peak and hole ($e \cdot Å^{-3}$)	0.831/–1.236	1.258/–1.740	2.225/–1.263
CCDC No.	1457076	1457074	1457075

Table S4. Crystallographic data for **7d[BPh$_4$]**·2CH_2Cl_2, **7e[BPh$_4$]**·2CH_2Cl_2.

	7d[BPh$_4$]·2CH_2Cl_2	**7e[BPh$_4$]**·2CH_2Cl_2
Formula	$C_{61}H_{67}Rh_2S_2BCl_4$	$C_{60}H_{64}Rh_2S_2BCl_5$
Formula weight	1222.70	1243.11
Crystal dimensions (mm^3)	0.42 × 0.32× 0.30	0.40 × 0.31 × 0.29
Crystal system	Triclinic	Triclinic
Space group	P–1	P–1
a (Å)	11.8737(5)	11.8882(4)
b (Å)	13.8883(6)	13.8454(5)
c (Å)	17.6708(8)	17.6084(6)
α (deg)	88.3611(14)	88.5777(13)
β (deg)	76.5046(13)	76.6031(12)
γ (deg)	80.2492(13)	79.8761(12)
Volume ($Å^3$)	2792.4(2)	2775.14(17)
Z	2	2
T (K)	100(2)	100(2)
D_{calcd} ($g \cdot cm^{-3}$)	1.454	1.488
μ (mm^{-1})	0.896	0.949
F (000)	1256	1272
No. of rflns. collected	71858	59082
No. of indep. rflns. / R_{int}	9784/0.0384	9759/0.0345
No. of obsd. rflns. [$I_0 > 2\sigma(I_0)$]	8974	8792
Data / restraints / parameters	9784/2/613	9759/423/613
R_1 / wR_2 [$I_0 > 2\sigma(I_0)$][a]	0.0317/0.0841	0.0465/0.1126
R_1 / wR_2 (all data)[a]	0.0363/0.0887	0.0527/0.1164
GOF (on F^2)[a]	1.003	1.091
Largest diff. peak and hole ($e \cdot Å^{-3}$)	1.060/–1.636	3.086/–3.536
CCDC No.	1457077	1457078

Figure S1. ORTEP diagram of **1[BF_4]**·CH_2Cl_2

Hydrogen atoms, counteranion BF_4 and one co-crystallized CH_2Cl_2 molecule are omitted for clarity (thermal ellipsoids shown at 50% probability level)

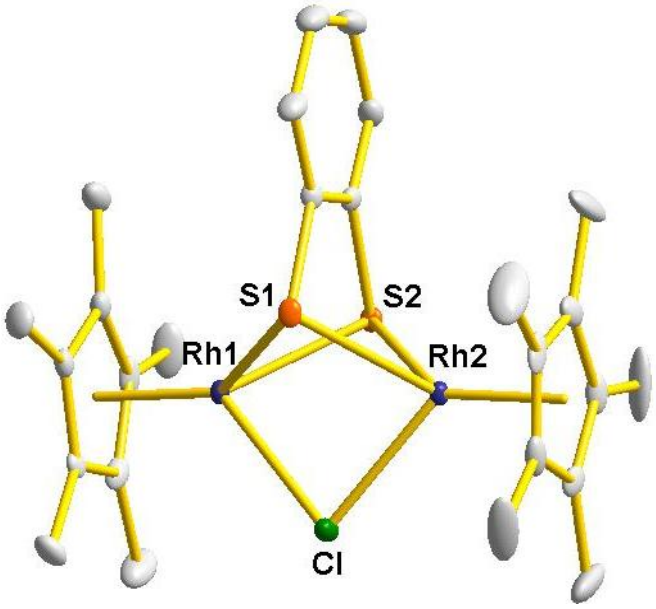

Table S5. Selected bond distances (Å) and bond angles (deg) for **1[BF_4]**·CH_2Cl_2

Distances (Å)			
Rh1–Rh2	3.1708(5)	Rh1–Cl	2.4440(11)
Rh2–Cl	2.4442(11)	Rh1–S1	2.4037(12)
Rh1–S2	2.4052(11)	Rh2–S1	2.4066(12)
Rh2–S2	2.4106(11)	Rh1–Cp*1	1.7786(3)
Rh2–Cp*2	1.7814(3)		
Angles (deg)			
Rh1–S1–Rh2	82.47(4)	Rh1–S2–Rh2	82.36(3)
S1–Rh2–Rh1	48.72(3)	S2–Rh1–Rh2	48.89(3)
S2–Rh2–Rh1	48.75(3)	S1–Rh2–S2	75.90(4)
S1–Rh1–S2	76.05(4)	S1–Rh1–Rh2	48.80(3)
Rh1–Cl–Rh2	80.88(3)		
Torsion angles (deg)			
S1–Rh1Rh2–S2	70.20(5)	Cp*1–Cp*2	2.11(24)

Figure S2. ORTEP diagram of **2**

Hydrogen atoms are omitted for clarity (thermal ellipsoids shown at 50% probability level)

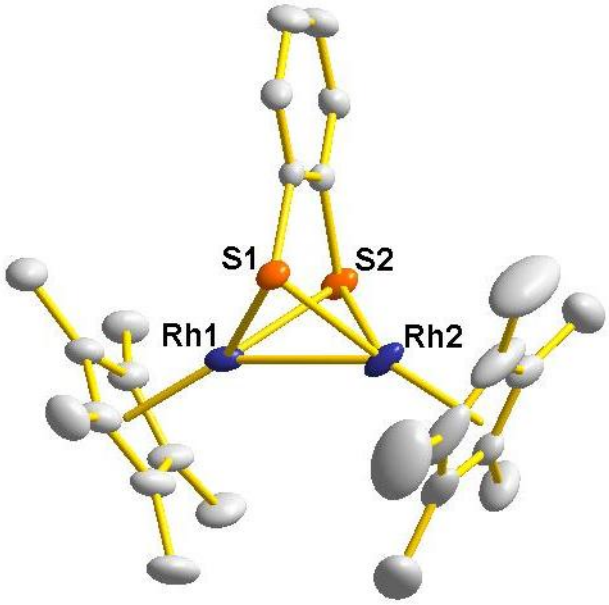

Table S6. Selected bond distances (Å) and bond angles (deg) for **2**

Distances (Å)			
Rh1–Rh2	2.6101(8)	Rh2–S1	2.3335(15)
Rh1–S1	2.3460(15)	Rh2–S2	2.3358(15)
Rh1–S2	2.3376(18)	Rh1–Cp*1	1.8266(5)
Rh2–Cp*2	1.8288(4)		
Angles (deg)			
Rh1–S1–Rh2	67.80(4)	S1–Rh1–S2	79.52(5)
S1–Rh2–S2	79.81(5)	Rh2–Rh1–S1	55.87(4)
Rh2–Rh1–S2	56.01(4)	Rh1–Rh2–S1	56.33(4)
Rh1–Rh2–S2	56.08(5)	Rh1−S2−Rh2	67.91(5)
Torsion angles (deg)			
S1–Rh1Rh2–S2	78.94(6)	Cp*1–Cp*2	59.39(26)

Figure S3. ORTEP diagram of **3[BPh_4]**

Hydrogen atoms, counteranion BPh_4 are omitted for clarity (thermal ellipsoids shown at 50% probability level)

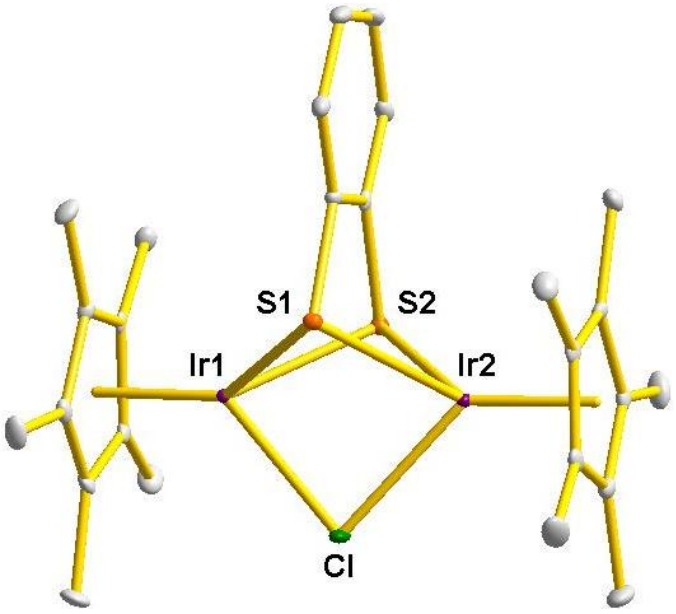

Table S7. Selected bond distances (Å) and bond angles (deg) for **3[BPh_4]**

Distances (Å)			
Ir1–Ir2	3.2956(2)	Ir1–Cl	2.4387(8)
Ir2–Cl	2.4462(8)	Ir1–S1	2.4224(8)
Ir1–S2	2.4018(8)	Ir2–S1	2.4164(8)
Ir2–S2	2.3957(8)	Ir1–Cp*1	1.7814(2)
Ir2–Cp*2	1.7829(2)		
Angles (deg)			
Ir1–S1–Ir2	85.86(3)	Ir1–S2–Ir2	86.78(11)
S1–Ir2–Ir1	47.15(2)	S2–Ir1–Ir2	46.54(2)
S2–Ir2–Ir1	46.69(2)	S1–Ir2–S2	74.62(3)
S1–Ir1–S2	74.40(3)	S1–Ir1–Ir2	47.00(2)
Ir1−Cl−Ir2	84.85(2)		
Torsion angles (deg)			
S1–Ir1Ir2–S2	63.83(4)	Cp*1–Cp*2	5.81(15)

Figure S4. ORTEP diagram of **4**

Hydrogen atoms are omitted for clarity (thermal ellipsoids shown at 50% probability level)

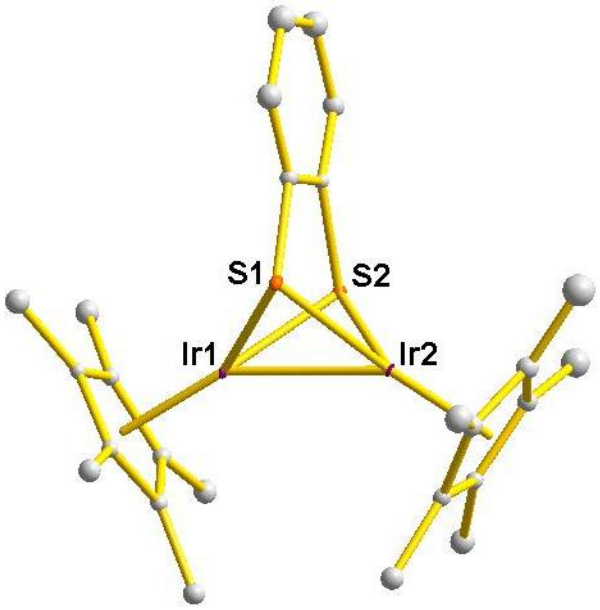

Table S8. Selected bond distances (Å) and bond angles (deg) for **4**

Distances (Å)			
Ir1–Ir2	2.6441(4)	Ir2–S1	2.3482(18)
Ir1–S1	2.3374(18)	Ir2–S2	2.3241(17)
Ir1–S2	2.3418(18)	Ir1–Cp*1	1.8165(3)
Ir2–Cp*2	1.8285(3)		
Angles (deg)			
Ir1–S1–Ir2	68.71(5)	S1–Ir1–S2	77.71(6)
S1–Ir2–S2	77.84(6)	Ir2–Ir1–S1	55.84(4)
Ir2–Ir1–S2	55.16(4)	Ir1–Ir2–S1	55.45(4)
Ir1–Ir2–S2	55.80(4)	Ir1−S2−Ir2	69.04(5)
Torsion angles (deg)			
S1–Ir1Ir2–S2	80.86(7)	Cp*1–Cp*2	66.24(30)

Figure S5. ORTEP diagram of **5[PF_6]**

Hydrogen atoms except for the bridging hydride, counteranion PF_6 are omitted for clarity (thermal ellipsoids shown at 50% probability level)

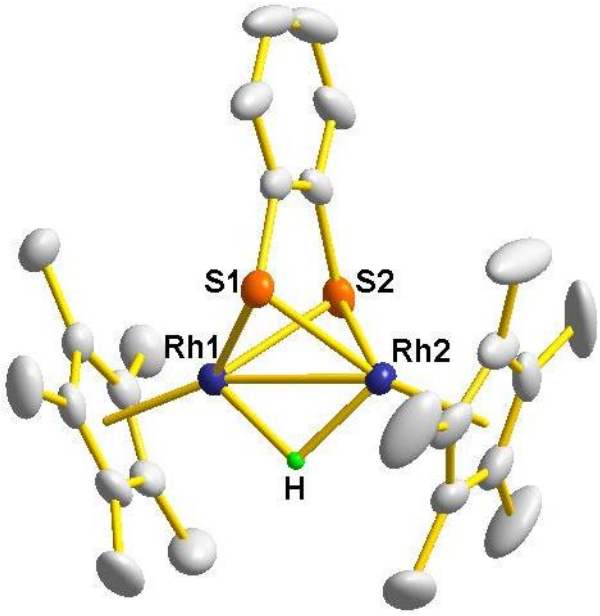

Table S9. Selected bond distances (Å) and bond angles (deg) for **5[PF_6]**

Distances (Å)			
Rh1–Rh2	2.6924(4)	Rh1–H	1.79(5)
Rh2–H	1.82(4)	Rh1–S1	2.3754(10)
Rh1–S2	2.3774(10)	Rh2–S1	2.3777(9)
Rh2–S2	2.3655(10)	Rh1–Cp*1	1.7973(3)
Rh2–Cp*2	1.7909(3)		
Angles (deg)			
Rh1–S1–Rh2	69.01(3)	Rh1–S2–Rh2	69.18(3)
S1–Rh2–Rh1	55.46(2)	S2–Rh1–Rh2	55.20(2)
S2–Rh2–Rh1	55.62(2)	S1–Rh2–S2	78.10(3)
S1–Rh1–S2	77.91(3)	S1–Rh1–Rh2	55.54(2)
Torsion angles (deg)			
S1–Rh1Rh2–S2	80.35(3)	Cp*1–Cp*2	40.87(18)

Figure S6. ORTEP diagram of **6[BF_4]**

Hydrogen atoms except for the bridging hydride, counteranion BF_4 are omitted for clarity (thermal ellipsoids shown at 50% probability level)

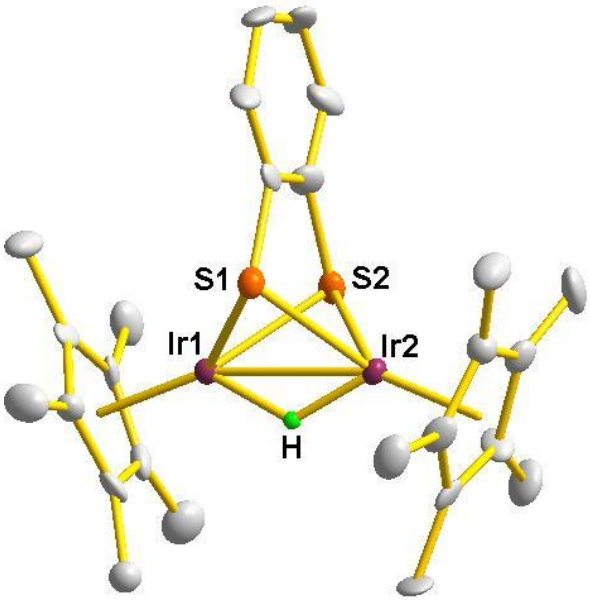

Table S10. Selected bond distances (Å) and bond angles (deg) for **6[BF_4]**

Distances (Å)			
Ir1–Ir2	2.7256(9)	Ir1–H	1.60(12)
Ir2–H	1.49(12)	Ir1–S1	2.391(3)
Ir1–S2	2.390(3)	Ir2–S1	2.390(3)
Ir2–S2	2.388(3)	Ir1–Cp*1	1.7943(7)
Ir2–Cp*2	1.8007(7)		
Angles (deg)			
Ir1–S1–Ir2	69.52(7)	Ir1–S2–Ir2	69.57(7)
S1–Ir2–Ir1	55.25(7)	S2–Ir1–Ir2	55.19(7)
S2–Ir2–Ir1	55.24(7)	S1–Ir2–S2	77.23(9)
S1–Ir1–S2	77.19(10)	S1–Ir1–Ir2	55.23(7)
Torsion angles (deg)			
S1–Ir1Ir2–S2	81.14(8)	Cp*1–Cp*2	39.85(42)

Figure S7. ORTEP diagram of **7a[BPh_4]**

Hydrogen atoms on carbons except for the bridging vinyl group, counteranion BPh_4 are omitted for clarity (thermal ellipsoids shown at 50% probability level)

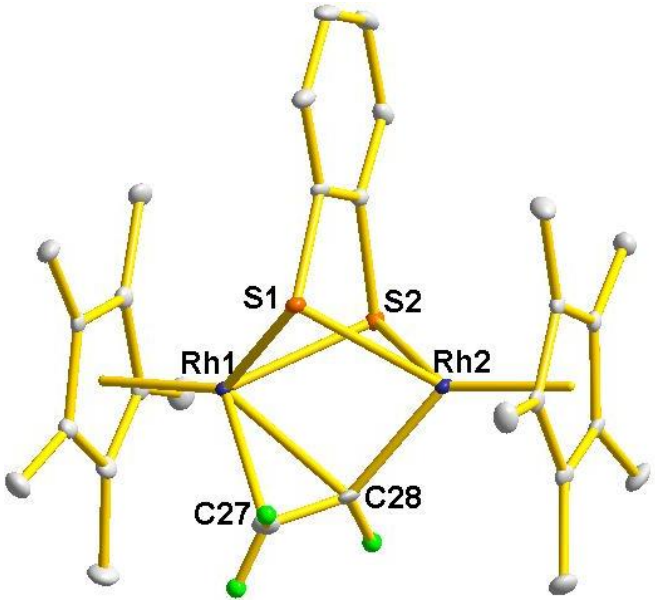

Table S11. Selected bond distances (Å) and bond angles (deg) for **7a[BPh_4]**

Distances (Å)			
Rh1–Rh2	3.1832(3)	Rh1–C27	2.299(2)
Rh1−C28	2.303(2)	Rh2–C28	2.047(2)
Rh1–S1	2.3895(6)	Rh1–S2	2.4007(6)
Rh2–S1	2.4047(6)	Rh2–S2	2.3805(6)
Rh1–Cp*1	1.8137(2)	Rh2–Cp*2	1.8177(2)
C27–C28	1.358(4)		
Angles (deg)			
Rh1–S1–Rh2	83.21(2)	Rh1–S2–Rh2	83.48(2)
S1–Rh2–Rh1	48.19(1)	S2–Rh1–Rh2	47.99(1)
S2–Rh2–Rh1	48.53(1)	S1–Rh2–S2	75.88(2)
S1–Rh1–S2	75.79(2)	S1–Rh1–Rh2	48.60(1)
Torsion angles (deg)			
S1–Rh1Rh2–S2	69.30(2)	Cp*1–Cp*2	5.12(11)

Figure S8. ORTEP diagram of **7b[BPh_4]**

Hydrogen atoms on carbons except for C27 atom, counteranion BPh_4 are omitted for clarity (thermal ellipsoids shown at 50% probability level)

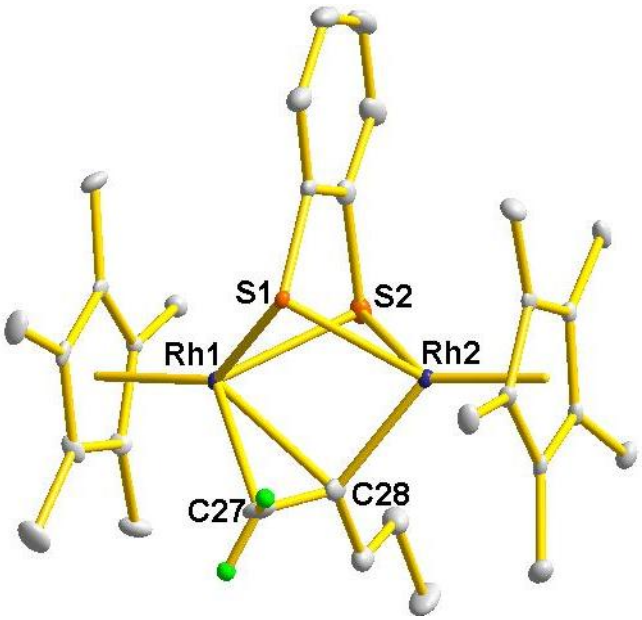

Table S12. Selected bond distances (Å) and bond angles (deg) for **7b[BPh_4]**

Distances (Å)			
Rh1–Rh2	3.1592(4)	Rh1–C27	2.299(4)
Rh1−C28	2.329(4)	Rh2–C28	2.091(4)
Rh1–S1	2.3960(9)	Rh1–S2	2.4065(11)
Rh2–S1	2.4138(9)	Rh2–S2	2.3868(11)
Rh1–Cp*1	1.8166(3)	Rh2–Cp*2	1.8152(3)
C27–C28	1.334(7)		
Angles (deg)			
Rh1–S1–Rh2	82.11(3)	Rh1–S2–Rh2	82.46(3)
S1–Rh2–Rh1	48.70(2)	S2–Rh1–Rh2	48.50(3)
S2–Rh2–Rh1	49.04(3)	S1–Rh2–S2	76.20(4)
S1–Rh1–S2	76.16(3)	S1–Rh1–Rh2	49.19(2)
Torsion angles (deg)			
S1–Rh1Rh2–S2	69.99(4)	Cp*1–Cp*2	2.10(13)

Figure S9. ORTEP diagram of **7c[BPh_4]**·CH_2Cl_2

Hydrogen atoms on carbons except for C27 atom, counteranion BPh_4 and one co-crystallized CH_2Cl_2 molecule are omitted for clarity (thermal ellipsoids shown at 50% probability level)

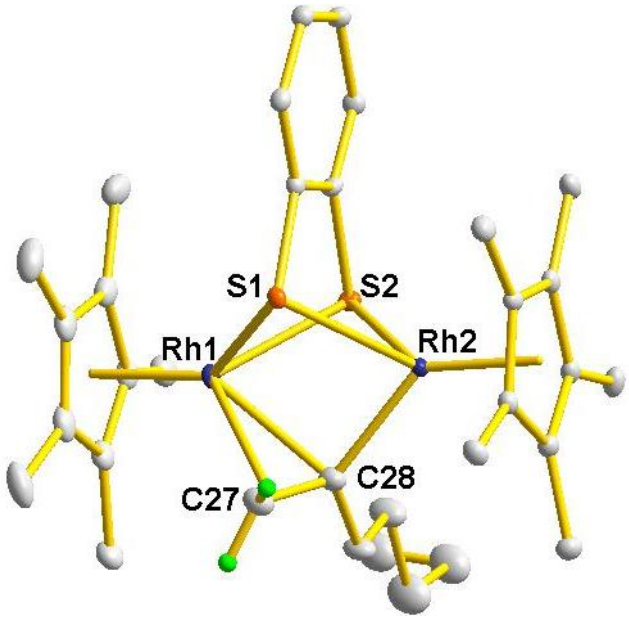

Table S13. Selected bond distances (Å) and bond angles (deg) for **7c[BPh_4]**·CH_2Cl_2

Distances (Å)			
Rh1–Rh2	3.1532(5)	Rh1–C27	2.299(5)
Rh1−C28	2.312(5)	Rh2–C28	2.084(5)
Rh1–S1	2.3641(11)	Rh1–S2	2.4131(11)
Rh2–S1	2.4006(11)	Rh2–S2	2.3951(11)
Rh1–Cp*1	1.8227(4)	Rh2–Cp*2	1.8175(3)
C27–C28	1.358(7)		
Angles (deg)			
Rh1–S1–Rh2	82.87(4)	Rh1–S2–Rh2	81.96(3)
S1–Rh2–Rh1	48.07(3)	S2–Rh1–Rh2	48.77(3)
S2–Rh2–Rh1	49.27(3)	S1–Rh2–S2	76.07(4)
S1–Rh1–S2	76.41(4)	S1–Rh1–Rh2	49.06 (3)
Torsion angles (deg)			
S1–Rh1Rh2–S2	69.73(4)	Cp*1–Cp*2	3.03(18)

Figure S10. ORTEP diagram of **7d[BPh_4]**·$2CH_2Cl_2$

Hydrogen atoms on carbons except for C27 atom, counteranion BPh_4 and two co-crystallized CH_2Cl_2 molecules are omitted for clarity (thermal ellipsoids shown at 50% probability level)

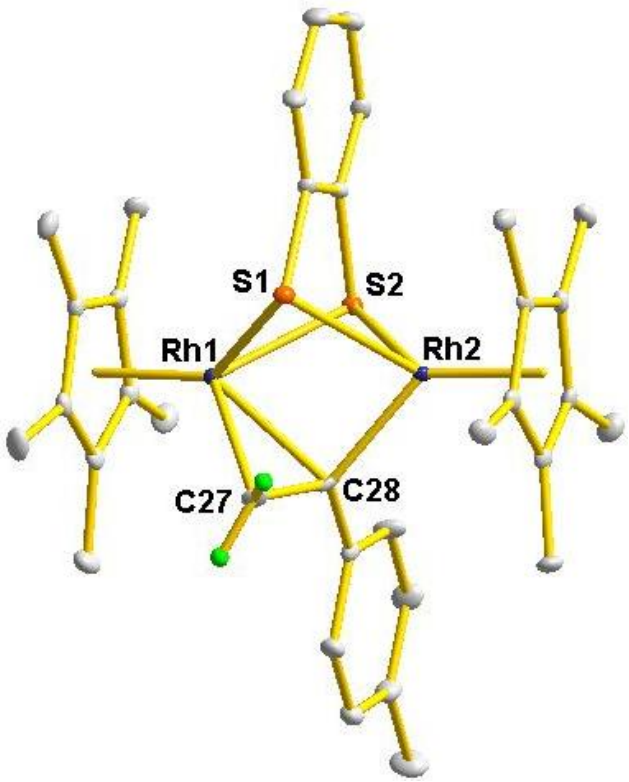

Table S14. Selected bond distances (Å) and bond angles (deg) for **7d[BPh_4]**·$2CH_2Cl_2$

Distances (Å)			
Rh1–Rh2	3.1378(3)	Rh1–C27	2.272(2)
Rh1−C28	2.311(2)	Rh2–C28	2.086(3)
Rh1–S1	2.3892(6)	Rh1–S2	2.4444(6)
Rh2–S1	2.4156(6)	Rh2–S2	2.4087(6)
Rh1–Cp*1	1.8101(4)	Rh2–Cp*2	1.8210(4)
C27–C28	1.363(4)		
Angles (deg)			
Rh1–S1–Rh2	81.54(2)	Rh1–S2–Rh2	80.56(2)
S1–Rh2–Rh1	48.87(2)	S2–Rh1–Rh2	49.22(2)
S2–Rh2–Rh1	50.22(2)	S1–Rh2–S2	76.35(2)
S1–Rh1–S2	76.16(2)	S1–Rh1–Rh2	49.59(2)
Torsion angles (deg)			
S1–Rh1Rh2–S2	71.39(2)	Cp*1–Cp*2	3.69(14)

Figure S11. ORTEP diagram of **7e[BPh_4]**·$2CH_2Cl_2$

Hydrogen atoms on carbons except for C27 atom, counteranion BPh_4 and two co-crystallized CH_2Cl_2 molecules are omitted for clarity (thermal ellipsoids shown at 50% probability level)

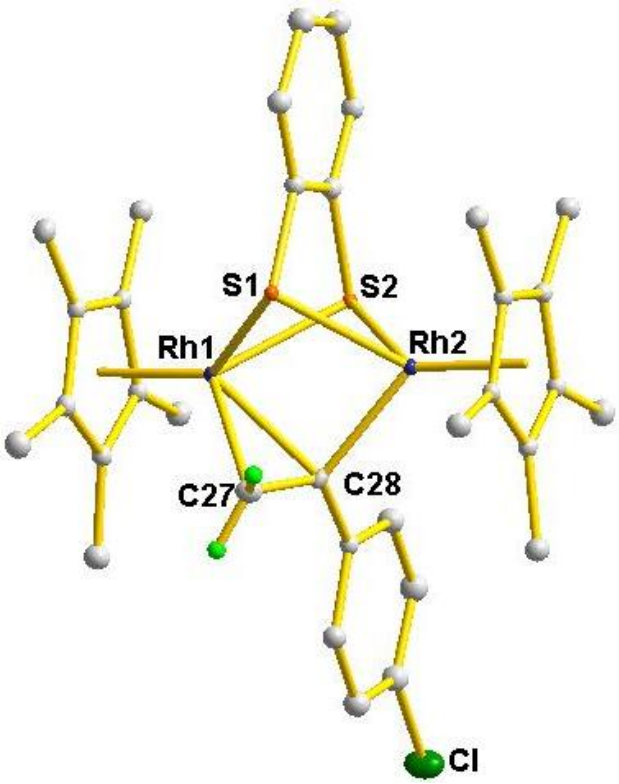

Table S15. Selected bond distances (Å) and bond angles (deg) for **7e[BPh_4]**·$2CH_2Cl_2$

Distances (Å)			
Rh1–Rh2	3.1381(5)	Rh1–C27	2.269(5)
Rh2−C28	2.133(5)	Rh1–C28	2.306(4)
Rh1–S1	2.3949(11)	Rh1–S2	2.4406(11)
Rh2–S1	2.4107(11)	Rh2–S2	2.4104(11)
Rh1–Cp*1	1.8137(3)	Rh2–Cp*2	1.8162(3)
C27–C28	1.272(7)		
Angles (deg)			
Rh1–S1–Rh2	81.54(3)	Rh1–S2–Rh2	80.61(3)
S1–Rh2–Rh1	49.01(3)	S2–Rh1–Rh2	49.27(3)
S2–Rh2–Rh1	50.11(2)	S1–Rh2–S2	76.08(4)
S1–Rh1–S2	75.81(4)	S1–Rh1–Rh2	49.45(3)
Torsion angles (deg)			
S1–Rh1Rh2–S2	71.88(4)	Cp*1–Cp*2	3.49(21)

V. NMR Spectra

Figure S12. The ^{1}H NMR spectrum of **1[BF_4]** in CD_2Cl_2

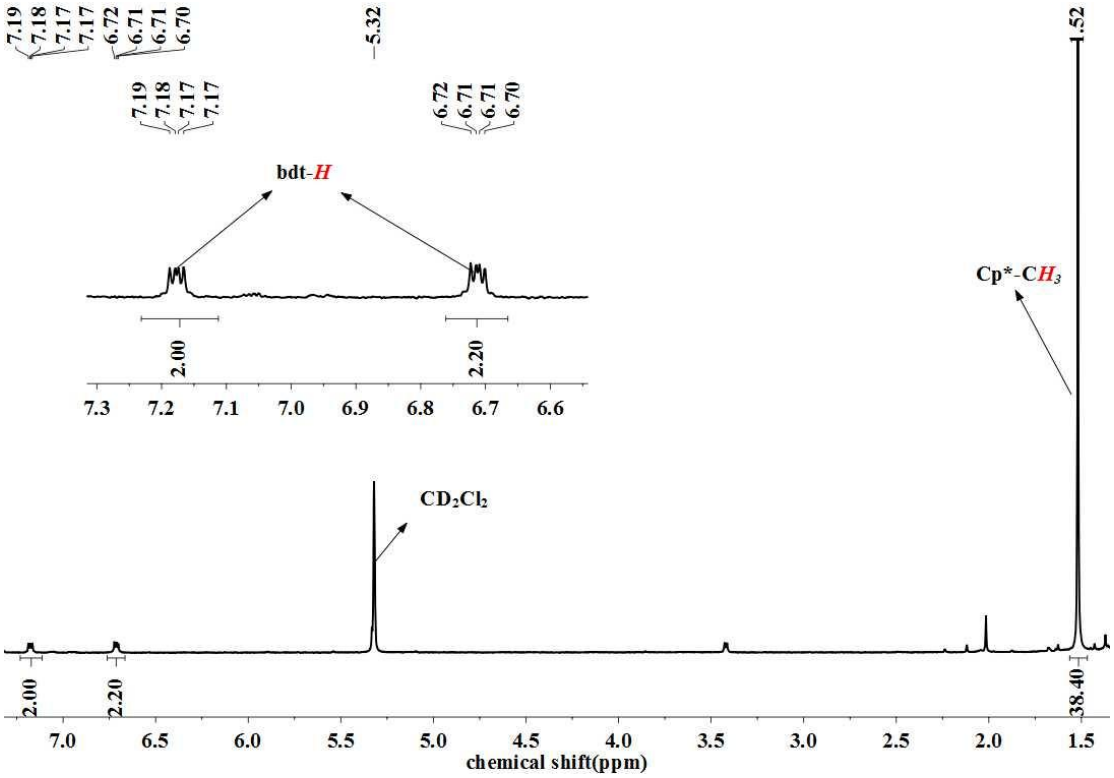

Figure S13. The ^{13}C NMR spectrum of **1[BF_4]** in CD_2Cl_2

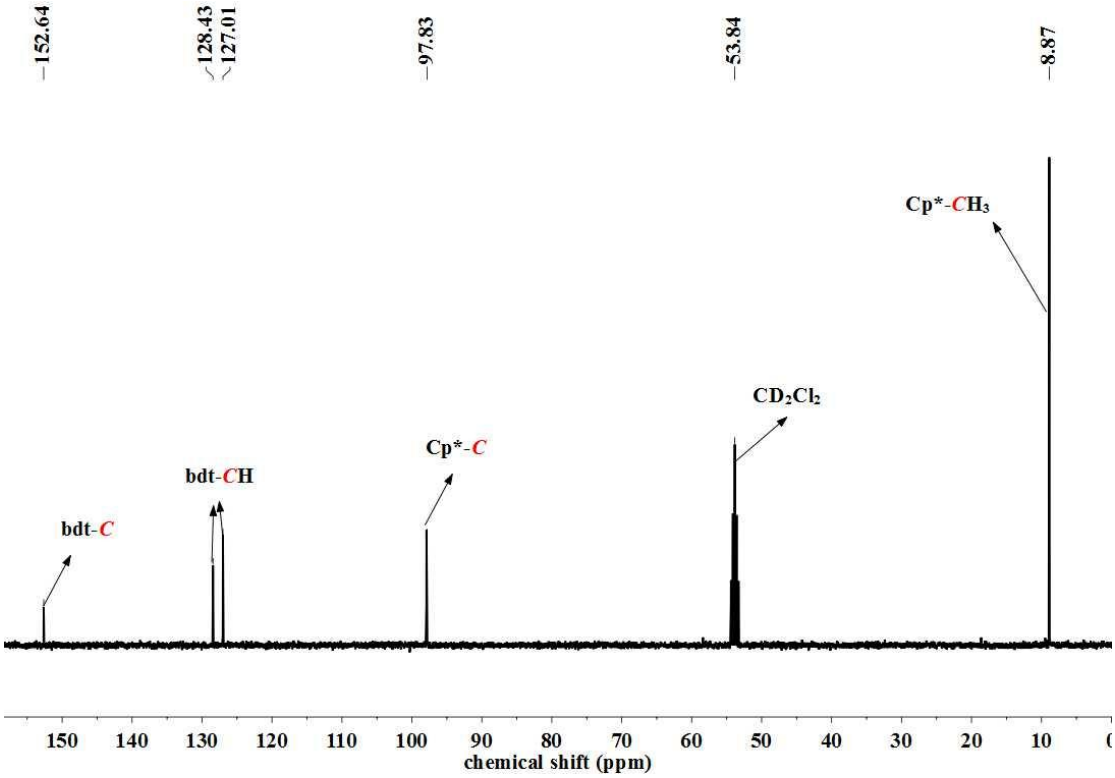

Figure S14. The ^{1}H NMR spectrum of **2** in CD_2Cl_2

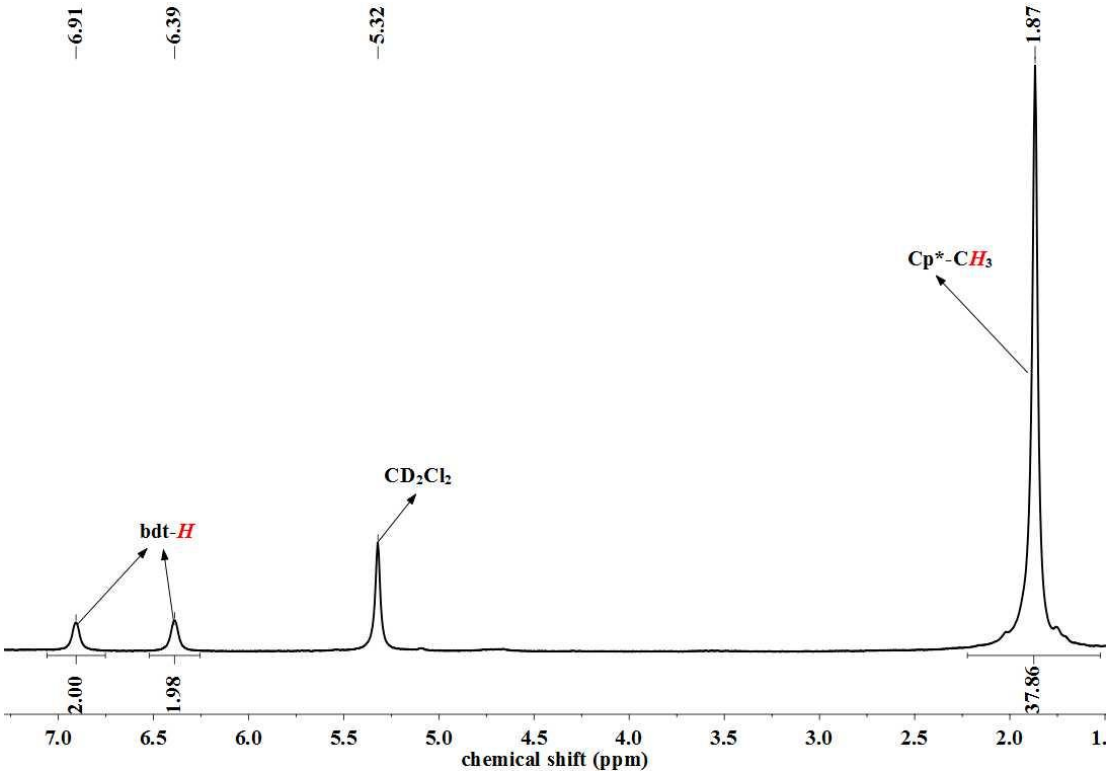

Figure S15. The ^{13}C NMR spectrum of **2** in CD_2Cl_2

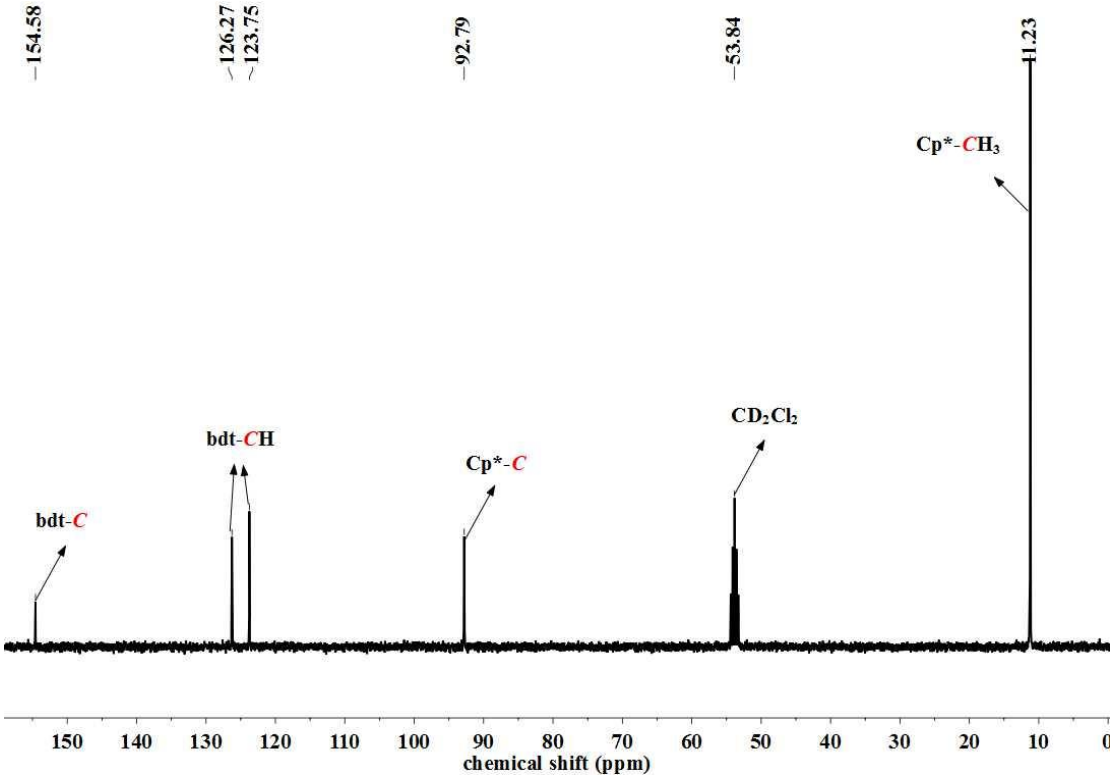

Figure S16. The ^{1}H NMR spectrum of **3[BPh$_4$]** in CD_2Cl_2

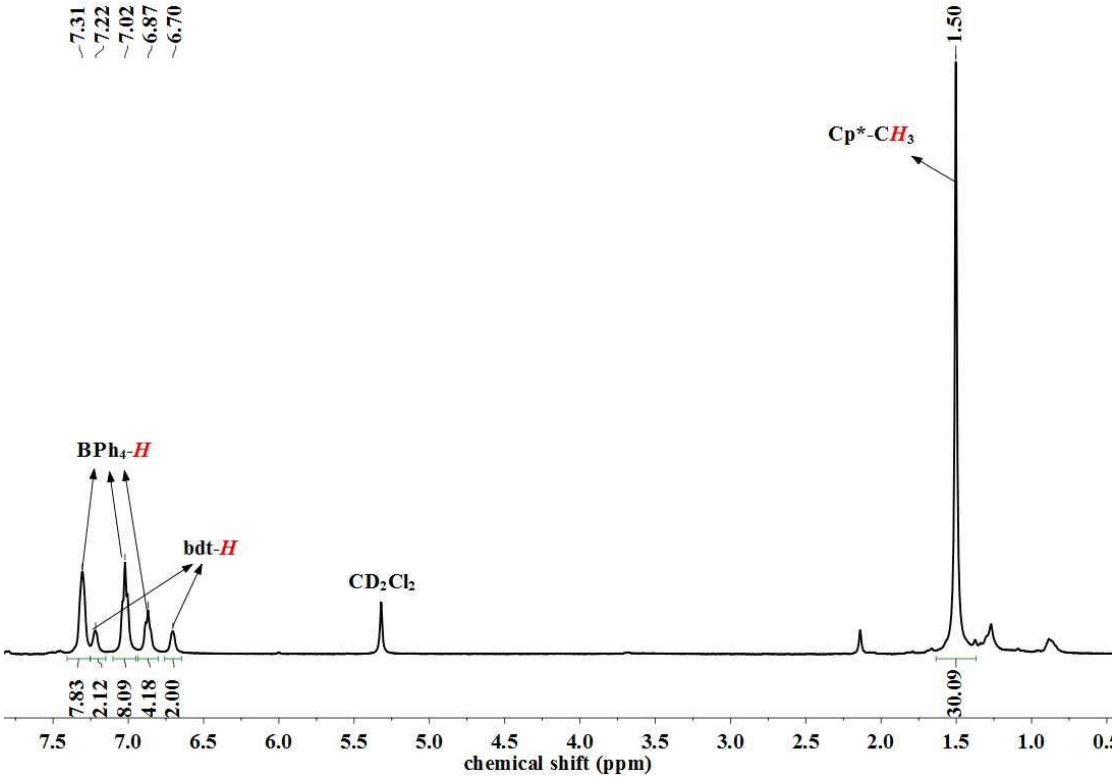

Figure S17. The ^{13}C NMR spectrum of **3[BPh$_4$]** in CD_2Cl_2

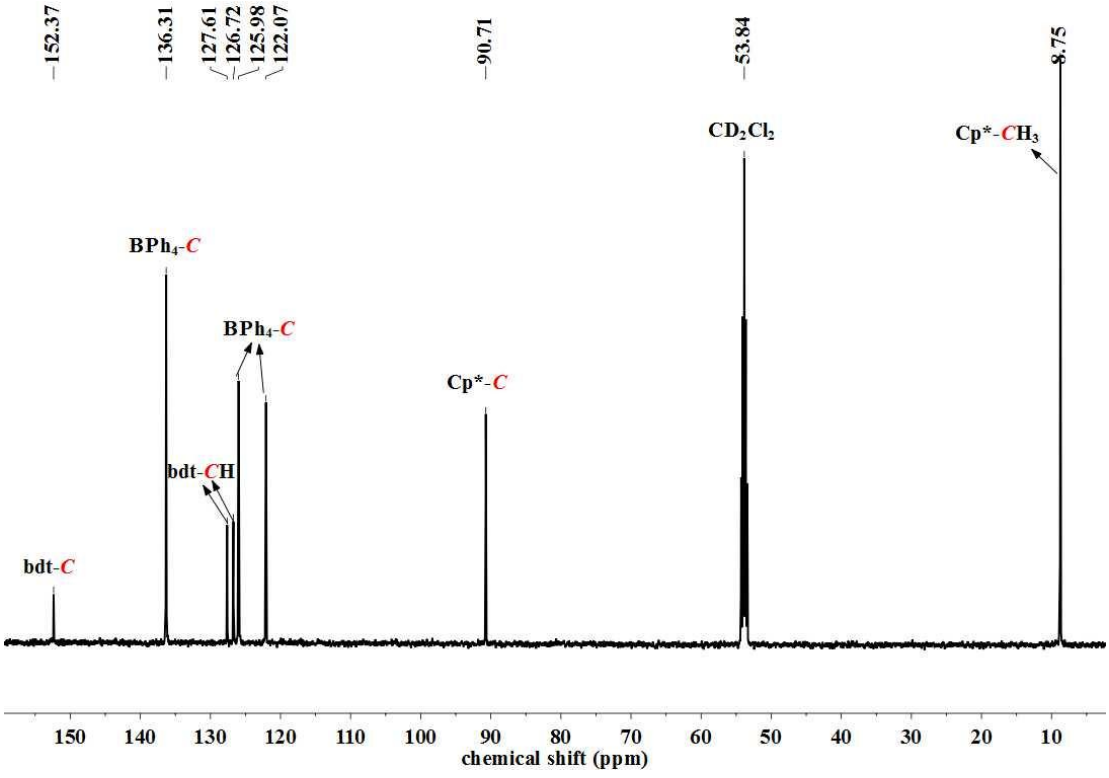

Figure S18. The ^{1}H NMR spectrum of **4** in CD_2Cl_2

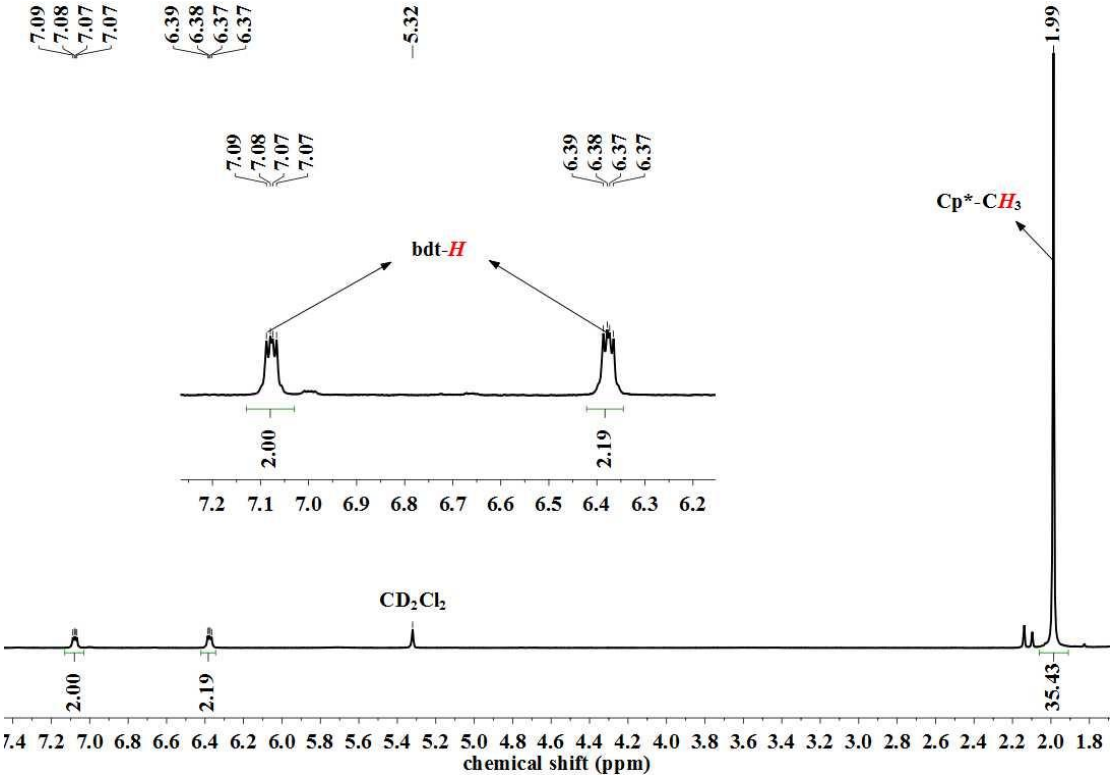

Figure S19. The ^{13}C NMR spectrum of **4** in CD_2Cl_2

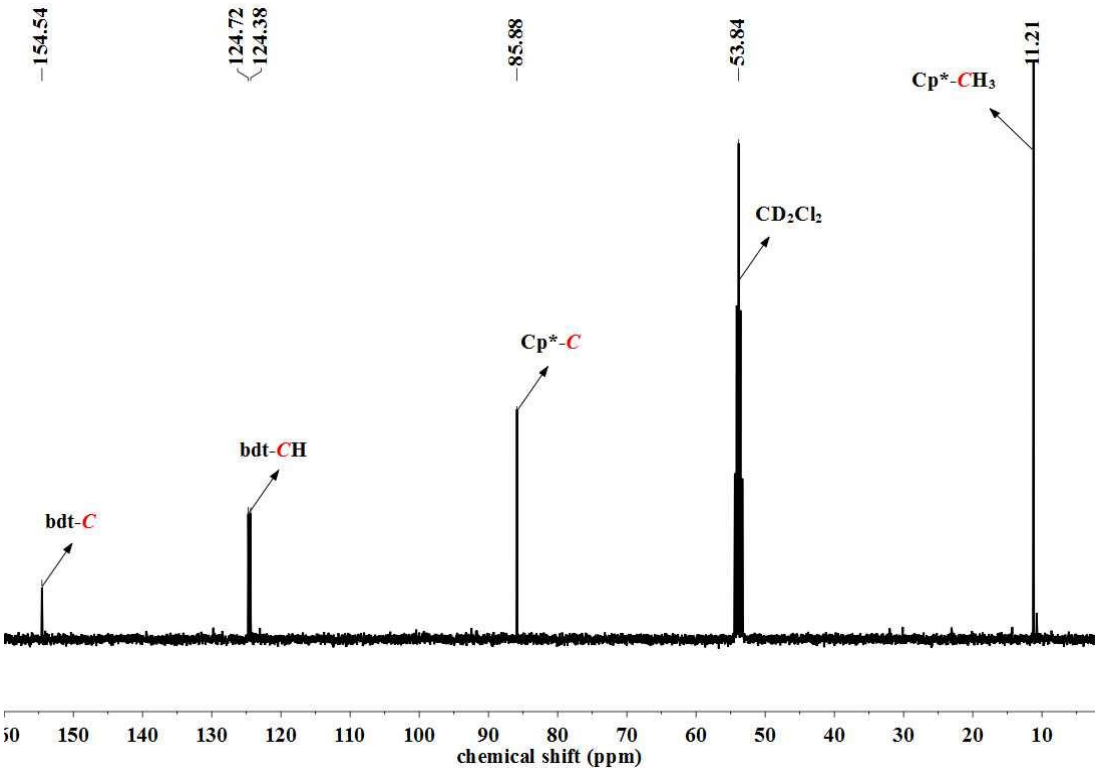

Figure S20. The ^{1}H NMR spectrum of **5[PF_6]** in CD_2Cl_2

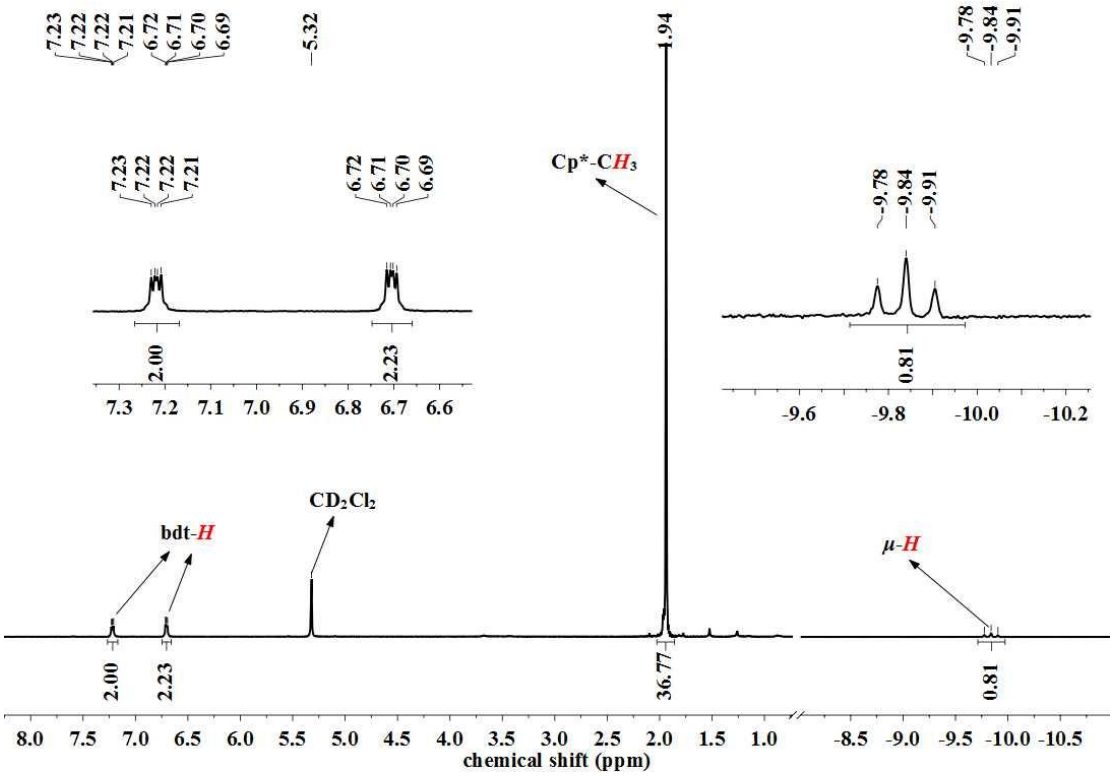

Figure S21. The ^{1}H NMR spectrum of D-**5[PF_6]** in CD_2Cl_2

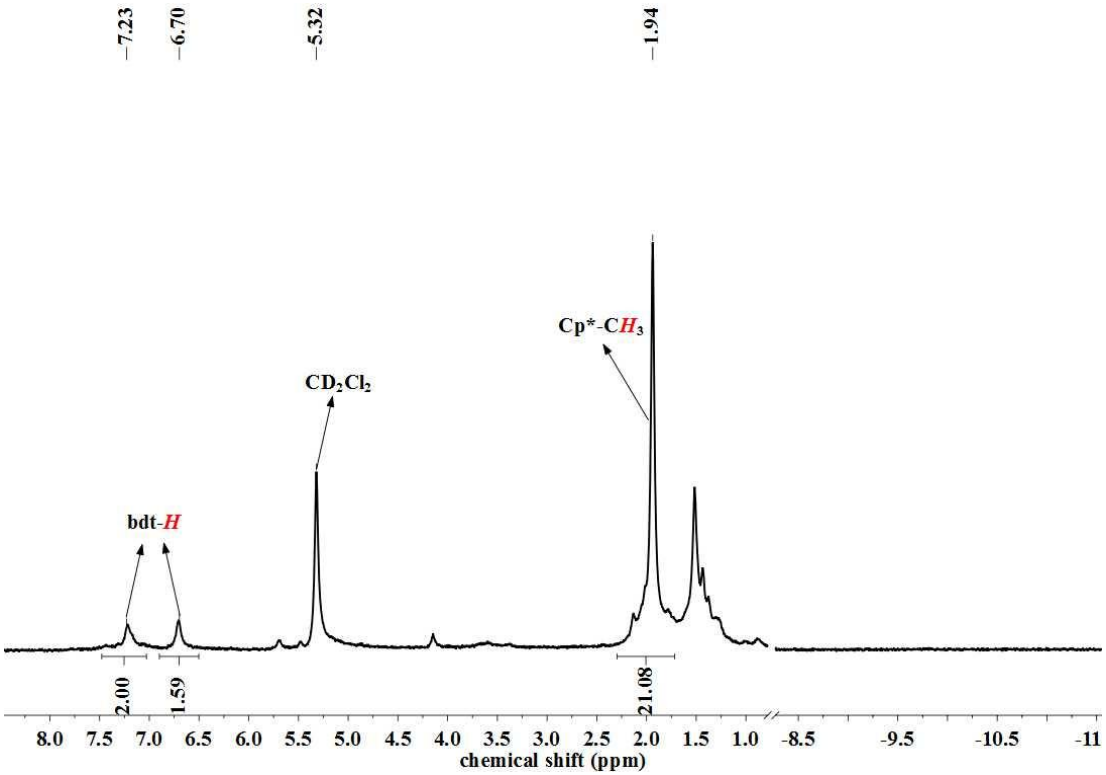

Figure S22. The ^{13}C NMR spectrum of **5[PF_6]** in CD_2Cl_2

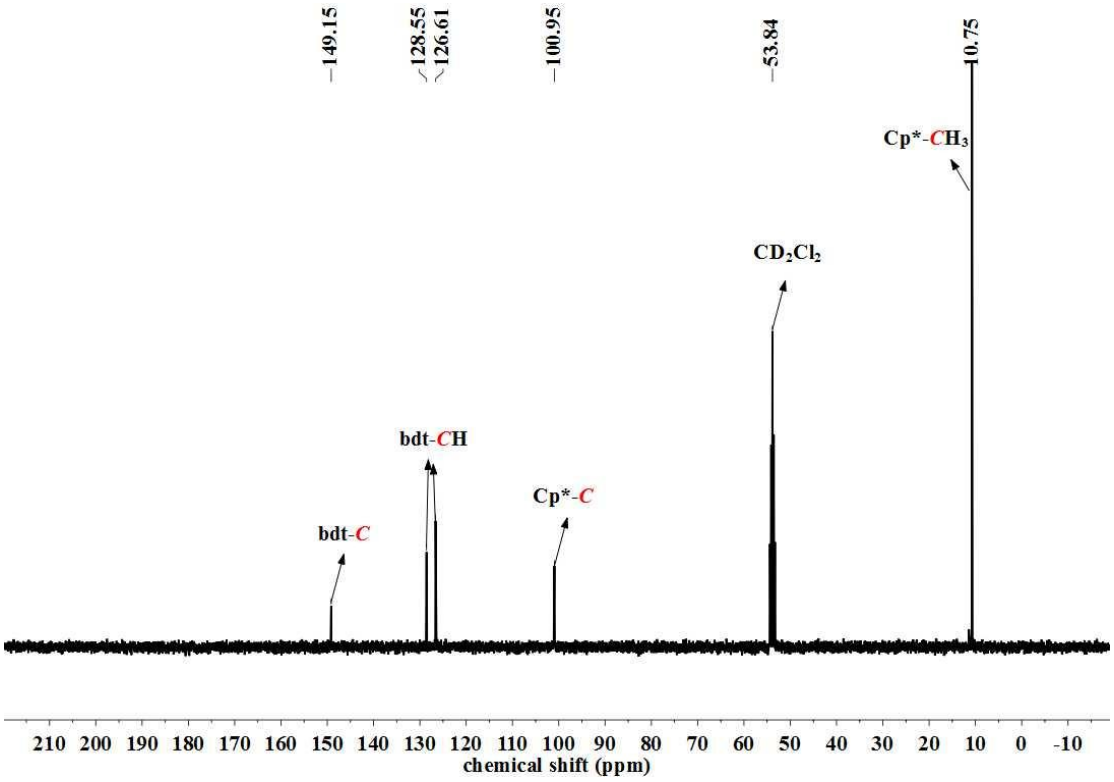

Figure S23. The ^{1}H NMR spectrum of **5[BF_4]** in CD_2Cl_2

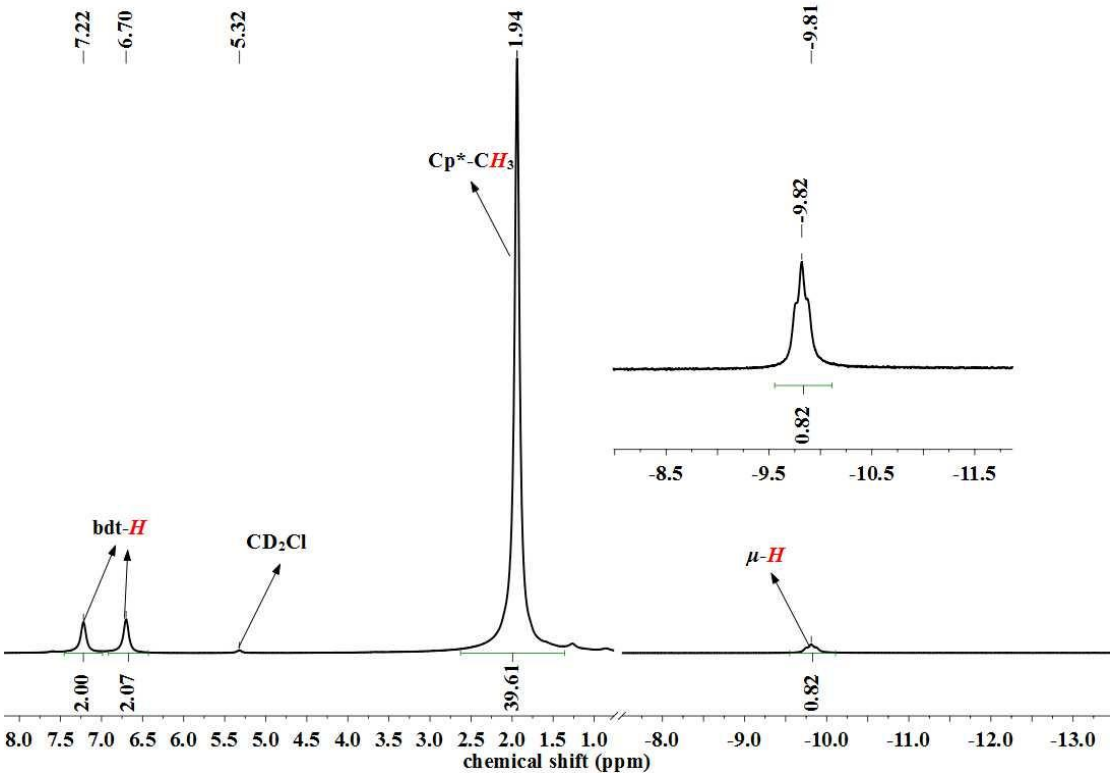

Figure S24. The ^{13}C NMR spectrum of **5[BF_4]** in CD_2Cl_2

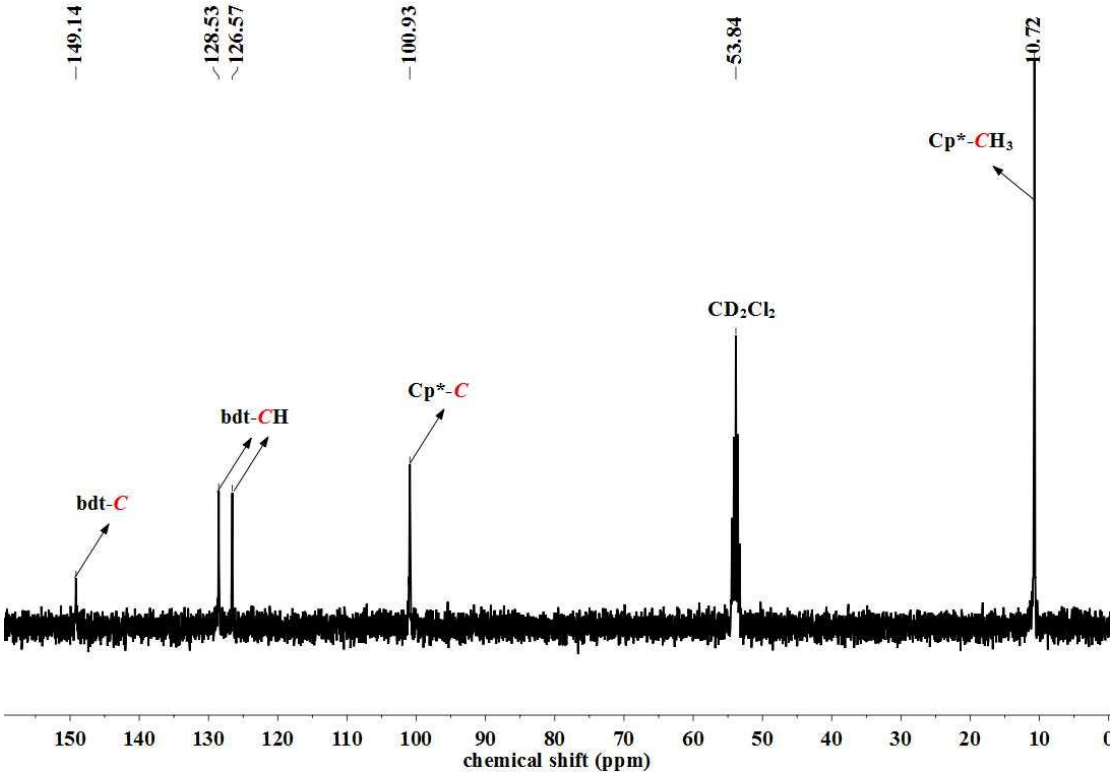

Figure S25. The ^{1}H NMR spectrum of **6[PF_6]** in CD_2Cl_2

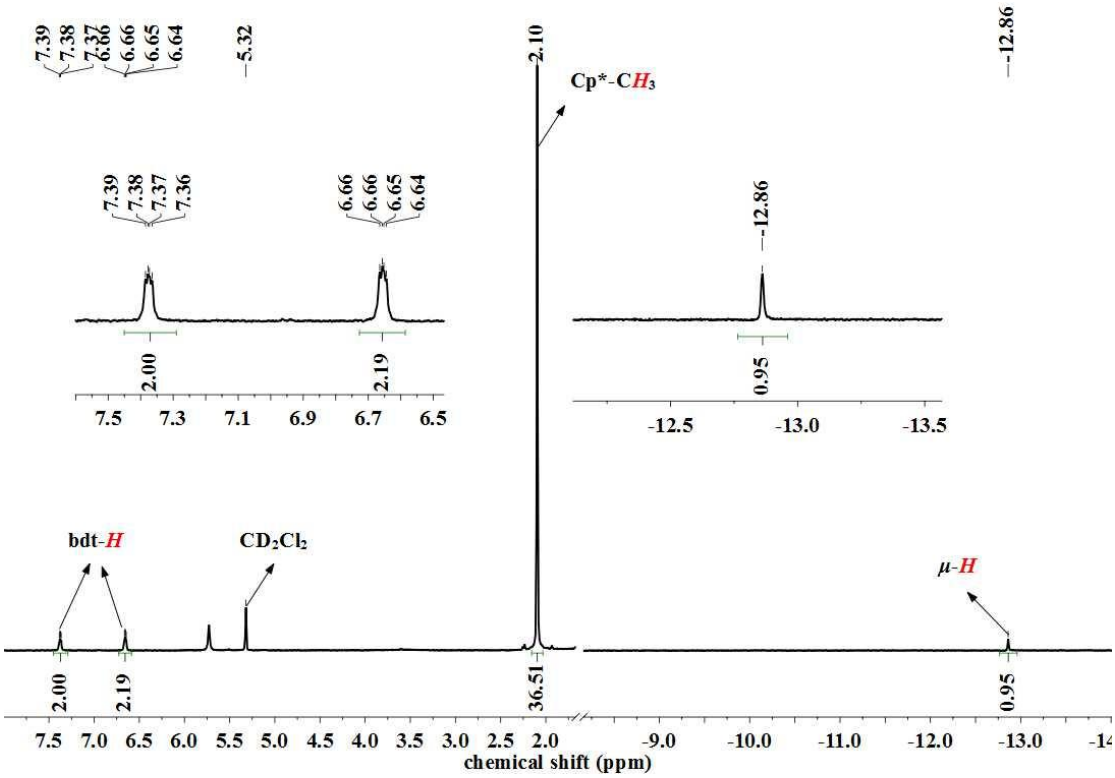

Figure S26. The ^{1}H NMR spectrum of D-**6[PF$_6$]** in CD_2Cl_2

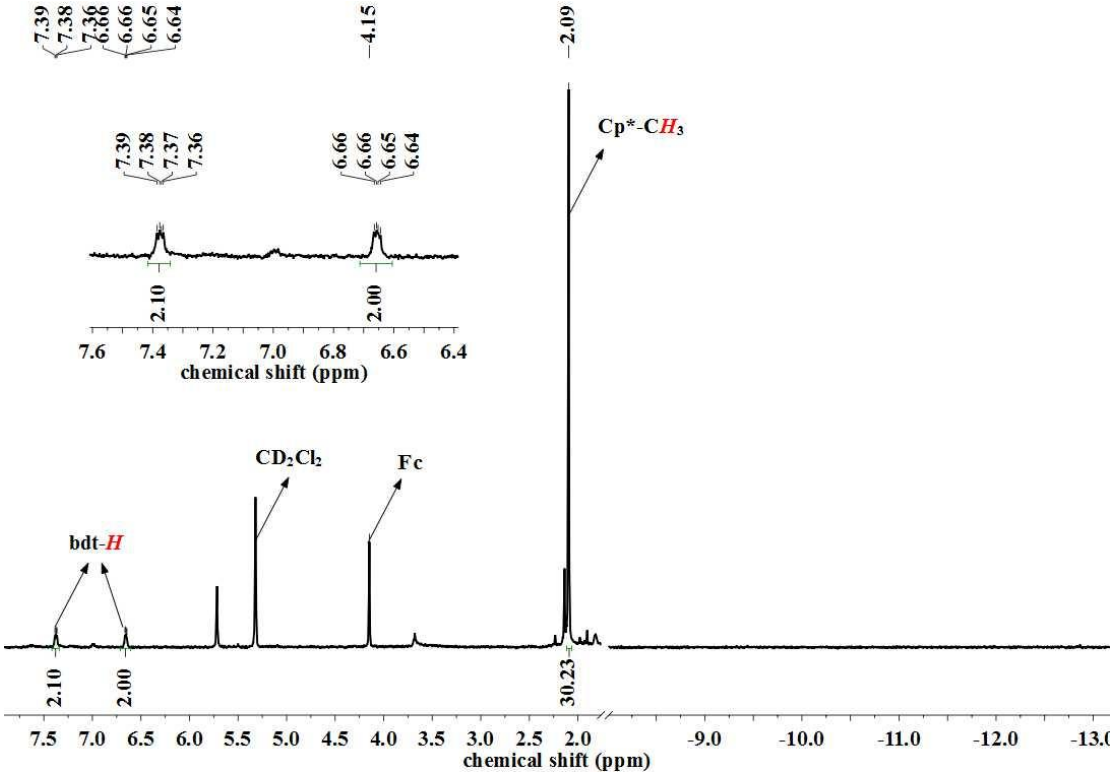

Figure S27. The ^{13}C NMR spectrum of **6[PF$_6$]** in CD_2Cl_2

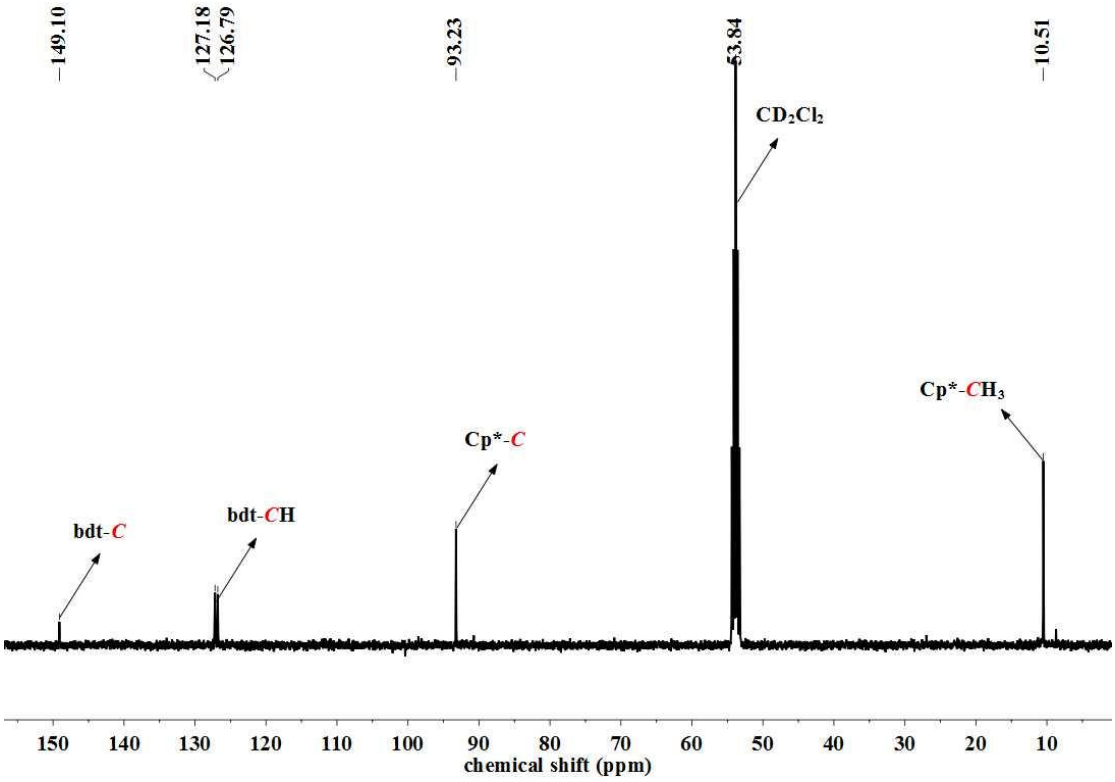

Figure S28. The ^{1}H NMR spectrum of **6[BF_4]** in CD_2Cl_2

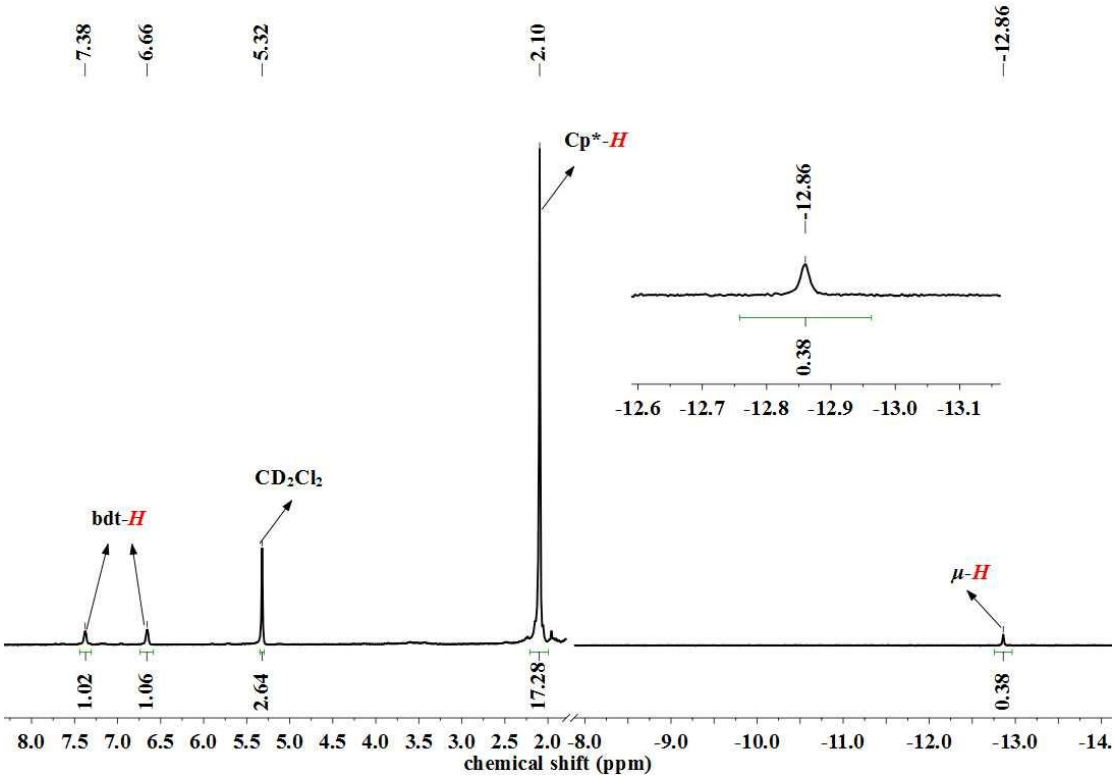

Figure S29. The ^{13}C NMR spectrum of **6[BF_4]** in CD_2Cl_2

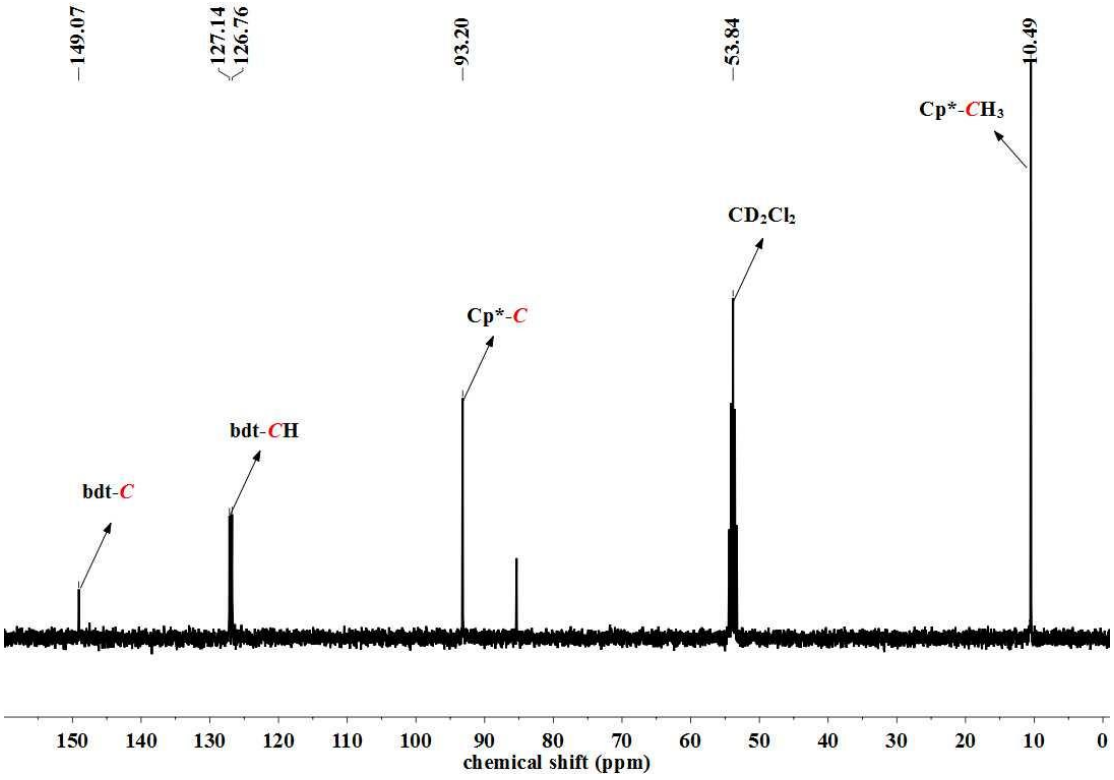

Figure S30. The ^{1}H NMR spectrum of **7a[BPh$_4$]** in CD_2Cl_2

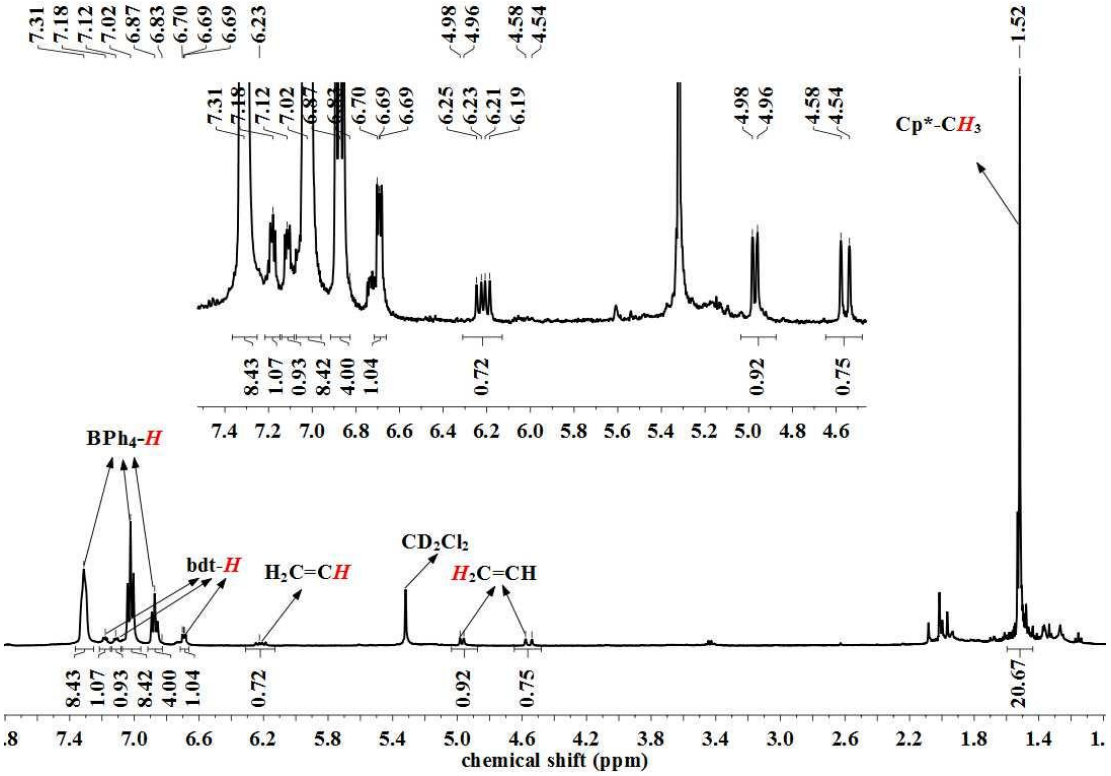

Figure S31. The ^{13}C NMR spectrum of **7a[BPh$_4$]** in CD_2Cl_2

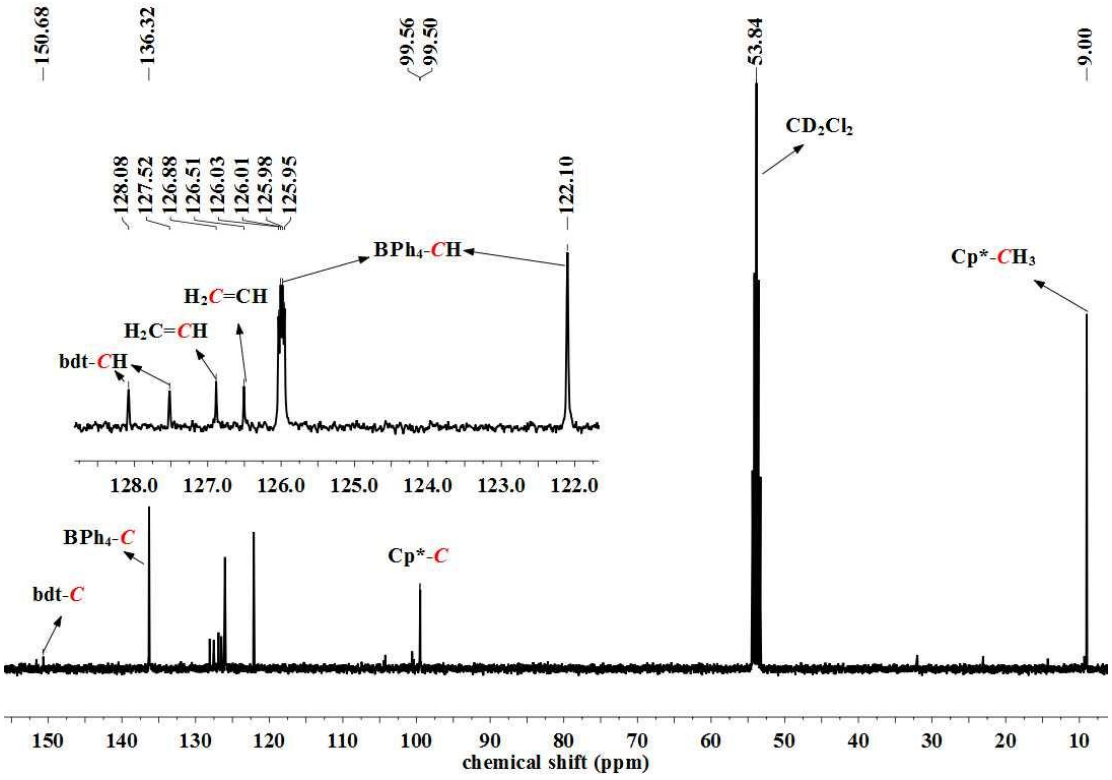

Figure S32. The ^{1}H NMR spectrum of **7b[BPh$_4$]** in CD_2Cl_2

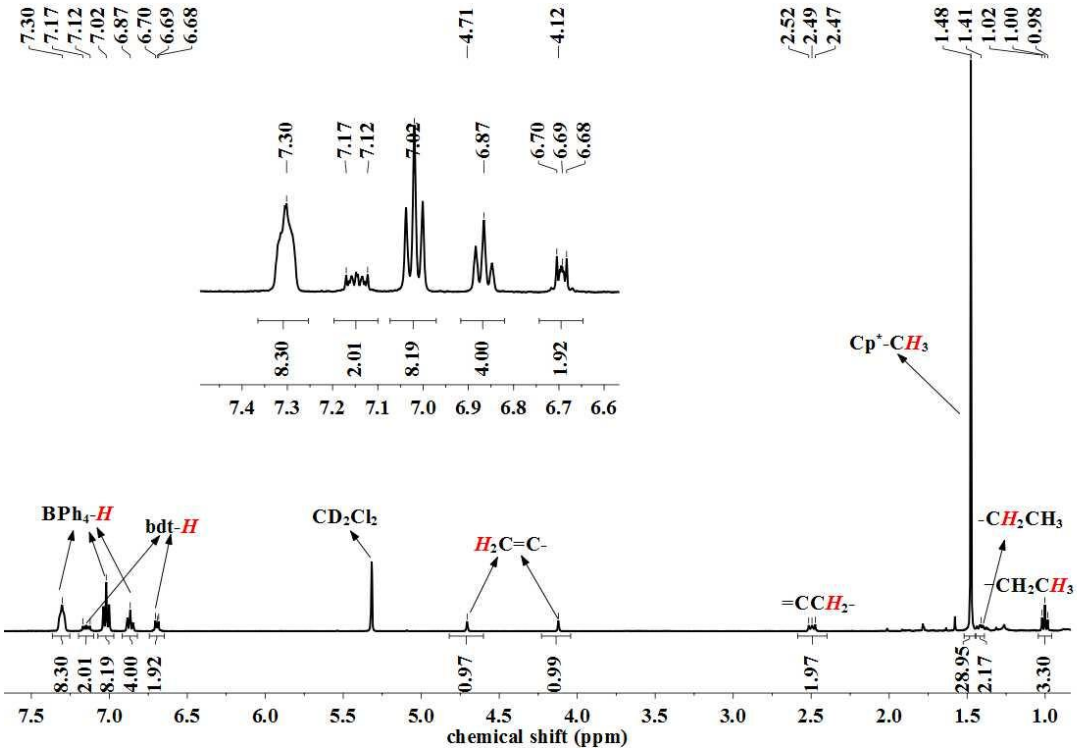

Figure S33. The ^{13}C NMR spectrum of **7b[BPh$_4$]** in CD_2Cl_2

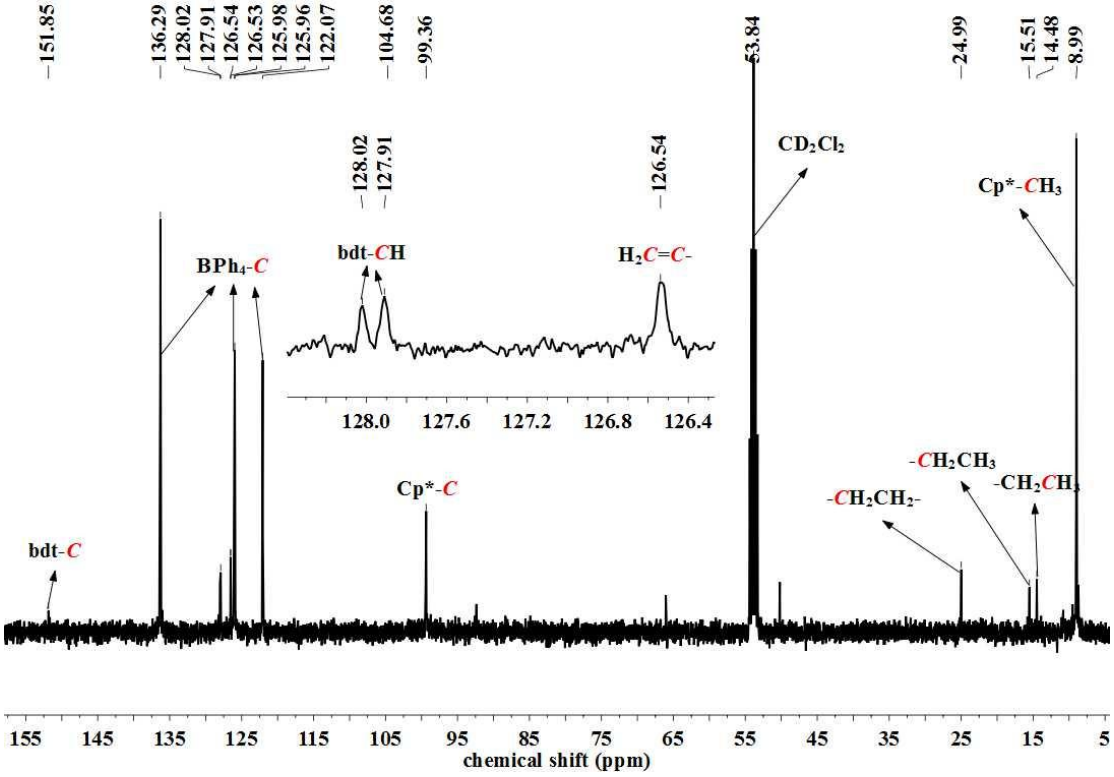

Figure S34. The ^{1}H NMR spectrum of **7c[BPh$_4$]** in CD_2Cl_2

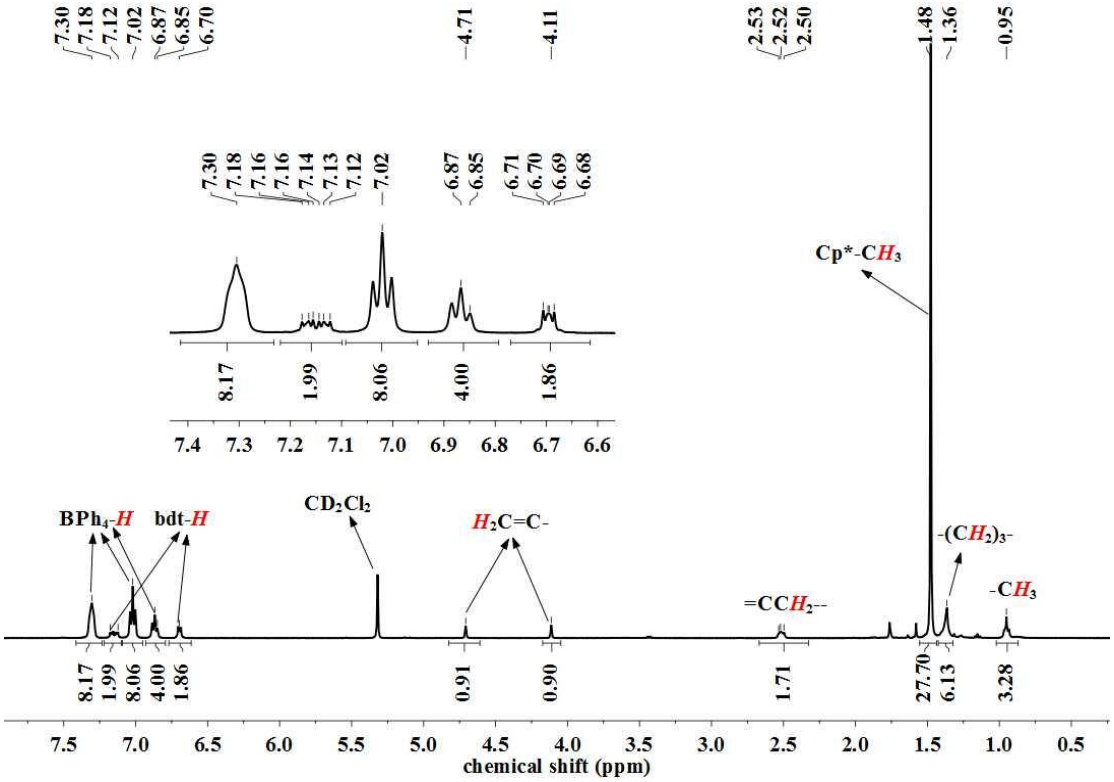

Figure S35. The ^{13}C NMR spectrum of **7c[BPh$_4$]** in CD_2Cl_2

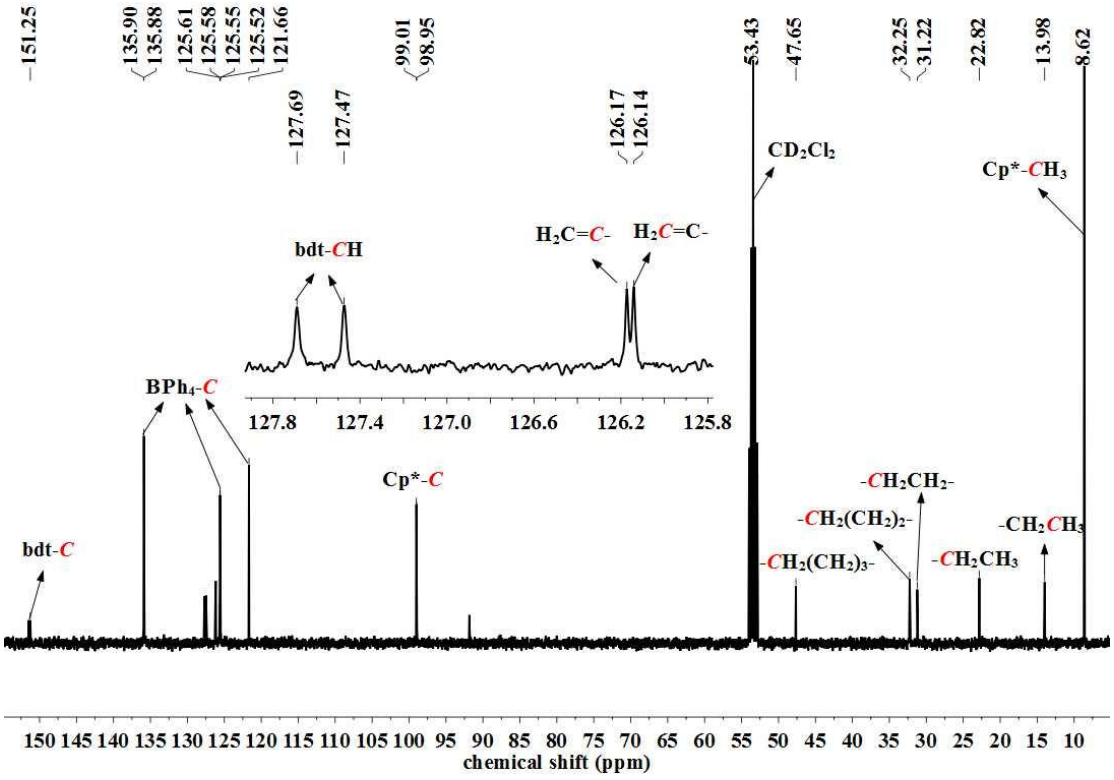

Figure S36. The ^{1}H NMR spectrum of **7d[BPh$_4$]** in CD_2Cl_2

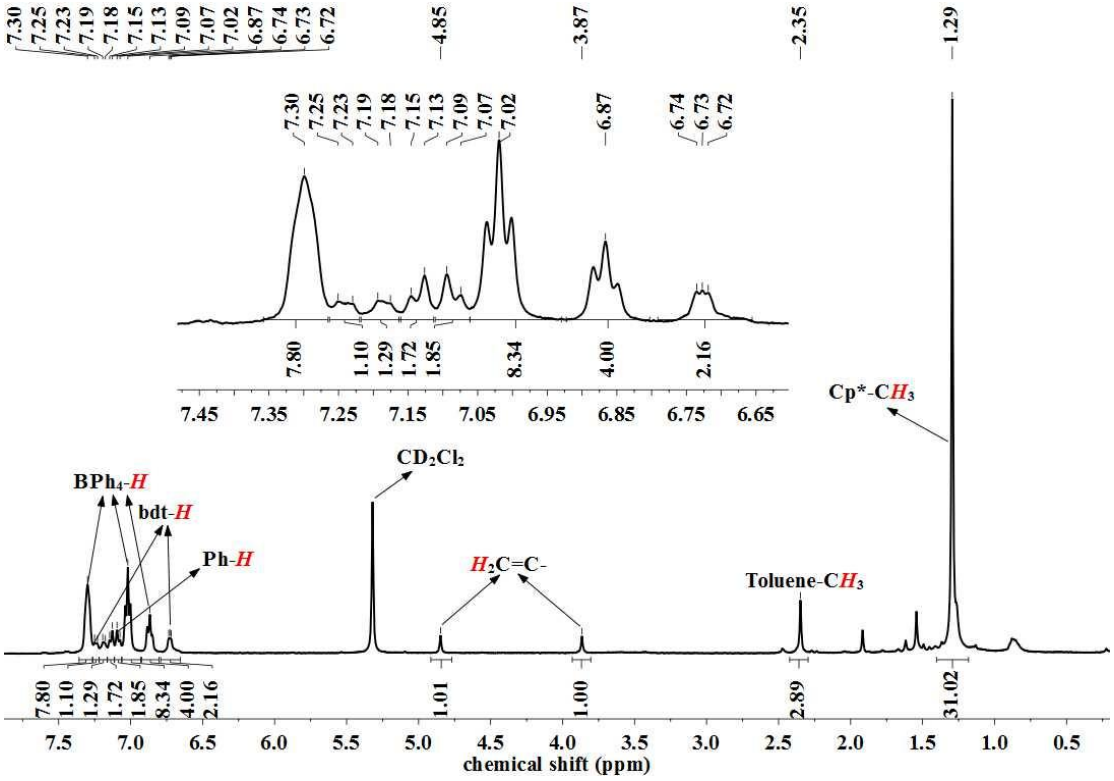

Figure S37. The ^{13}C NMR spectrum of **7d[BPh$_4$]** in CD_2Cl_2

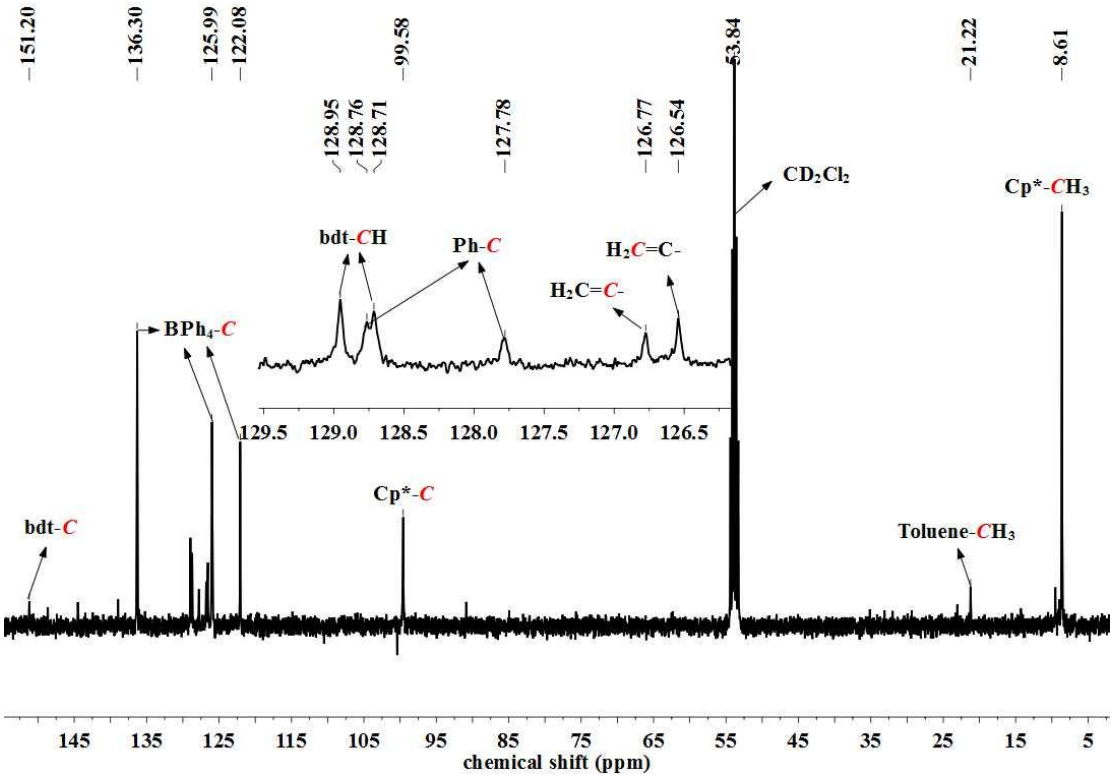

Figure S38. The ^{1}H NMR spectrum of **7e[BPh$_4$]** in CD_2Cl_2

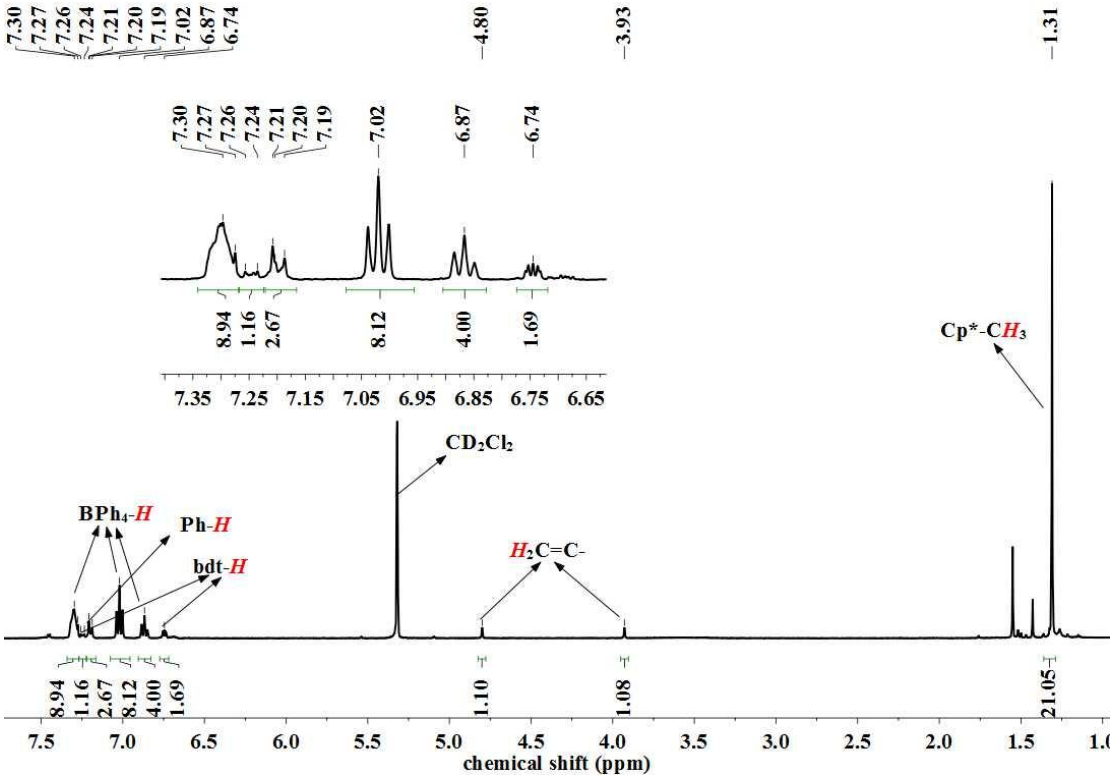

Figure S39. The ^{13}C NMR spectrum of **7e[BPh$_4$]** in CD_2Cl_2

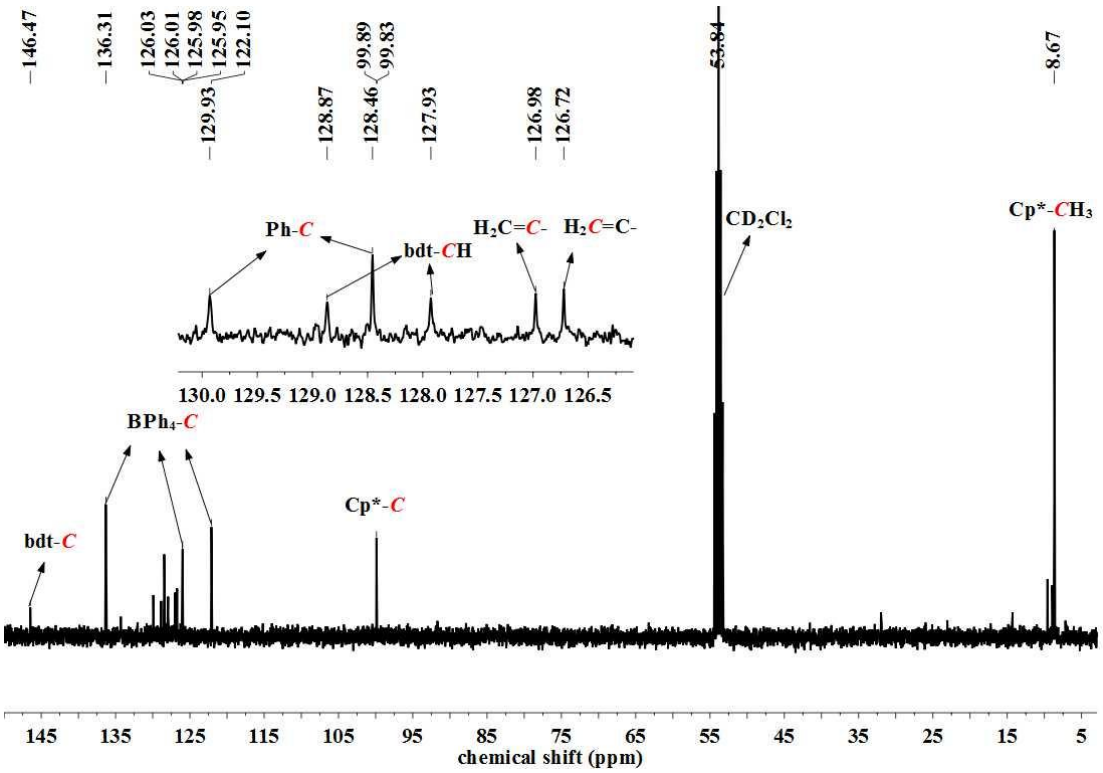

VI. ESI-HRMS

Figure S40. ESI-HRMS of **1[BF_4]** in CH_2Cl_2

(a) The signal at an m/z = 650.9912 corresponds to $[\mathbf{1}]^+$. (b) Calculated isotopic distribution for $[\mathbf{1}]^+$ (upper) and the amplifying experimental diagram for $[\mathbf{1}]^+$ (bottom).

(a)

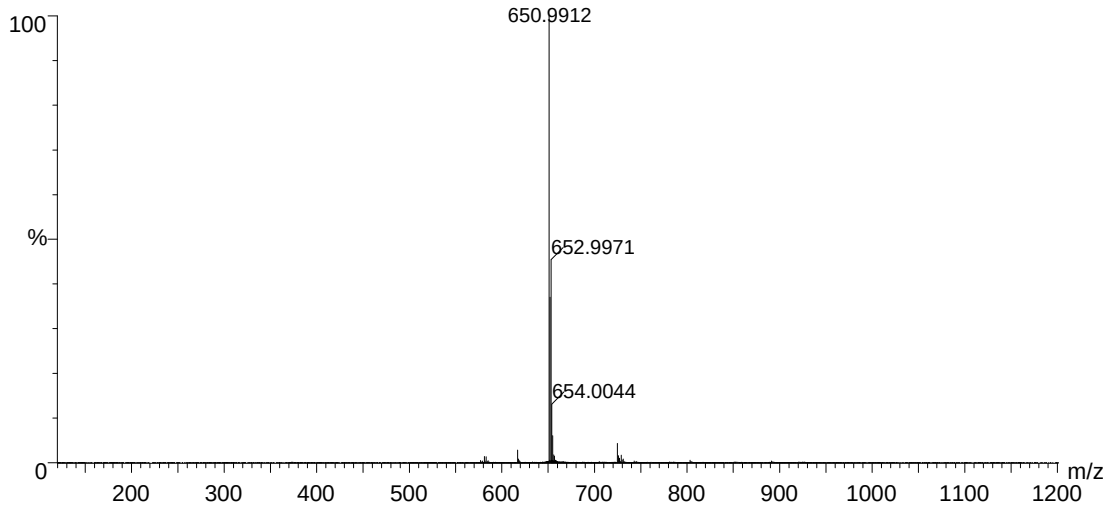

(b)

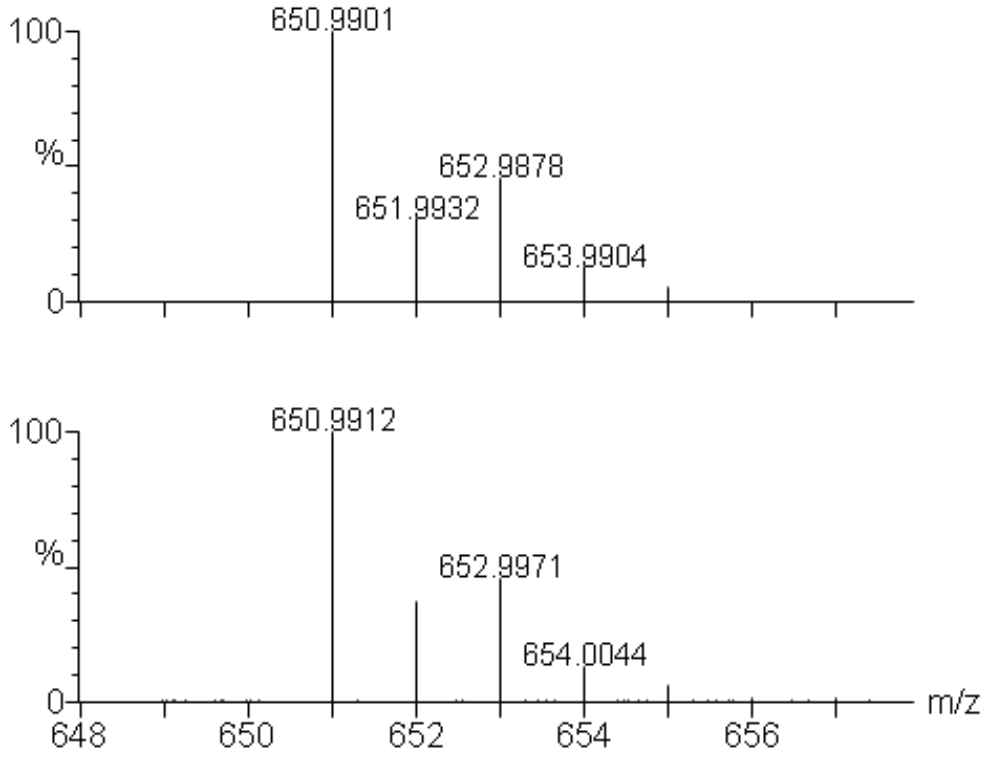

Figure S41. ESI-HRMS of **3[BPh$_4$]** in CH_2Cl_2

(a) The signal at an m/z = 831.1060 corresponds to $[\mathbf{3}]^+$. (b) Calculated isotopic distribution for $[\mathbf{3}]^+$ (upper) and the amplifying experimental diagram for $[\mathbf{3}]^+$ (bottom).

(a)

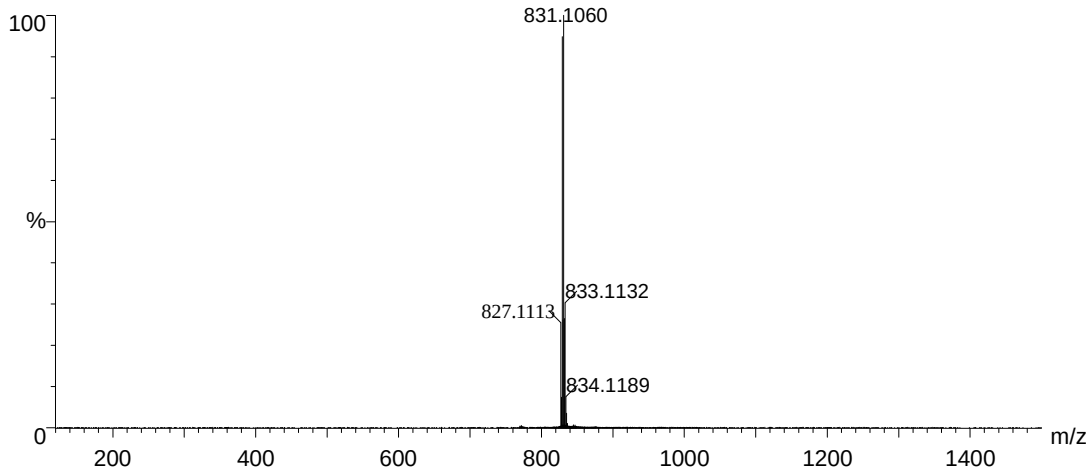

(b)

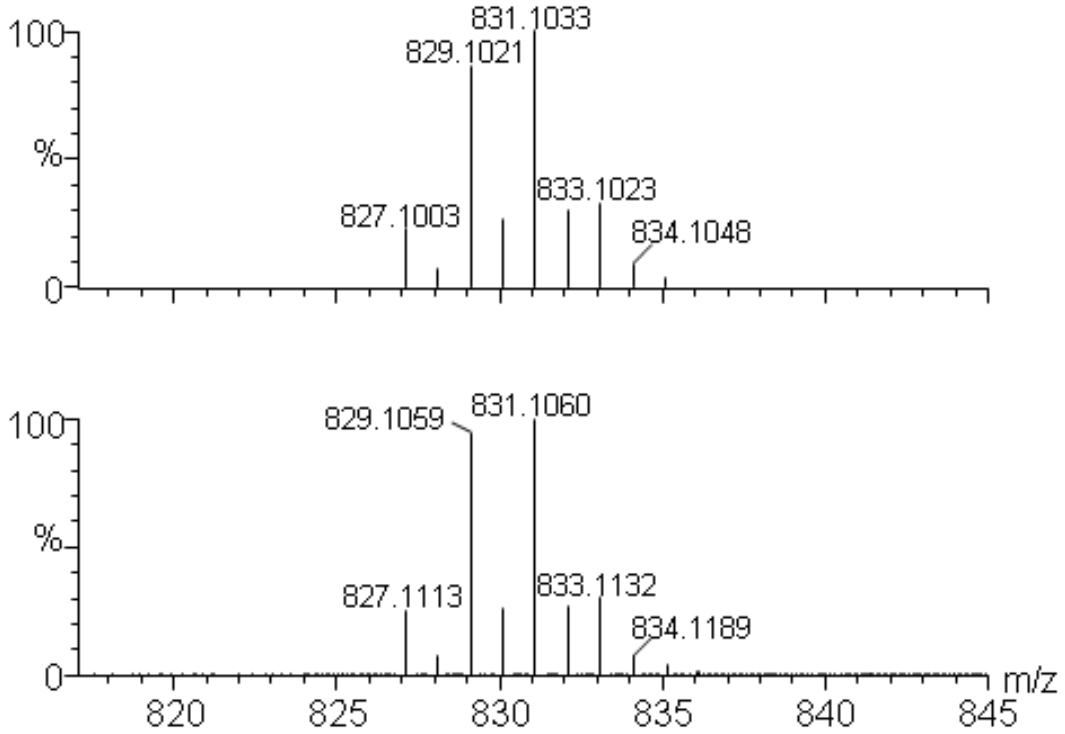

Figure S42. ESI-HRMS of **5[PF_6]** in CH_2Cl_2

(a) The signal at an m/z = 617.0285 corresponds to $[\mathbf{5}]^+$. (b) Calculated isotopic distribution for $[\mathbf{5}]^+$ (upper) and the amplifying experimental diagram for $[\mathbf{5}]^+$ (bottom).

(a)

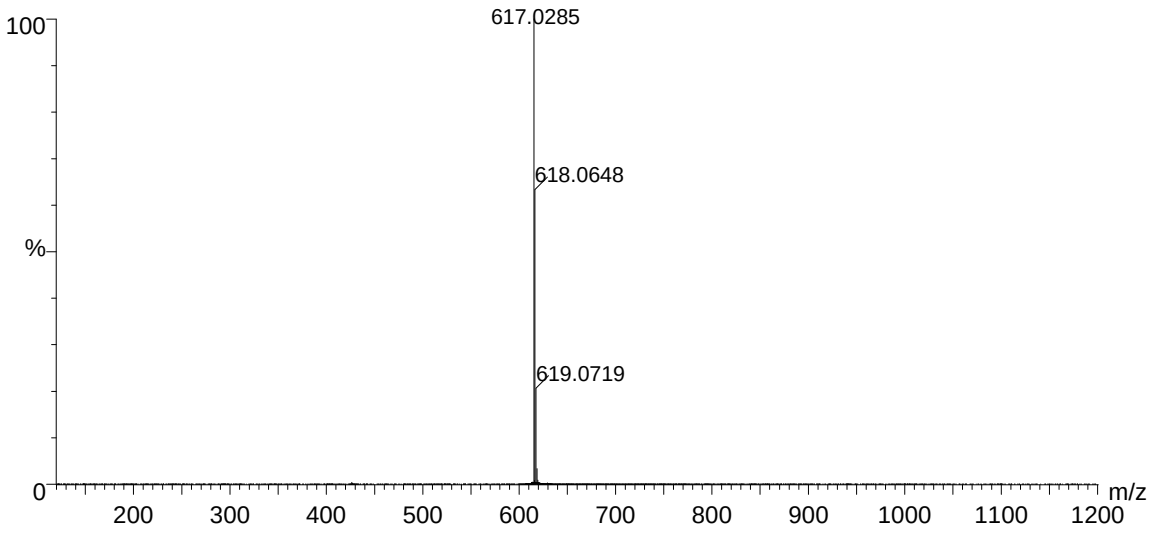

(b)

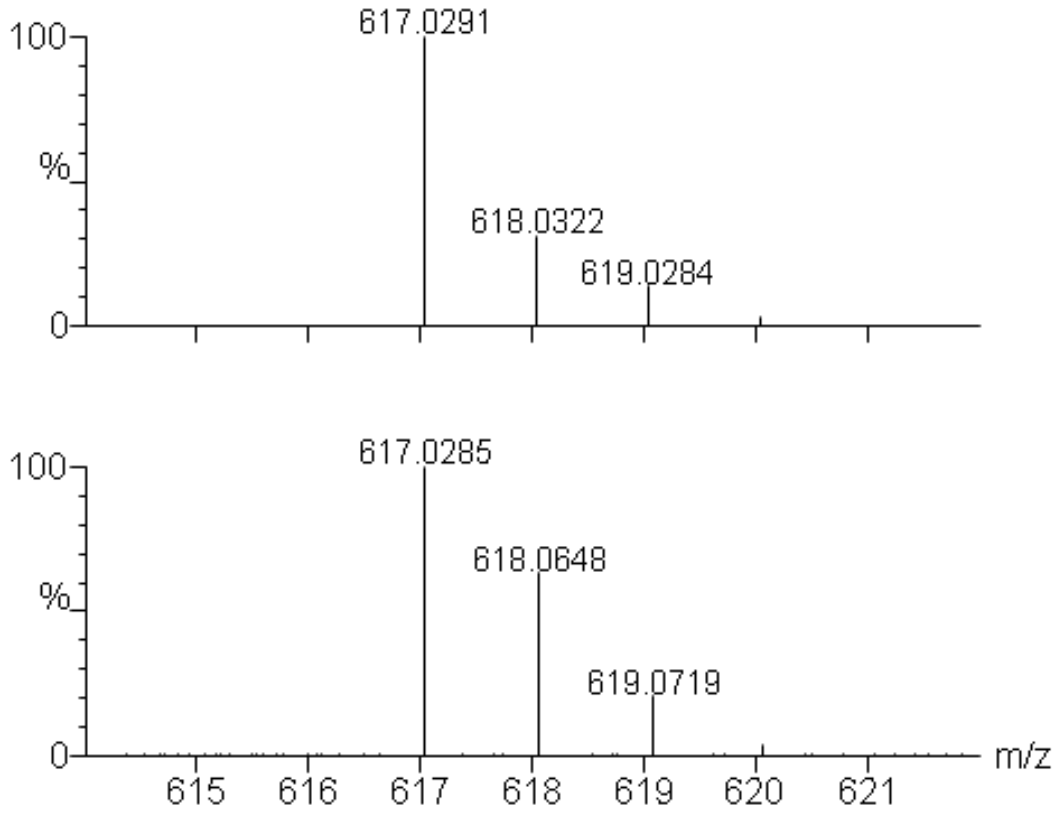

Figure S43. ESI-HRMS of **D-5[PF_6]** in CD_2Cl_2

(a) The signal at an m/z = 618.0349 corresponds to [D-**5**]$^+$ (b) Calculated isotopic distribution for [D-**5**]$^+$ (bottom) and the amplifying experimental diagram for [D-**5**]$^+$ (upper).

(a)

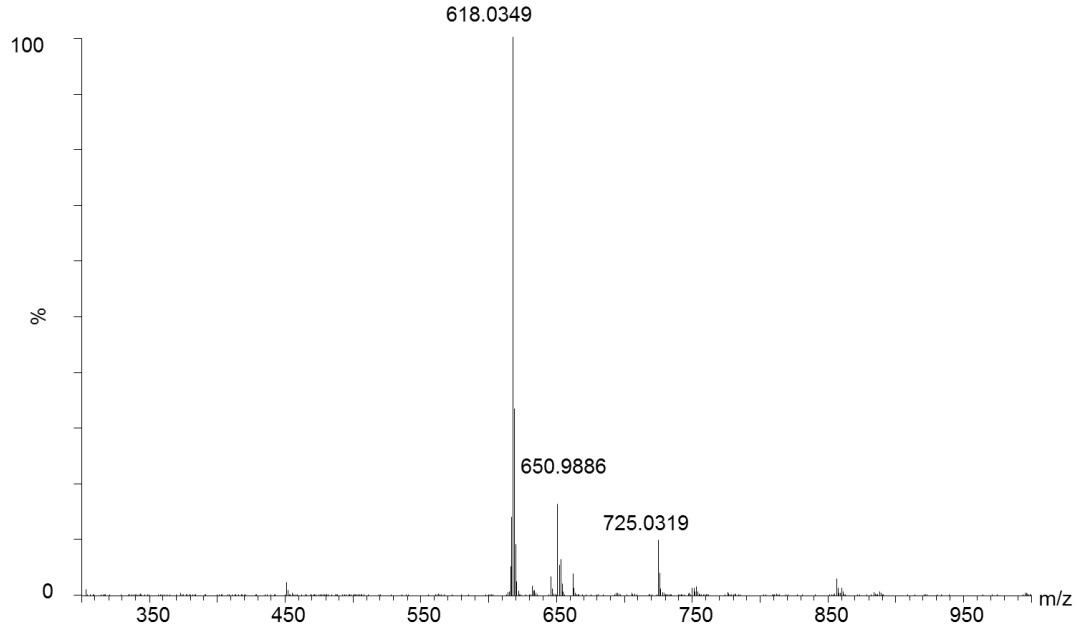

(b)

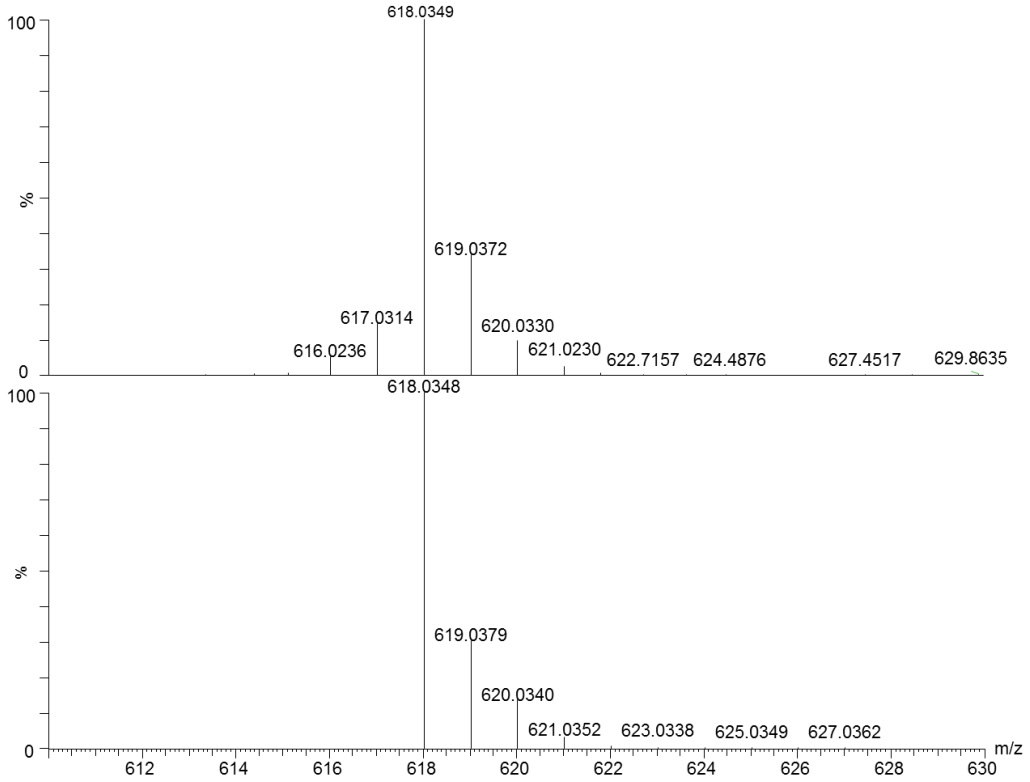

Figure S44. ESI-HRMS of **5[BF$_4$]** in CH_2Cl_2

(a) The signal at an m/z = 617.0285 corresponds to [**5**]$^+$ (b) Calculated isotopic distribution for [**5**]$^+$ (upper) and the amplifying experimental diagram for [**5**]$^+$ (bottom).

(a)

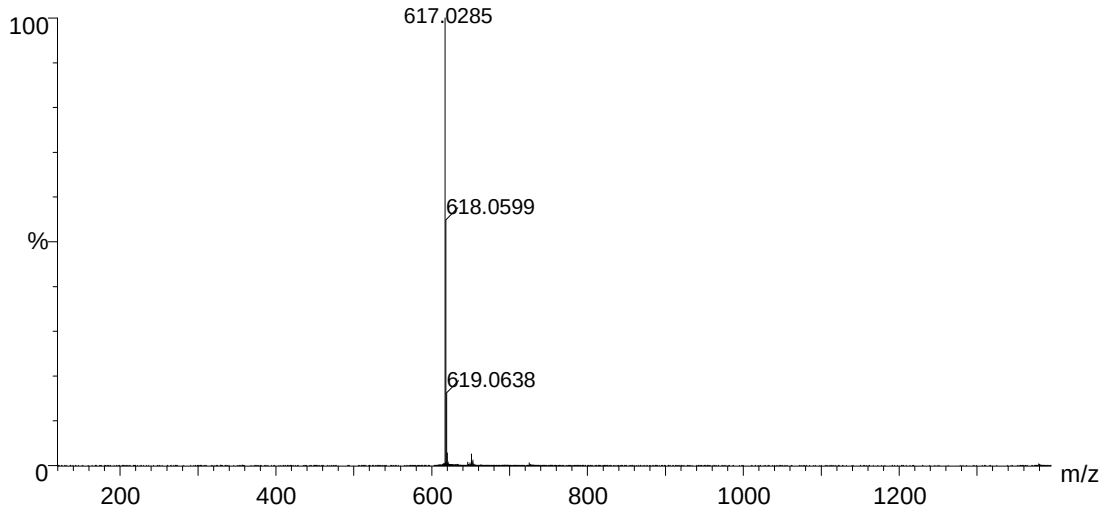

(b)

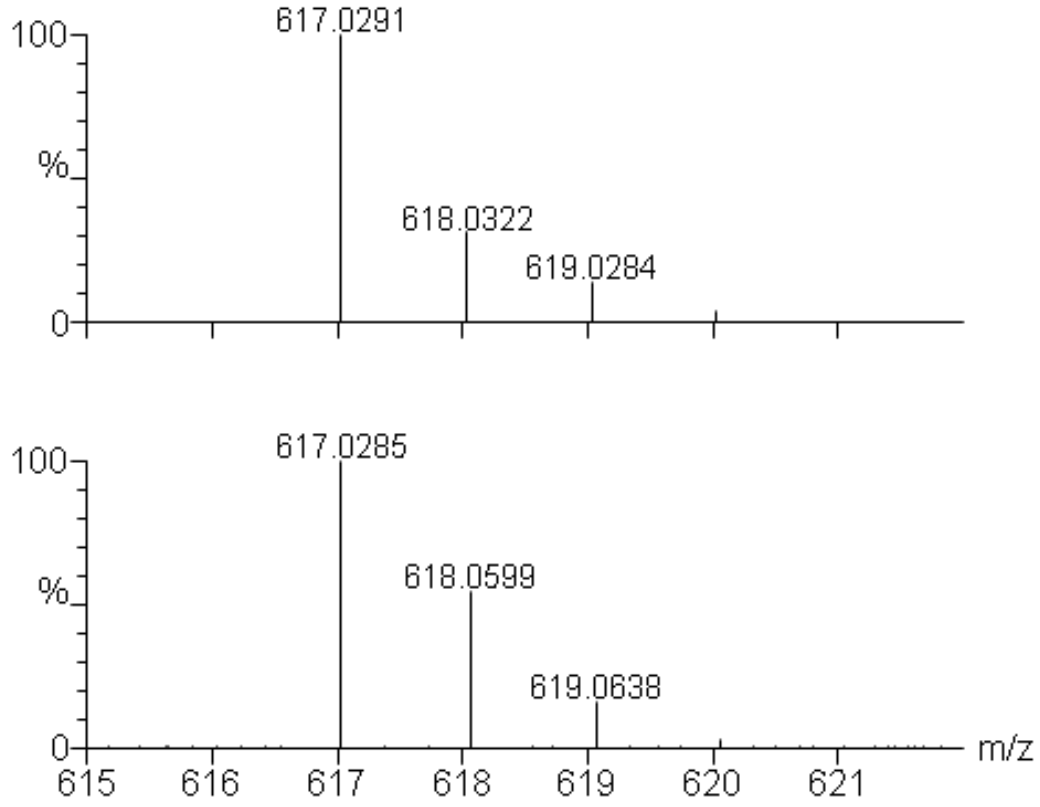

Figure S45. ESI-HRMS of **6[PF_6]** in CH_2Cl_2

(a) The signal at an m/z = 797.1454 corresponds to $[\mathbf{6}]^+$ (b) Calculated isotopic distribution for $[\mathbf{6}]^+$ (upper) and the amplifying experimental diagram for $[\mathbf{6}]^+$ (bottom).

(a)

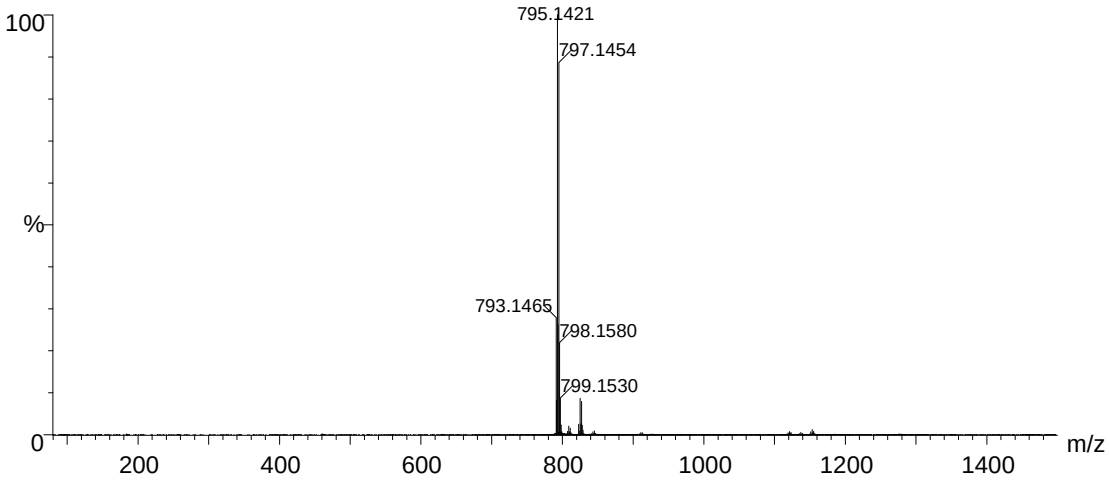

(b)

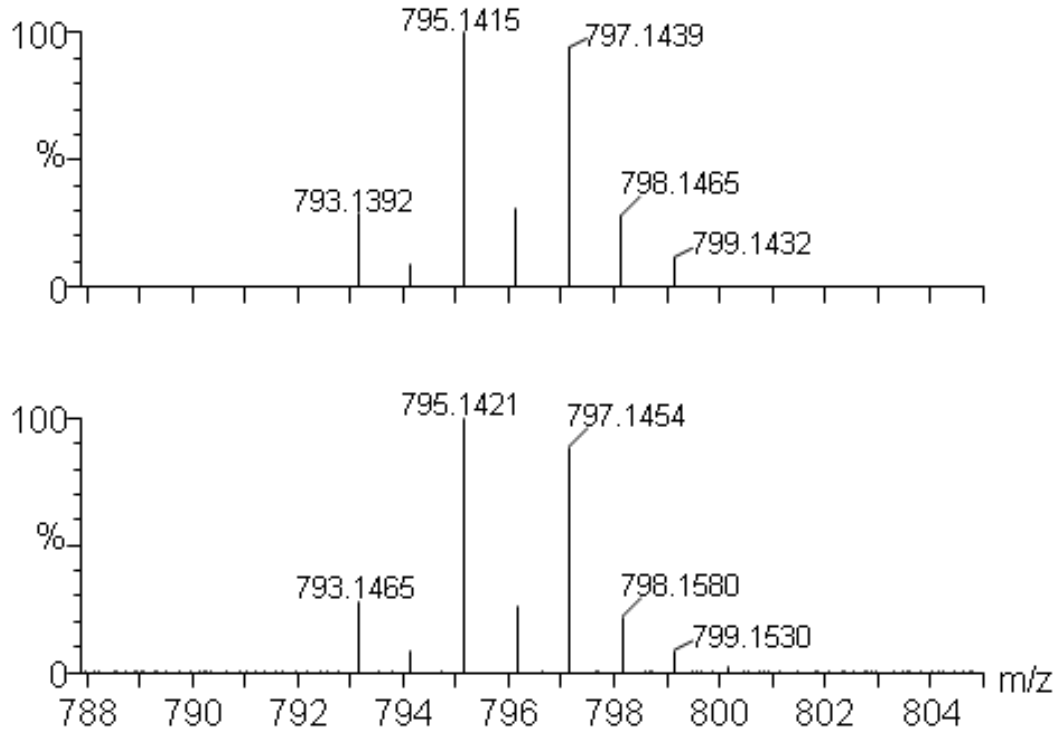

Figure S46. ESI-HRMS of **D-6[PF_6]** in CD_2Cl_2

(a) The signal at an m/z = 798.1494 corresponds to [D-**6**]$^+$ (b) Calculated isotopic distribution for [D-**6**]$^+$ (bottom) and the amplifying experimental diagram for [D-**6**]$^+$ (upper).

(a)

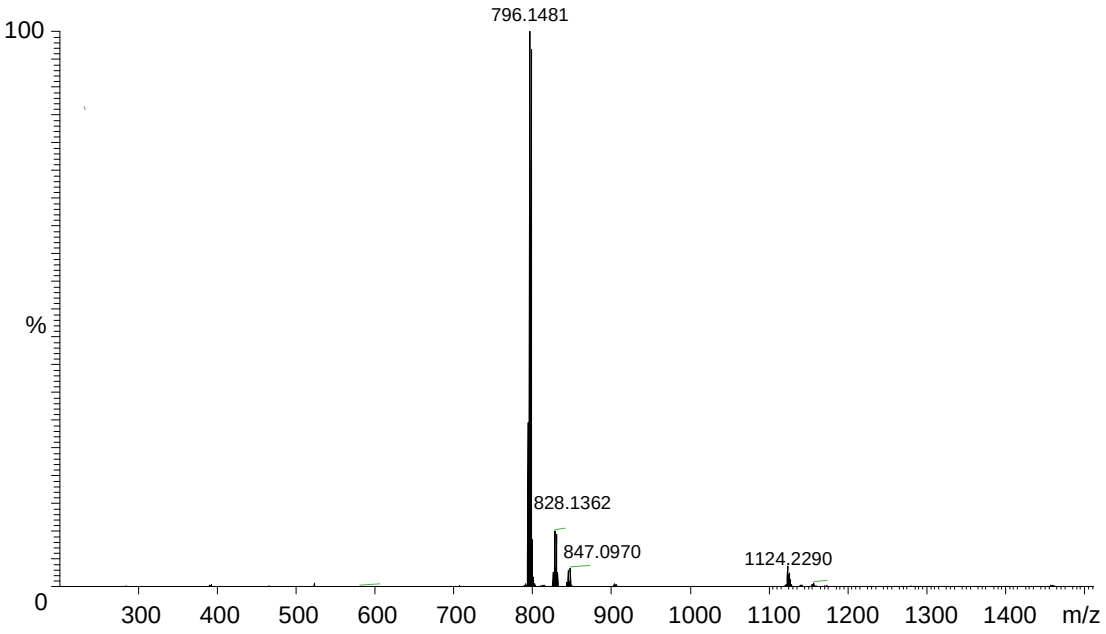

(b)

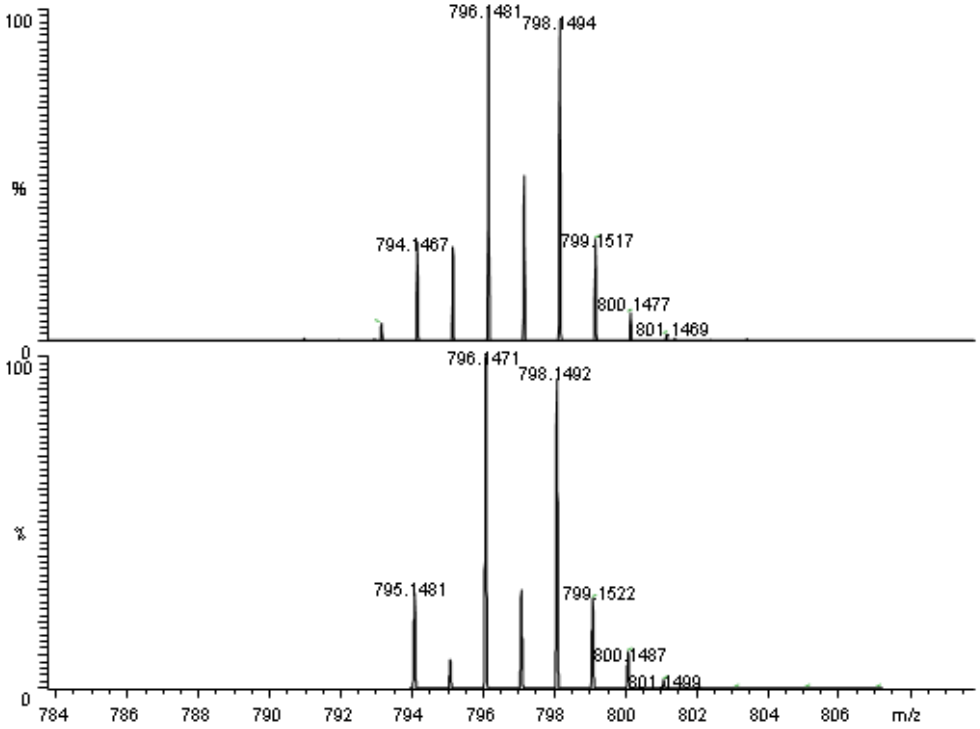

Figure S47. ESI-HRMS of **6[BF_4]** in CH_2Cl_2

(a) The signal at an m/z = 797.1447 corresponds to $[\mathbf{6}]^+$ (b) Calculated isotopic distribution for $[\mathbf{6}]^+$ (upper) and the amplifying experimental diagram for $[\mathbf{6}]^+$ (bottom).

(a)

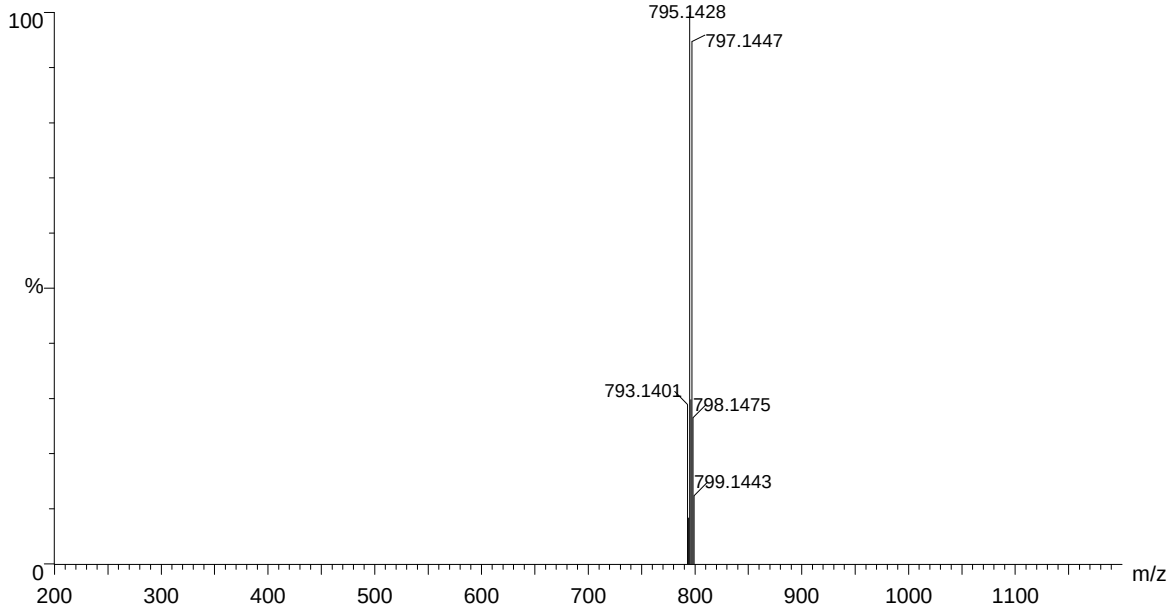

(b)

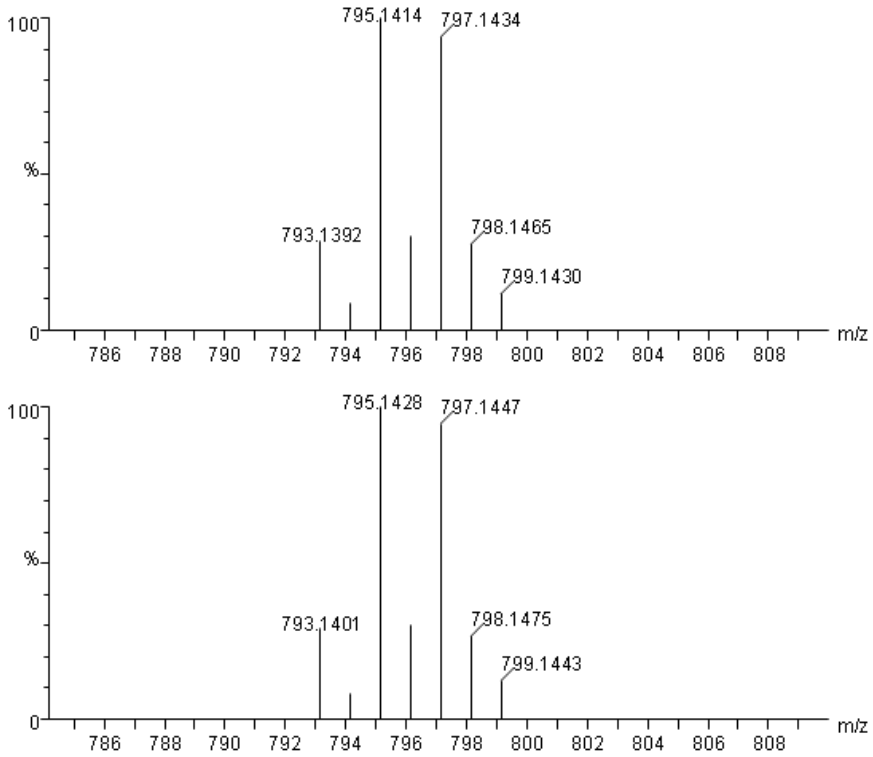

Figure S48. ESI-HRMS of **7a[BPh_4]** in CH_2Cl_2

(a) The signal at an m/z = 643.0457 corresponds to [**7a**]$^+$ (b) Calculated isotopic distribution for [**7a**]$^+$ (upper) and the amplifying experimental diagram for [**7a**]$^+$ (bottom).

(a)

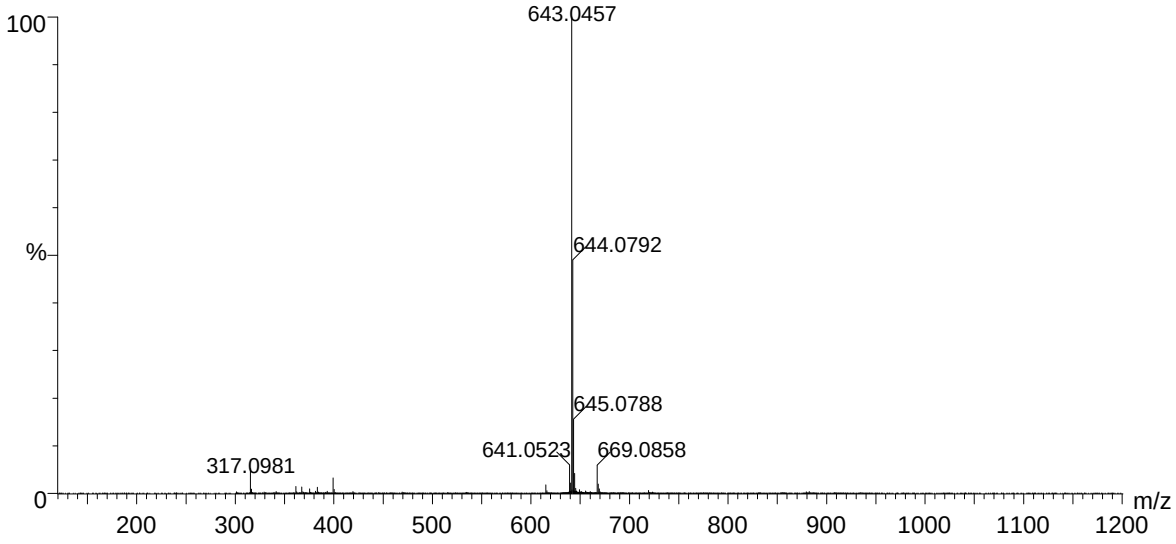

(b)

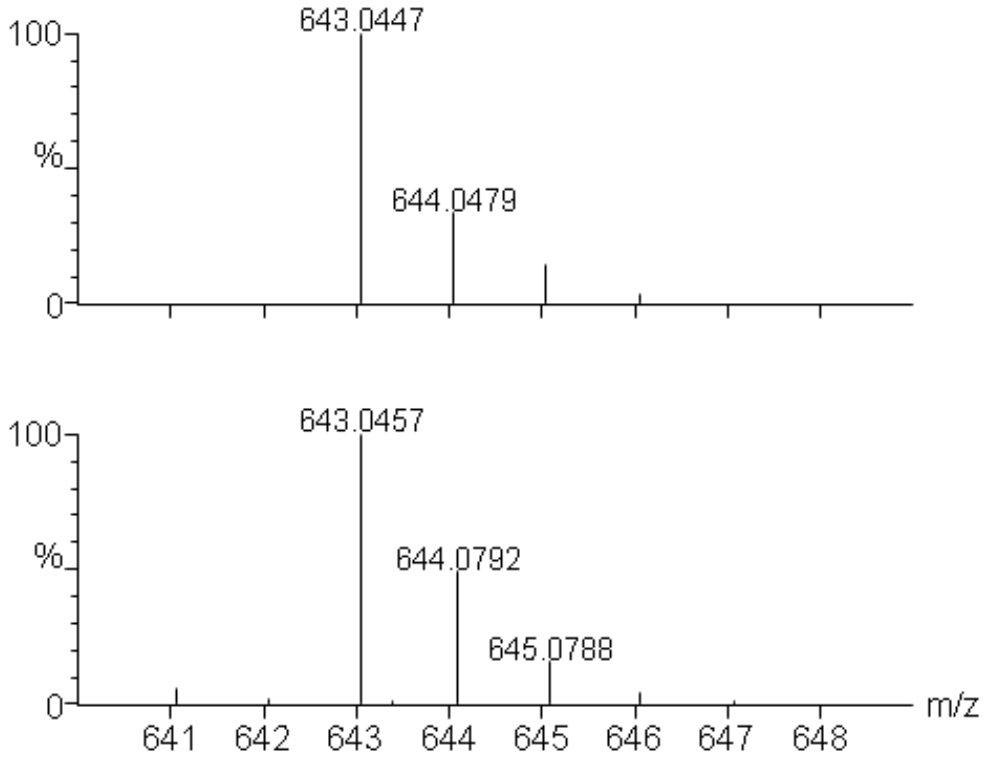

Figure S49. ESI-HRMS of **7b[BPh$_4$]** in CH_2Cl_2

(a) The signal at an m/z = 685.0923 corresponds to [**7b**]$^+$ (b) Calculated isotopic distribution for [**7b**]$^+$ (upper) and the amplifying experimental diagram for [**7b**]$^+$ (bottom).

(a)

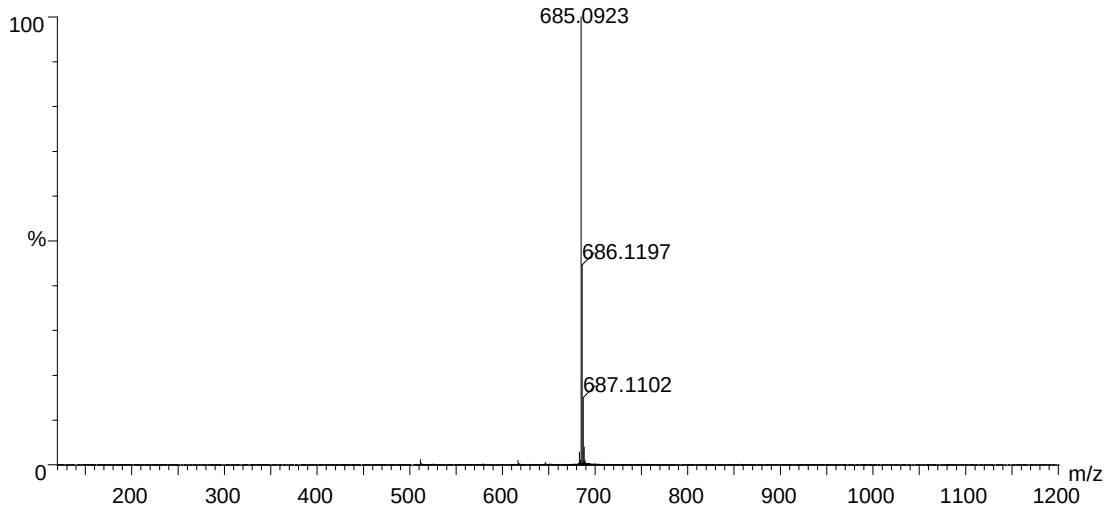

(b)

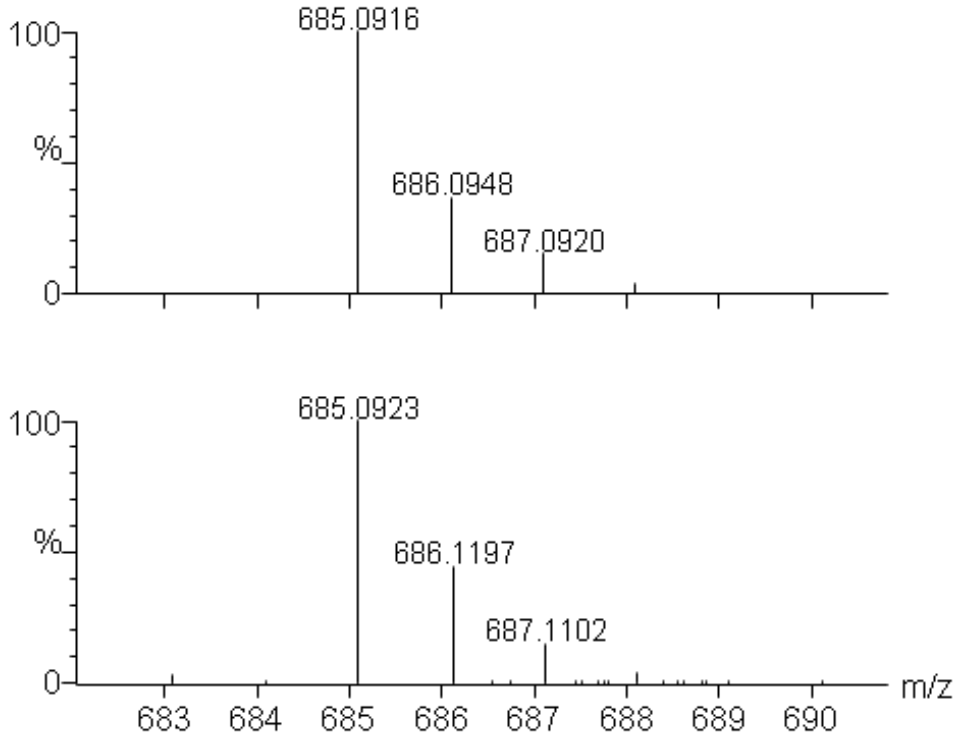

Figure S50. ESI-HRMS of **7c[BPh_4]** in CH_2Cl_2

(a) The signal at an m/z = 713.1223 corresponds to [**7c**]$^+$ (b) Calculated isotopic distribution for [**7c**]$^+$ (upper) and the amplifying experimental diagram for [**7c**]$^+$ (bottom).

(a)

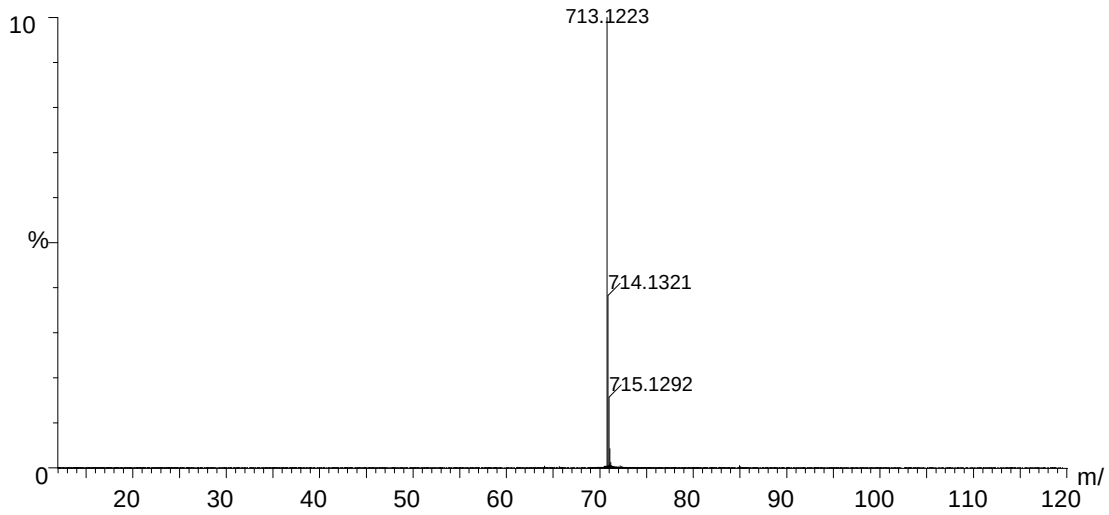

(b)

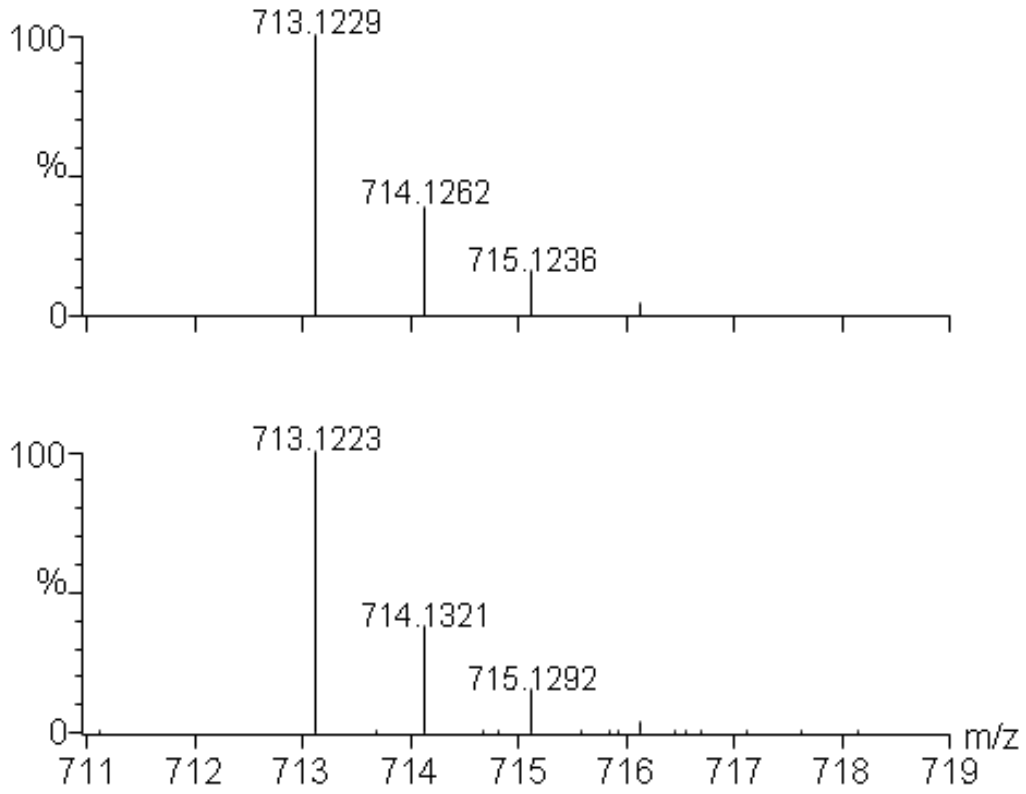

Figure S51. ESI-HRMS of **7d[BPh_4]** in CH_2Cl_2

(a) The signal at an m/z = 733.0918 corresponds to [**7d**]$^+$ (b) Calculated isotopic distribution for [**7d**]$^+$ (upper) and the amplifying experimental diagram for [**7d**]$^+$ (bottom).

(a)

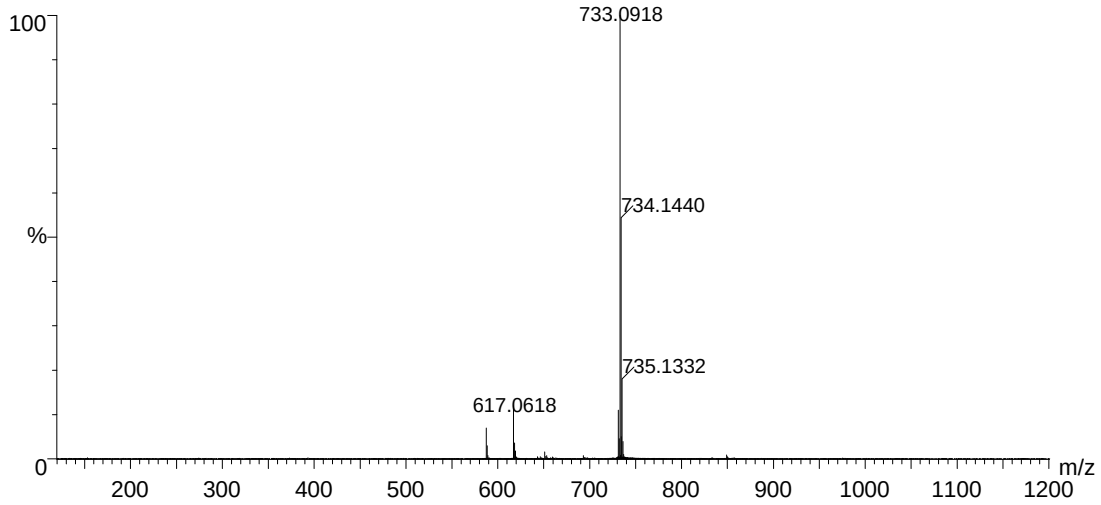

(b)

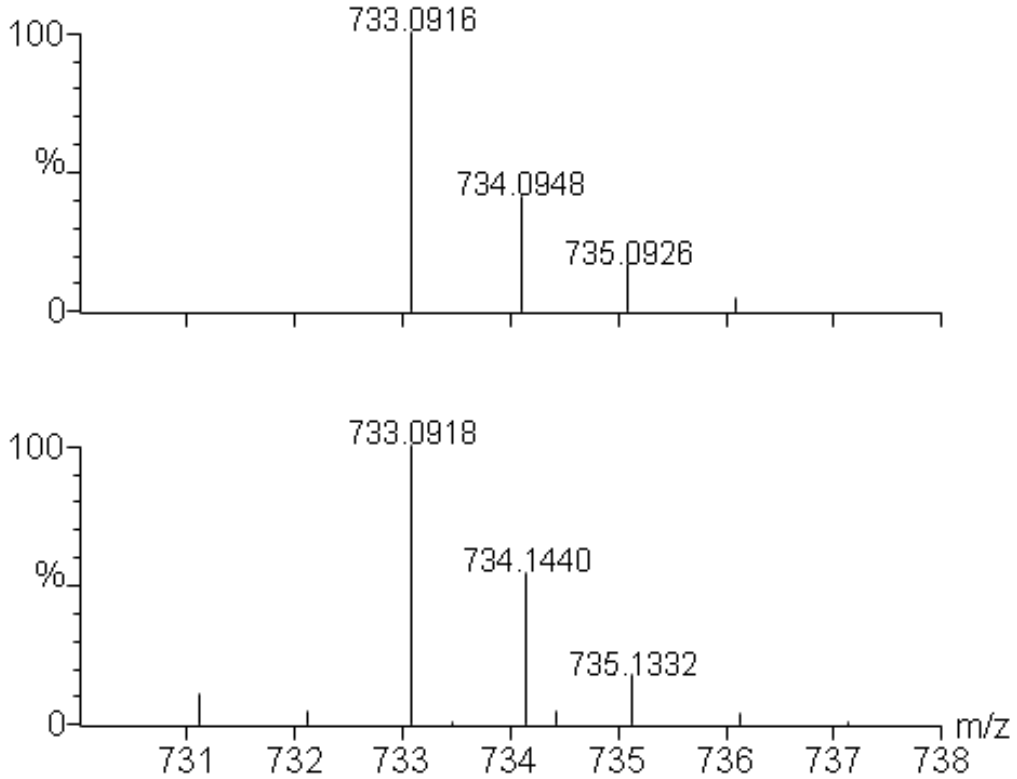

Figure S52. ESI-HRMS of **7e[BPh_4]** in CH_2Cl_2

(a) The signal at an m/z = 753.0381 corresponds to [**7e**]$^+$ (b) Calculated isotopic distribution for [**7e**]$^+$ (upper) and the amplifying experimental diagram for [**7e**]$^+$ (bottom).

(a)

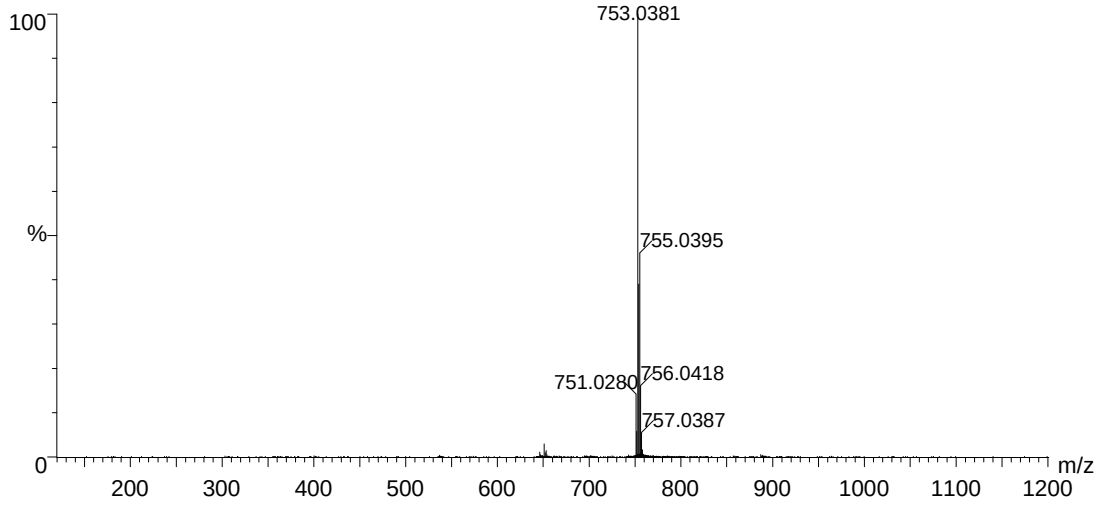

(b)

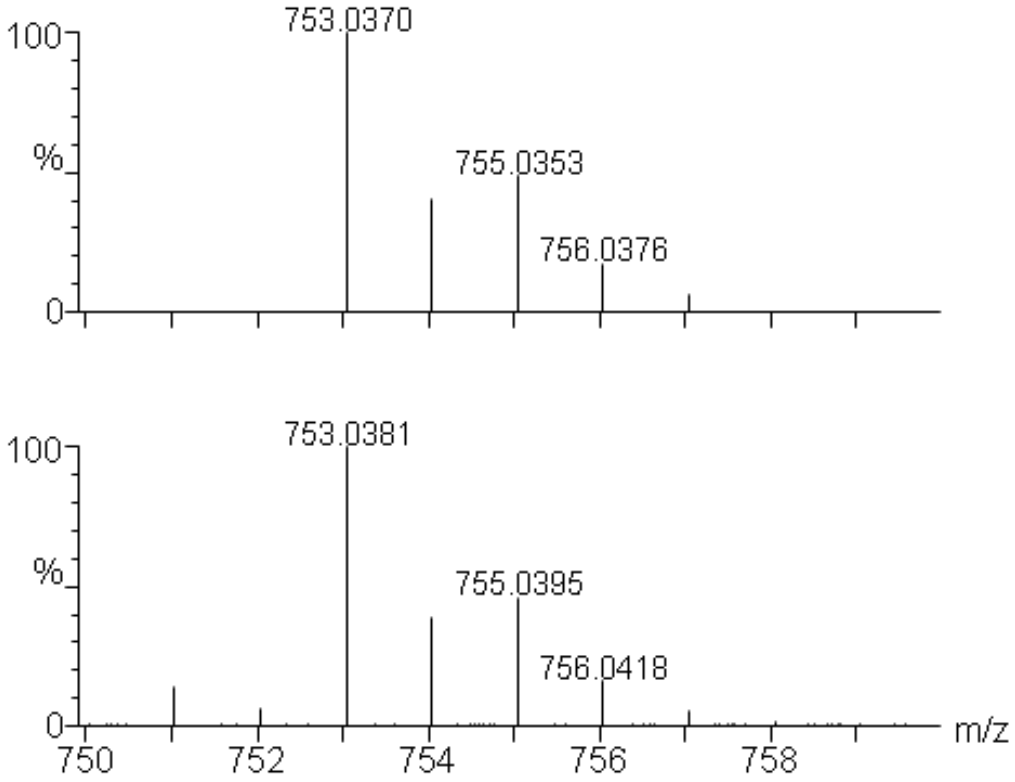

VII. IR Spectra

Figure S53. The IR (KBr) spectrum of **1[BF_4]**

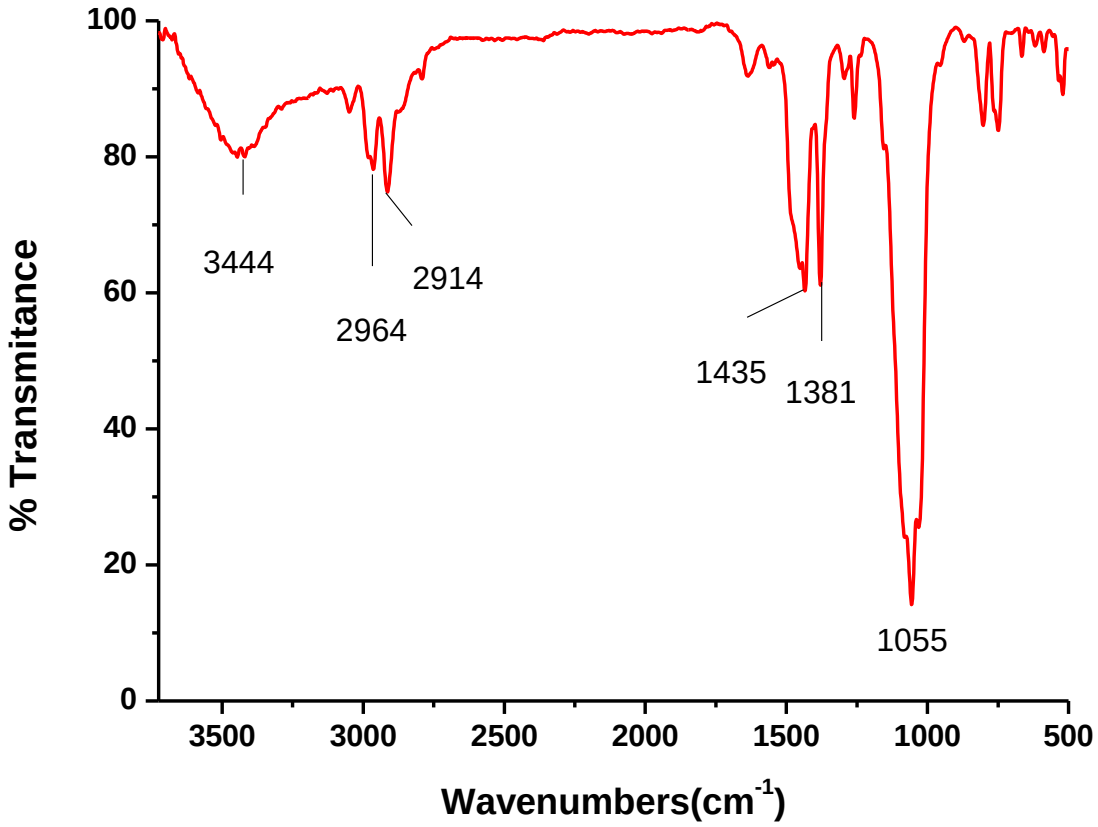

Figure S54. The IR (KBr) spectrum of **2**

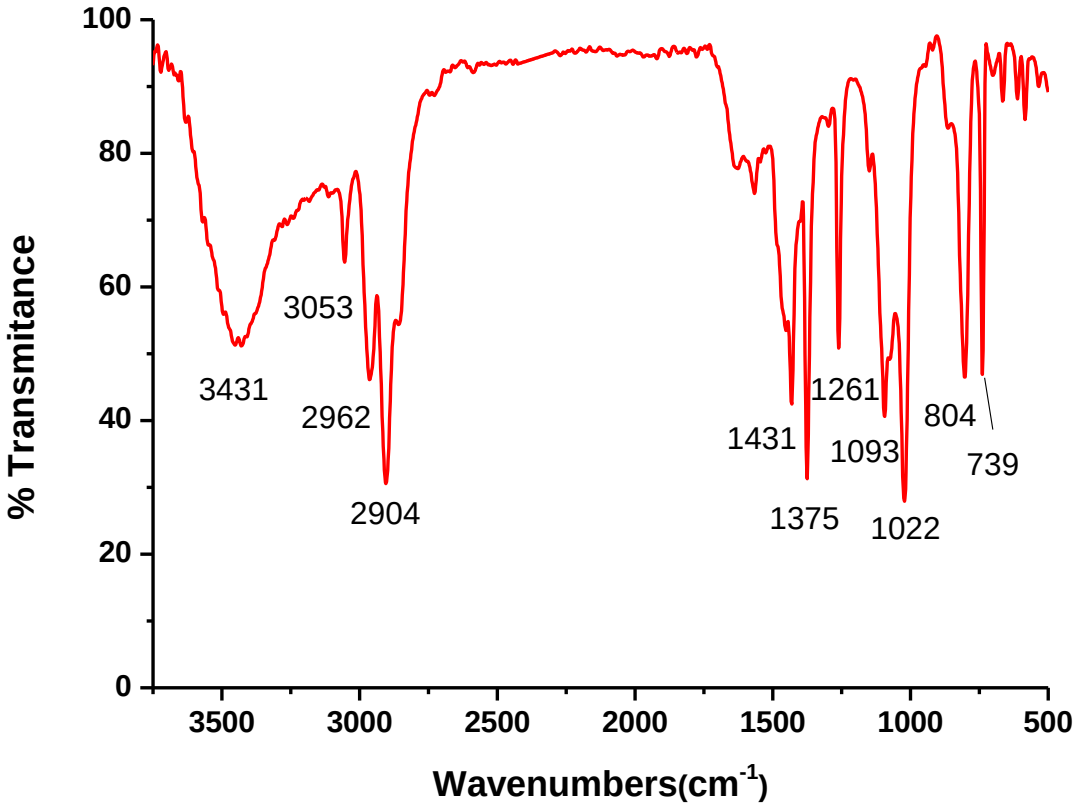

Figure S55. The IR (KBr) spectrum of **3[BPh_4]**

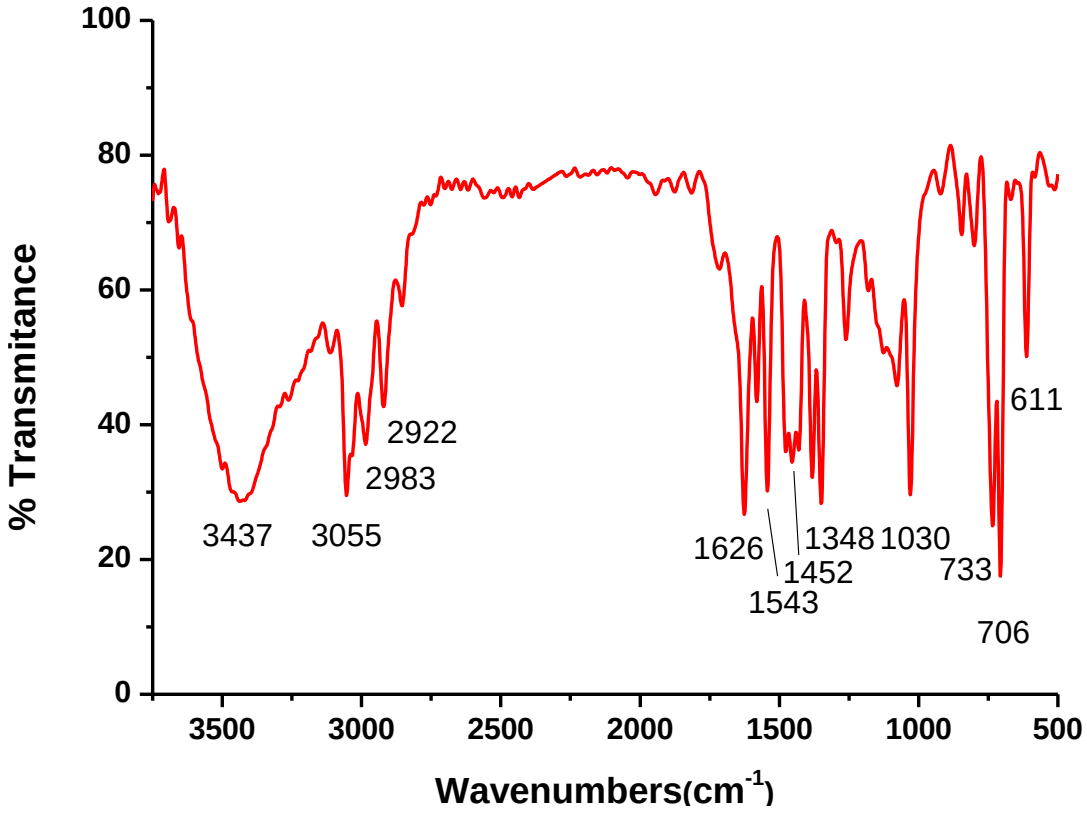

Figure S56. The IR (KBr) spectrum of **4**

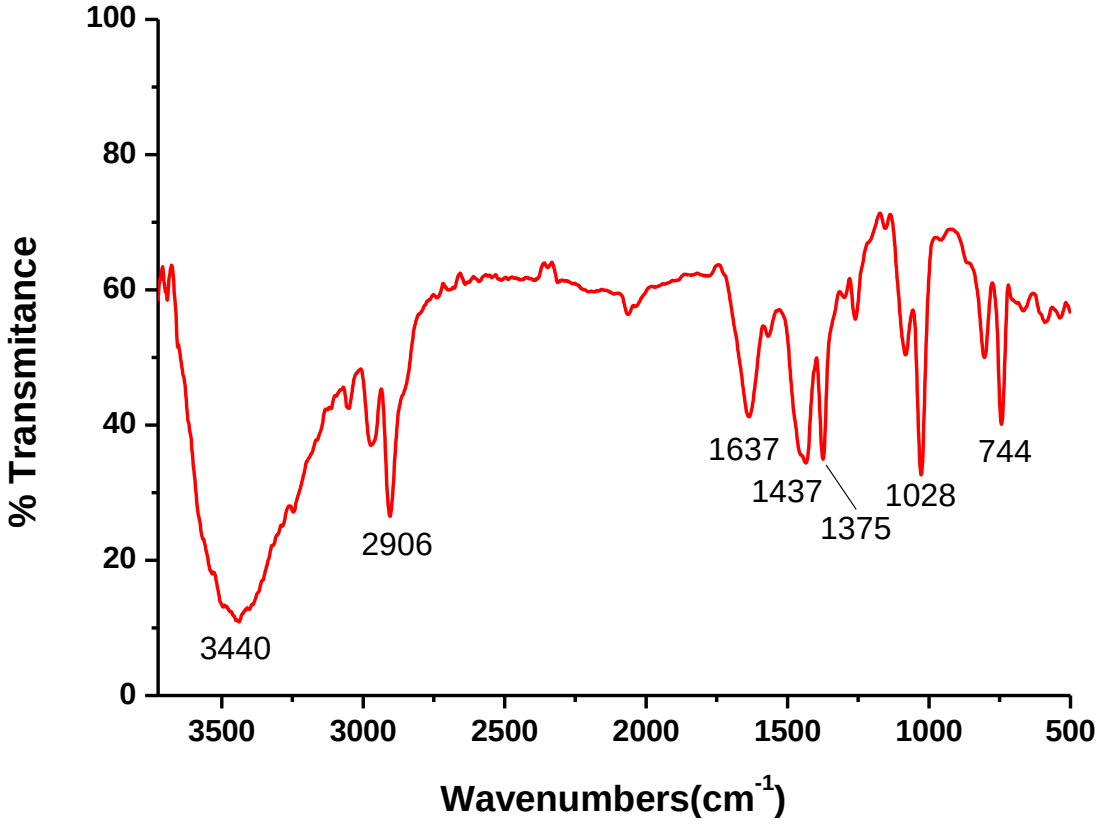

Figure S57 The IR (KBr) spectrum of **5[PF_6]**

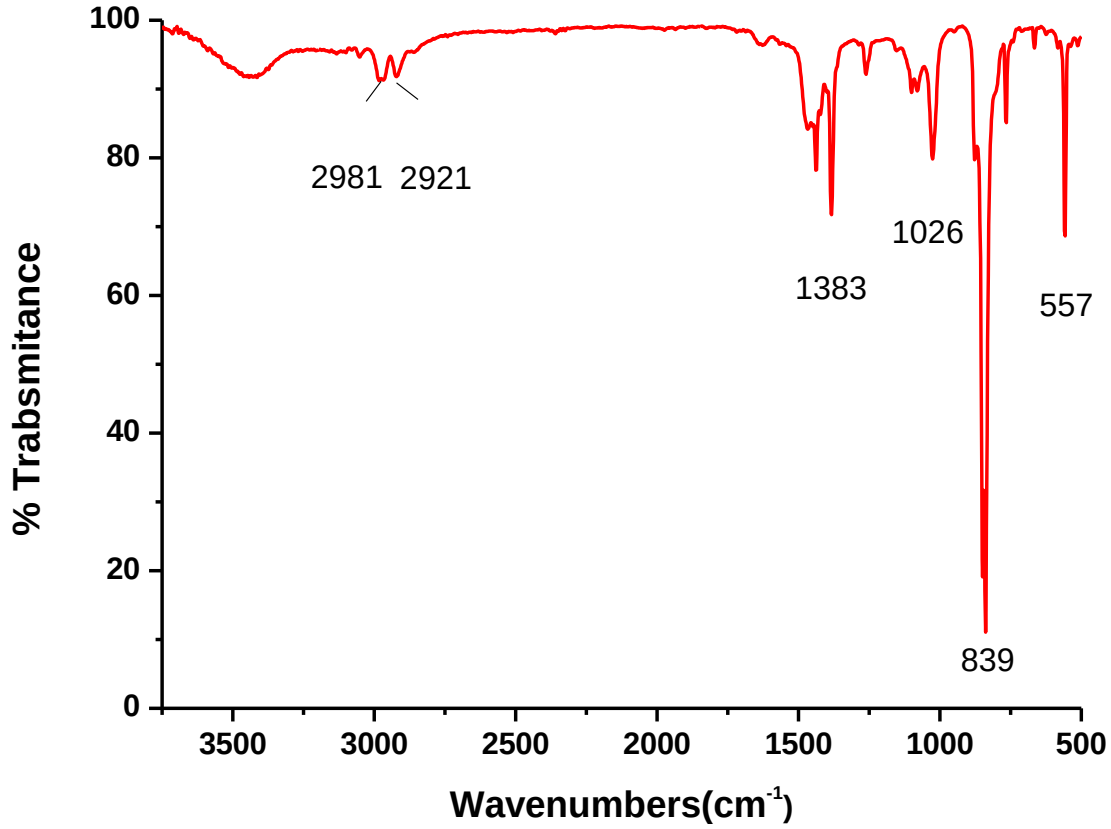

Figure S58. The IR (KBr) spectrum of **5[BF_4]**

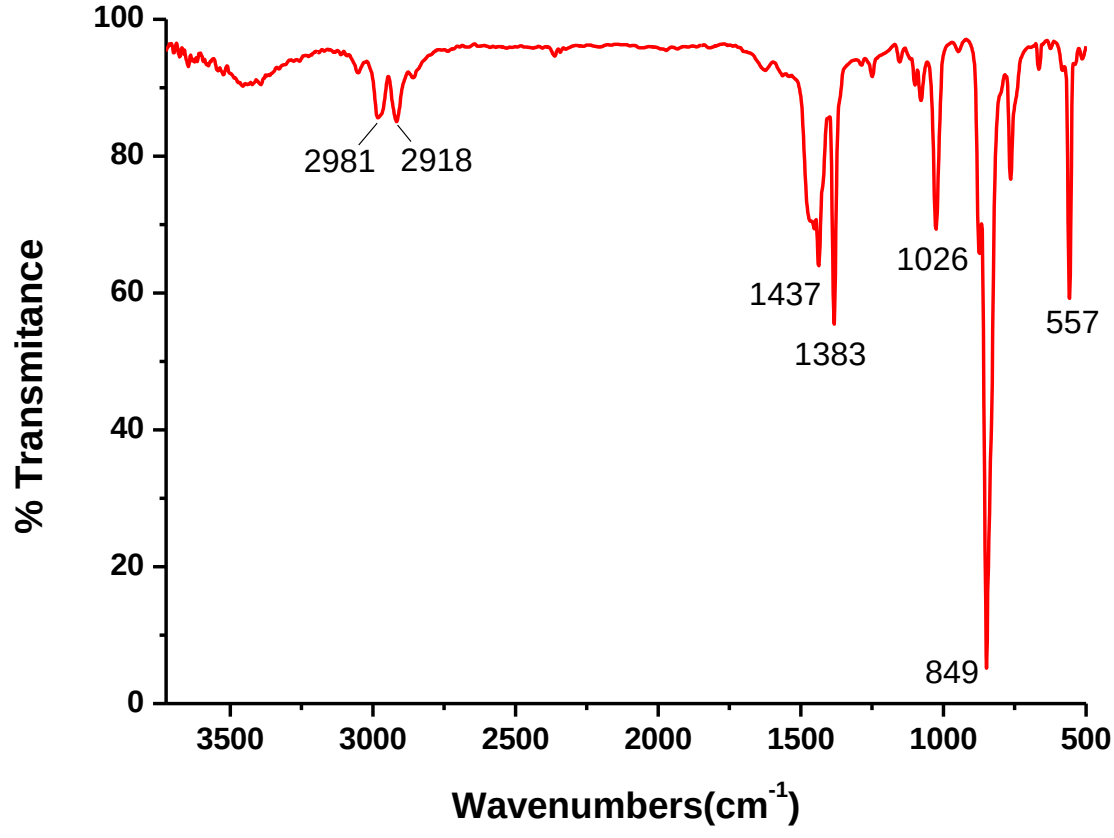

Figure S59. The IR (KBr) spectrum of **6[PF_6]**

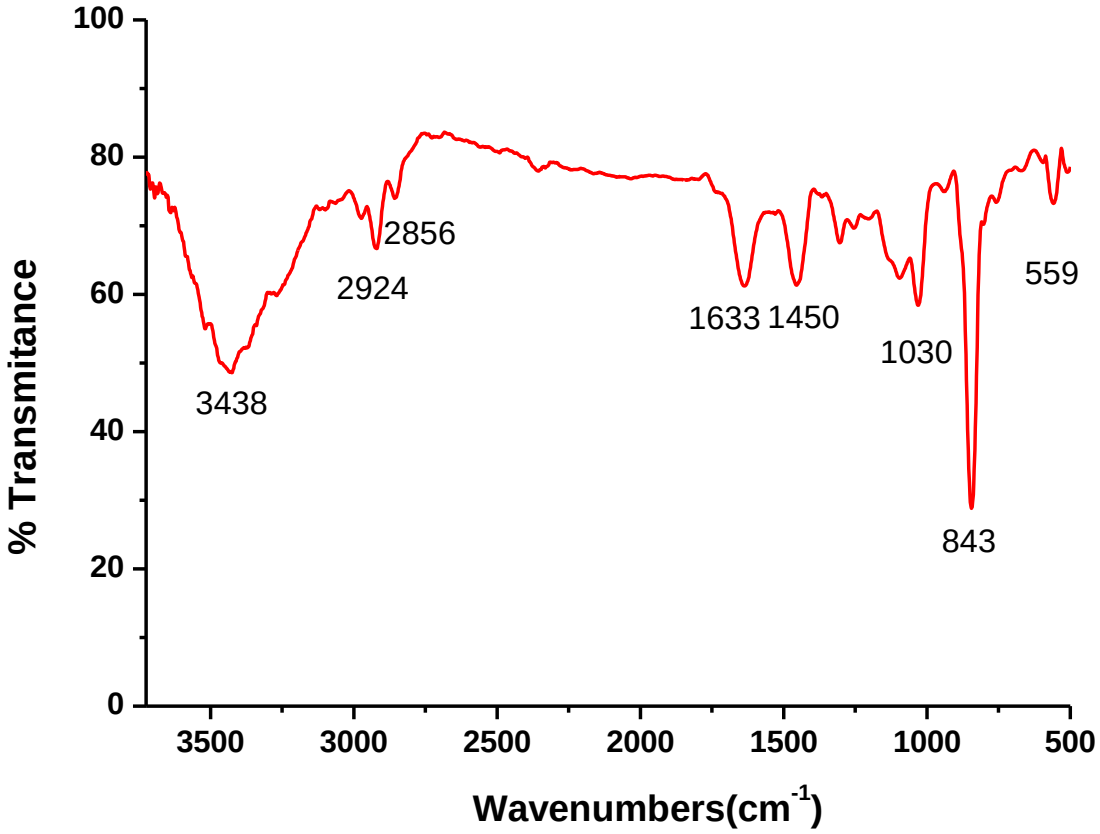

Figure S60. The IR (KBr) spectrum of **6[BF_4]**

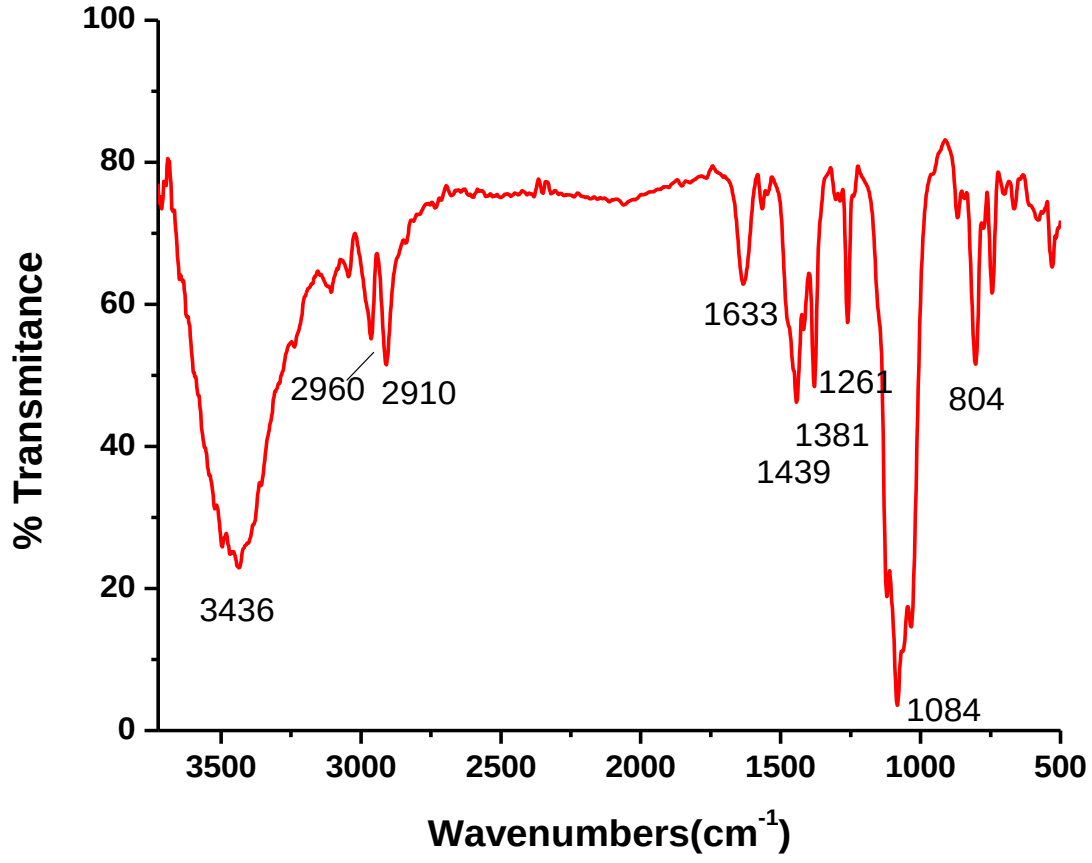

Figure S61. The IR (KBr) spectrum of **7a[BPh_4]**

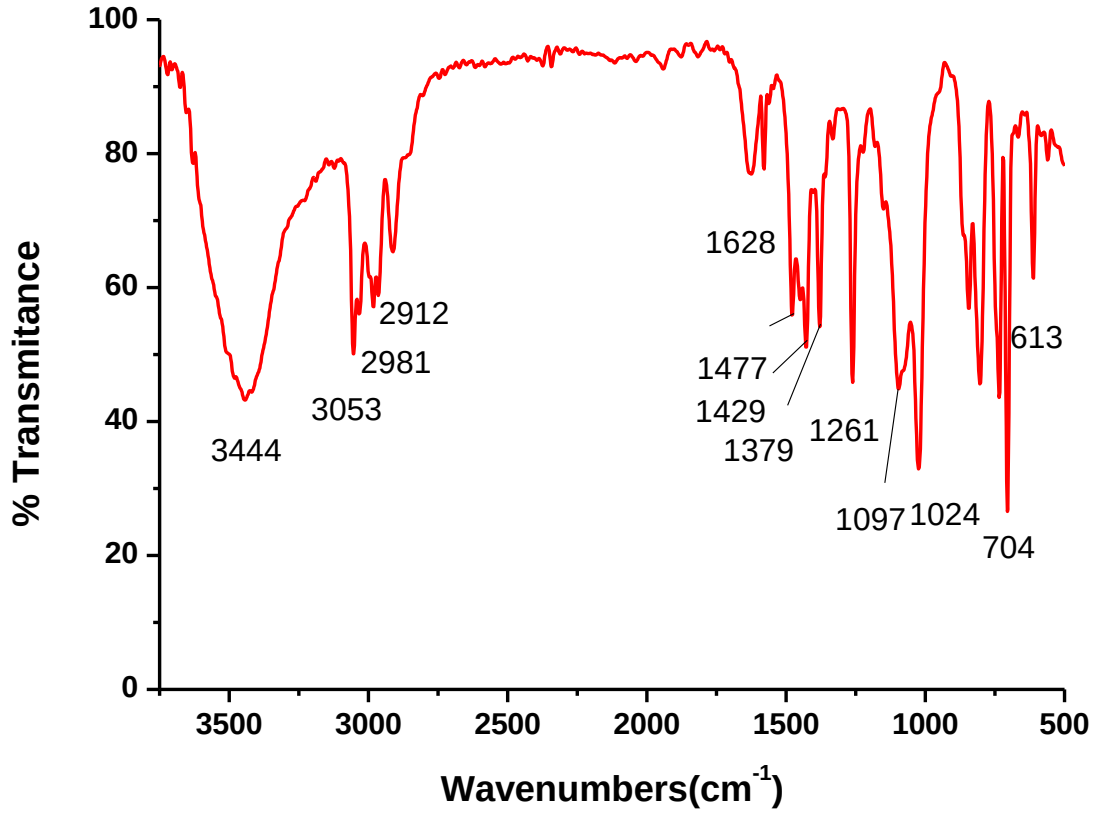

Figure S62. The IR (KBr) spectrum of **7b[BPh_4]**

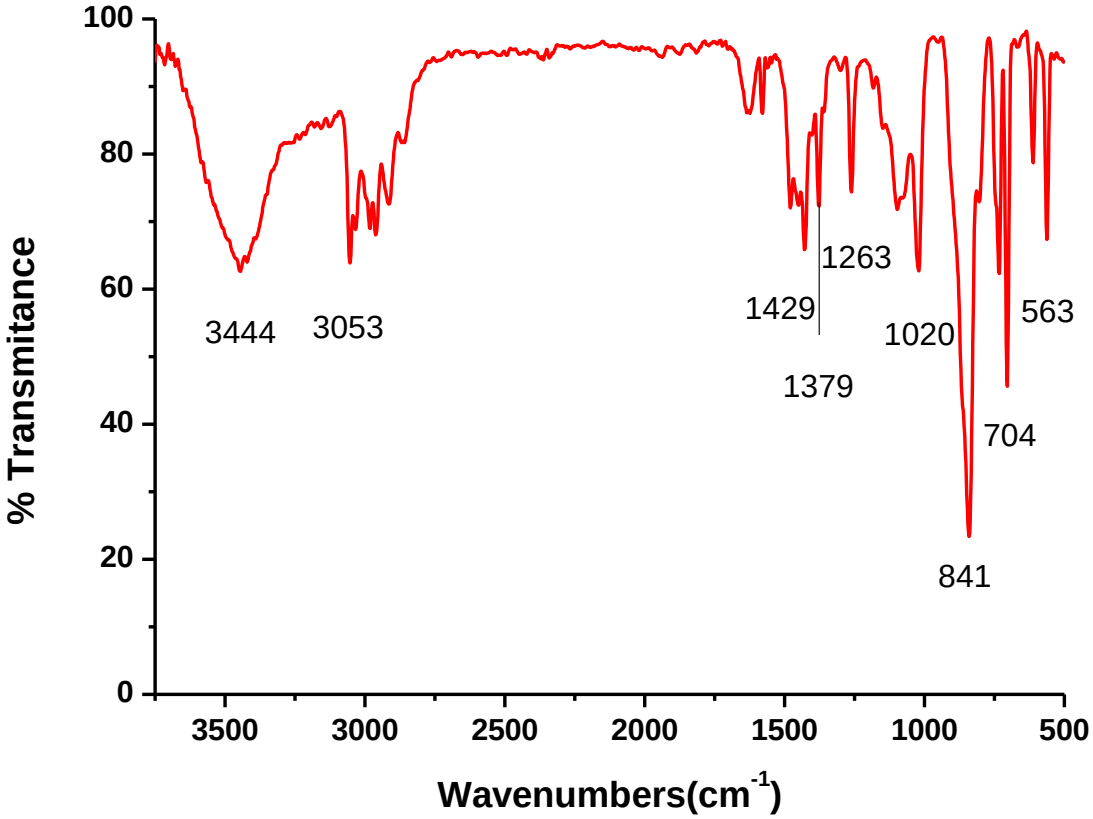

Figure S63. The IR (KBr) spectrum of **7c[BPh_4]**

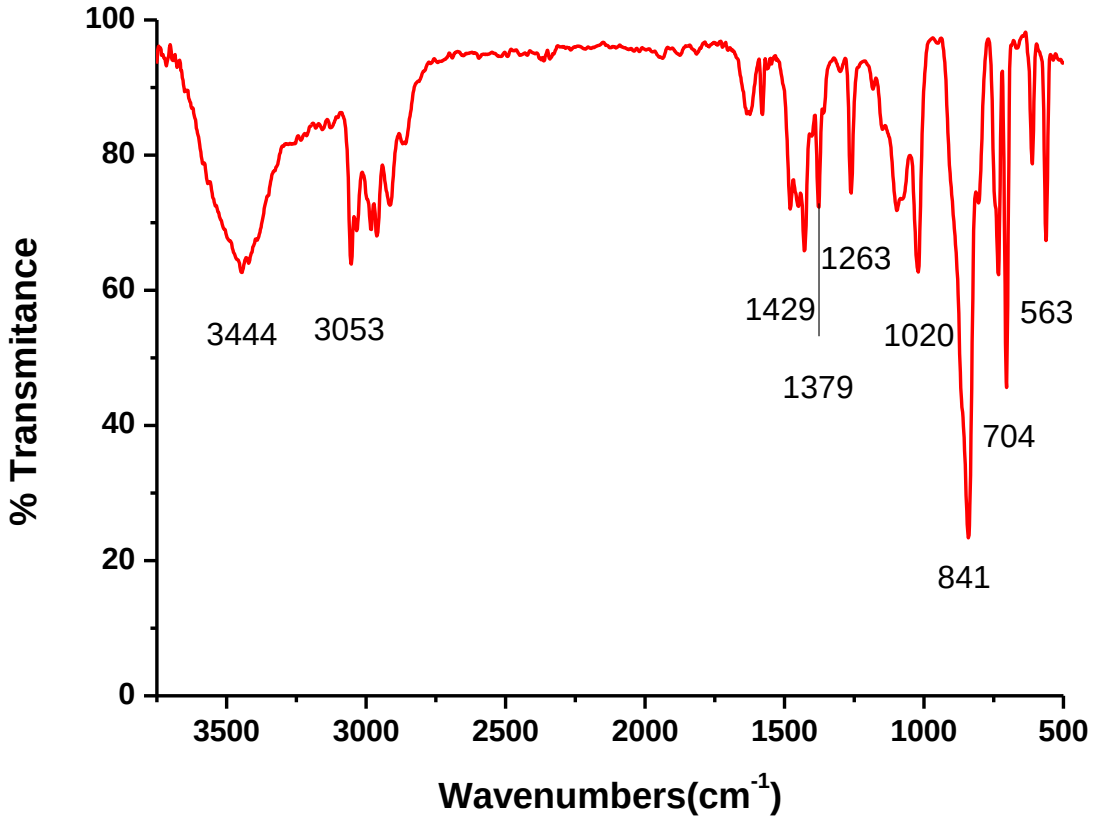

Figure S64. The IR (KBr) spectrum of **7d[BPh_4]**

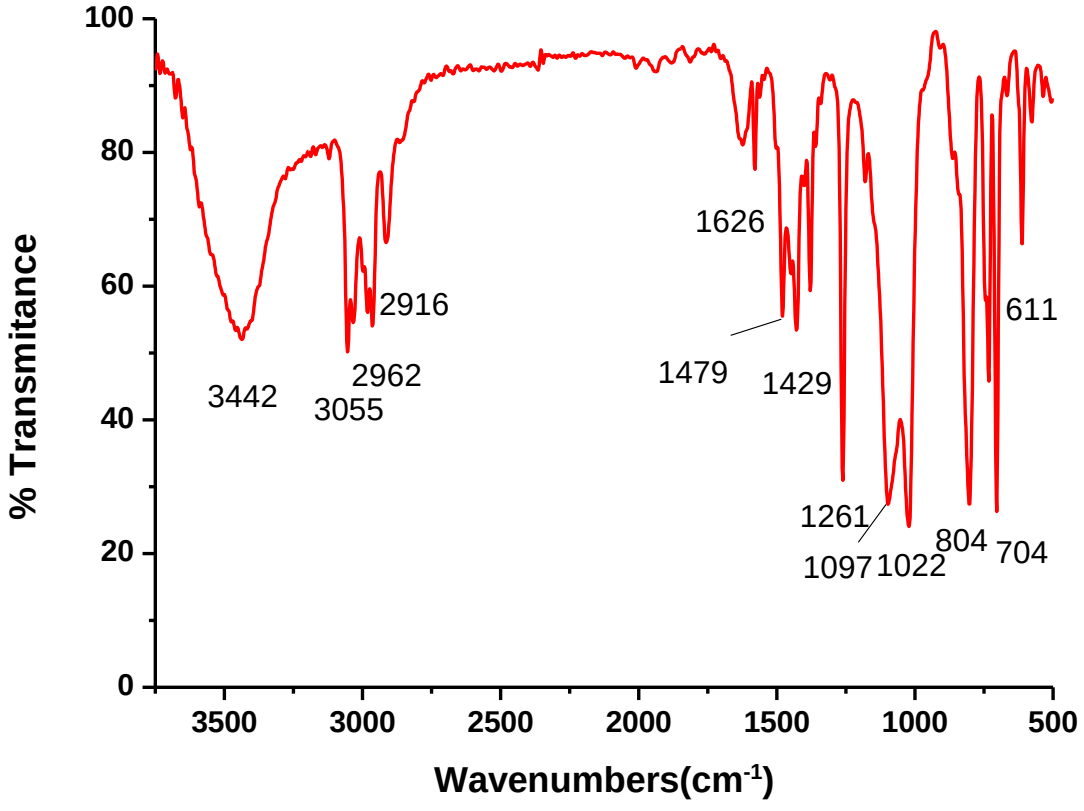

Figure S65. The IR (KBr) spectrum of **7e[BPh_4]**